Journal of Energy Storage 32 (2020) 101733

Contents lists available at ScienceDirect

Journal of Energy Storage

journal homepage: www.elsevier.com/locate/est

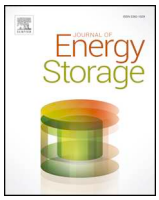

Systematic review on the use of heat pipes in latent heat thermal energy storage tanks

José Miguel Maldonado, Alvaro de Gracia, Luisa F. Cabeza*

GREiA Research Group, Universitat de Lleida, Pere de Cabrera s/n, 25001 Lleida, Spain

ARTICLE INFO

Keywords:
Heat pipe
Thermosiphon
Phase change material (PCM)
Thermal energy storage (TES)
Systematic review
Bibliometric analysis

ABSTRACT

This systematic review presents and discusses the previous research about hybrid devices which combine latent thermal energy storage (TES) technology and heat pipes. A bibliometric analysis of this issue shows how hybrid systems have globally grown popularity during time, providing details about the main researchers and research centres on this particular field. Then, the identified papers are assessed and categorized in two main sections, the experimental research carried out, and the numerical modelling of hybrid systems. Experimental research is later classified regarding the operating temperature range, and their final application. Numerical studies are also further categorized, accordingly to how heat pipes were modelled in this case. This review points out the lack of experimental studies at high temperatures, especially when many simulations extended their models (validated at low temperatures) to higher temperature designs. The paper provides details about the research performed, so the gap for future investigations can be spotted.

1. Introduction

This review explores in a systematic way all the available bibliography regarding hybrid systems of heat pipes and latent thermal energy storage (TES) systems and analyses their contribution to the state-of-the-art of this hybridization. The document also issues a bibliometric study, providing an overview of the interest in this particular topic along time and across the world. The synergy between heat pipes and latent TES arose from the necessity of improving the heat conductivity of the materials used in these TES systems, since heat pipes are one of the most efficient known devices to transfer heat [1]. By embedding heat pipes within TES devices, the heat transfer surface is enlarged. Increasing the heat transfer ratio between the TES material and the heat income (during loading process), and the heat output (when discharging); without adding extra pumping requirements to the system [2].

Thermal energy storage (TES) systems can be divided into sensible, latent, and thermochemical TES [3], the second one is the main target of this article. Latent TES, with phase change materials (PCM) as storing material, have a large capacity to store and release thermal energy by means of nearly isothermal processes [4]. There are many PCM with potential to become a good thermal energy storage material. Nonetheless, some properties must be possessed by the PCM, such as non-flammability, low toxicity, harmlessness, a melting and solidification according to the requirements, thermal stability, high heat of fusion, and high thermal conductivity; the latter property is hardly achieved by the PCM available today. Hence, due to the PCM low thermal conductivity, many researchers focused their efforts on developing new mechanisms which can overcome that drawback. Several designs and methods have been tested to improve heat transfer in these systems, such as adding different geometry fins, bubble agitation, including metal matrixes or other enhancement materials (such as graphite or nano-particles) into the PCM, and the insertion of heat pipes [3,5,6]. One of the simplest ways to increase the thermal conductivity in the storage tank is to enlarge the heat transfer surface. However, enlarging the PCM tank piping, where the heat transfer fluid flows through, can cause serious pressure drops and it reduces the effective PCM storage volume. By including heat pipes in the TES tank, at least one of the last issues would be avoided, since the number of heat pipes can be increased without affecting the heat transfer fluid (HTF) flow. The use of heat pipes is one of the most pursued ways to improve the already mentioned low heat conductivity of PCM [2], since heat pipes can be several thousand times as effective as the best metals in heat transporting [7].

Heat pipes are passive devices which are able to transport great heat amounts by using latent heat of an inner working fluid. Also, this heat transfer occurs at almost isothermal conditions, with a minimal temperature difference as driving force [8,9]. A heat pipe consists of three main parts: evaporator, adiabatic section, and condenser (Fig. 1). The

* Corresponding author.
E-mail address: lcabeza@diei.udl.cat (L.F. Cabeza).

https://doi.org/10.1016/j.est.2020.101733
Received 22 April 2020; Received in revised form 6 July 2020; Accepted 30 July 2020
Available online 11 August 2020

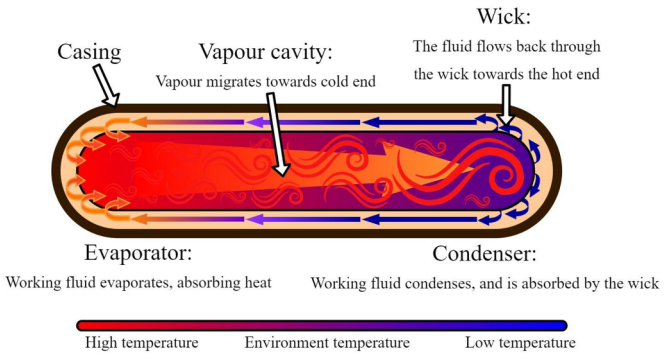

Fig. 1. Heat pipe scheme and working cycle.

heat input goes through the evaporator part, evaporating the working fluid inside the heat pipe. Then the vapour flows along the adiabatic section towards the condenser section. When condensing, the fluid goes back to the evaporator section, completing the cycle. The fluid return can happen by capillarity through an internal wick, or by gravity. The latter means a wickless heat pipe which is usually called thermosiphon instead of heat pipe. Among wicked heat pipes there are different types of wick systems to optimize the performance of capillary force in heat pipes, such as screen mesh, sintered metal, axial grooves, open annulus, or artery wick [9]. The wick selection depends on the heat pipe working condition and goal, to get the best wick design. Before choosing a heat pipe wick, three main parameters must be taken into account: minimum capillary radius, permeability, and effective thermal conductivity. For large capillary pressure, a small capillary radius is required. The permeability measures the axial liquid flow; the higher the permeability is, the lesser liquid pressure drop across the wick will be. Large values of effective thermal conductivity mean small temperature drop in the wick [9].

In 2015 Naghavi et al. [5] published a thorough review of hybrid applications. They concluded from the experimental literature that heat pipes with latent TES systems for solar applications improved their efficiency. Also, from the numerical research, they pointed out the use of 1-D and 2-D simulations due to the equation´s complexity. The

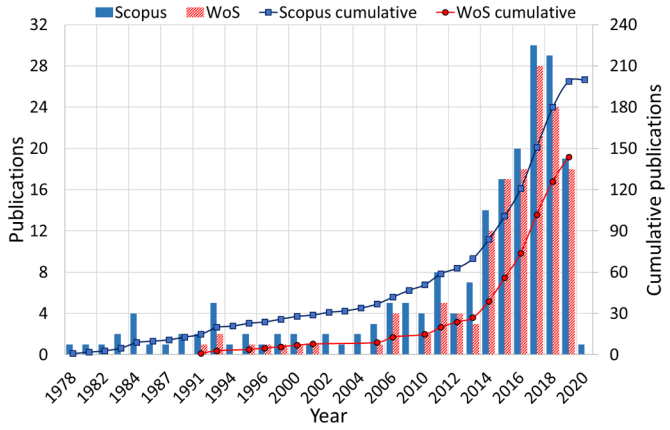

Fig. 3. Number and cumulative number of publications per year addressing heat pipes, PCM and latent TES.

present document provides an upgraded state-of-the-art, which is especially relevant in this case since the publications regarding hybrid system grew considerable in the last years, as it will be shown in Section 3.1. Also, the present review provides a different approach regarding the numerical research, by highlighting the heat pipe modelling in hybrid systems. Since regardless the system dimensions (1-D or 2-D), the model complexity can be eased by simulating the heat pipe as high thermal conductive solid, for instance, reducing the computing costs as well.

The research community interest on heat pipes and latent TES hybrid technology has increased within the last years. Therefore, the paper aims to provide updated guidelines for future research on this technology. The review classifies the studies according to their application, making it easier to spot what previous researchers have studied, and the new paths to pursue.

2. Methodology

This paper followed a systematic review methodology [10], starting with the definition of the adequate query to find the documents related

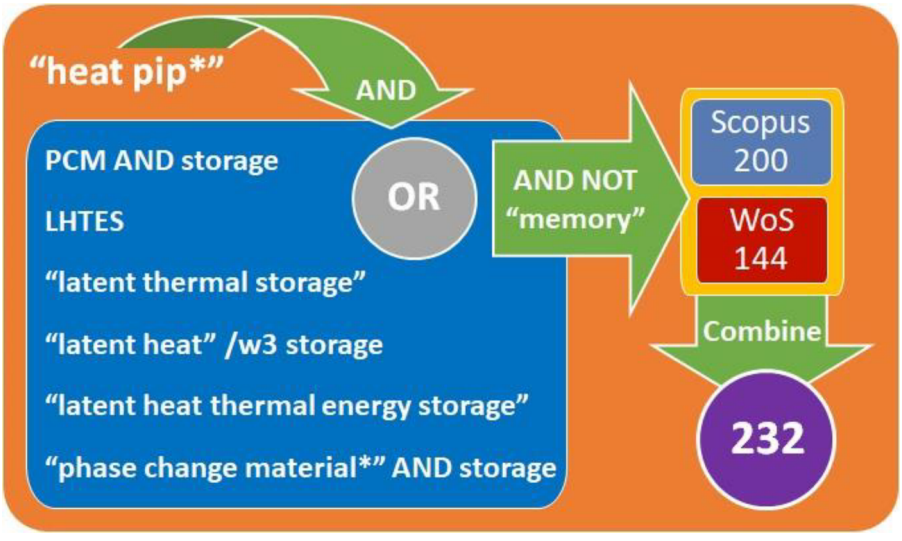

Fig. 2. Query performed to find the documents regarding the research on hybrid systems of PCM and heat pipes.

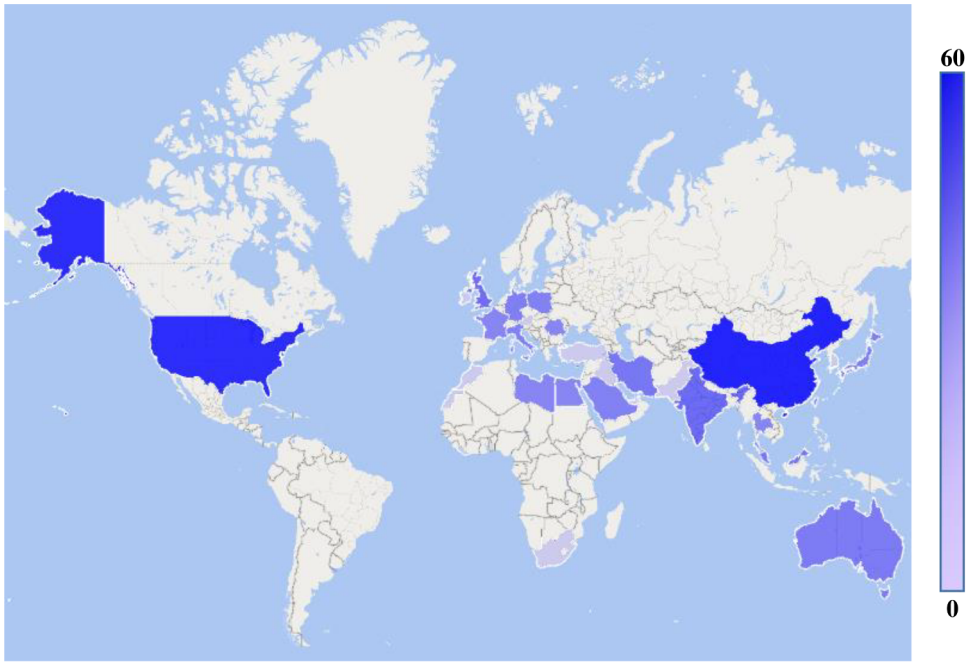

(a) Number of publications in Scopus

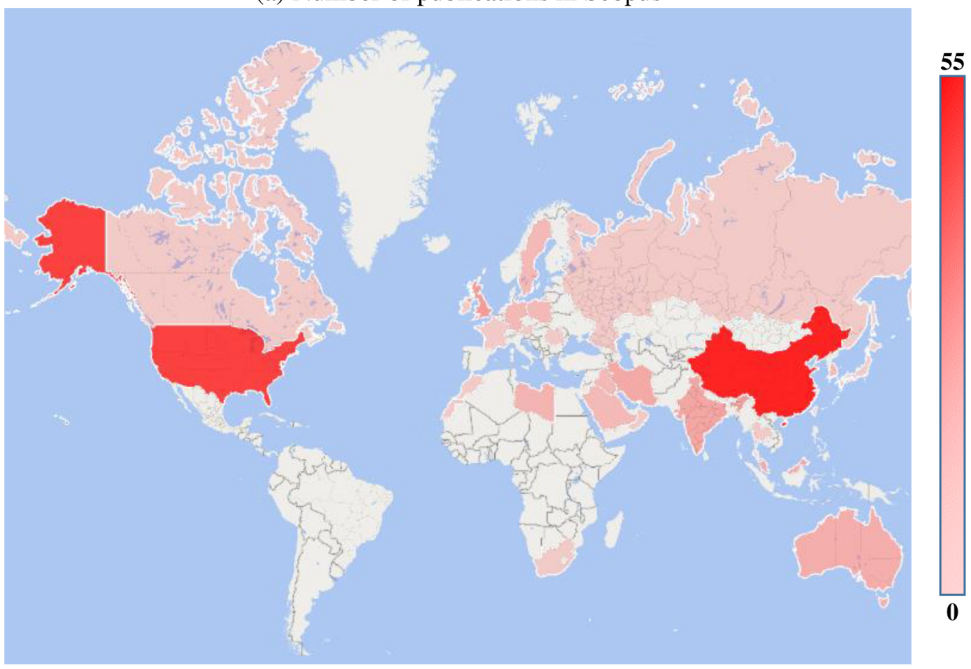

(b) Number of publications in Web of Science

Fig. 4. Geographical representation of the number of publications by country according to (a) Scopus, and (b) Web of Science.

to the topic of interest, followed by a bibliometric analysis of the found references, and finishing with the review of the state of the art.

In this study Elsevier Scopus and Web of Science (WoS) databases were used. The search query was “heat pip*” (the star character allows to search for words derived from “pip” such as pipe, pipes, piping and so on) and the time span considered all documents available in both databases. Initially, this search gave a total of 12712 and 7048 documents in Scopus and Web of Science, respectively. It has to be taken into account that when looking into Scopus database the searched words had to be found within the paper title, keywords or abstract; on the other hand, Web of Science considered the search words as topic. Since the scope of this study is to review the state-of-the-art in those systems which include both heat pipes and TES systems, all these documents are not related with the reviewed topic. Hence, an advanced query was performed. PCM and storage, “phase change material*” and storage, “latent heat storage”, "latent heat thermal energy storage",

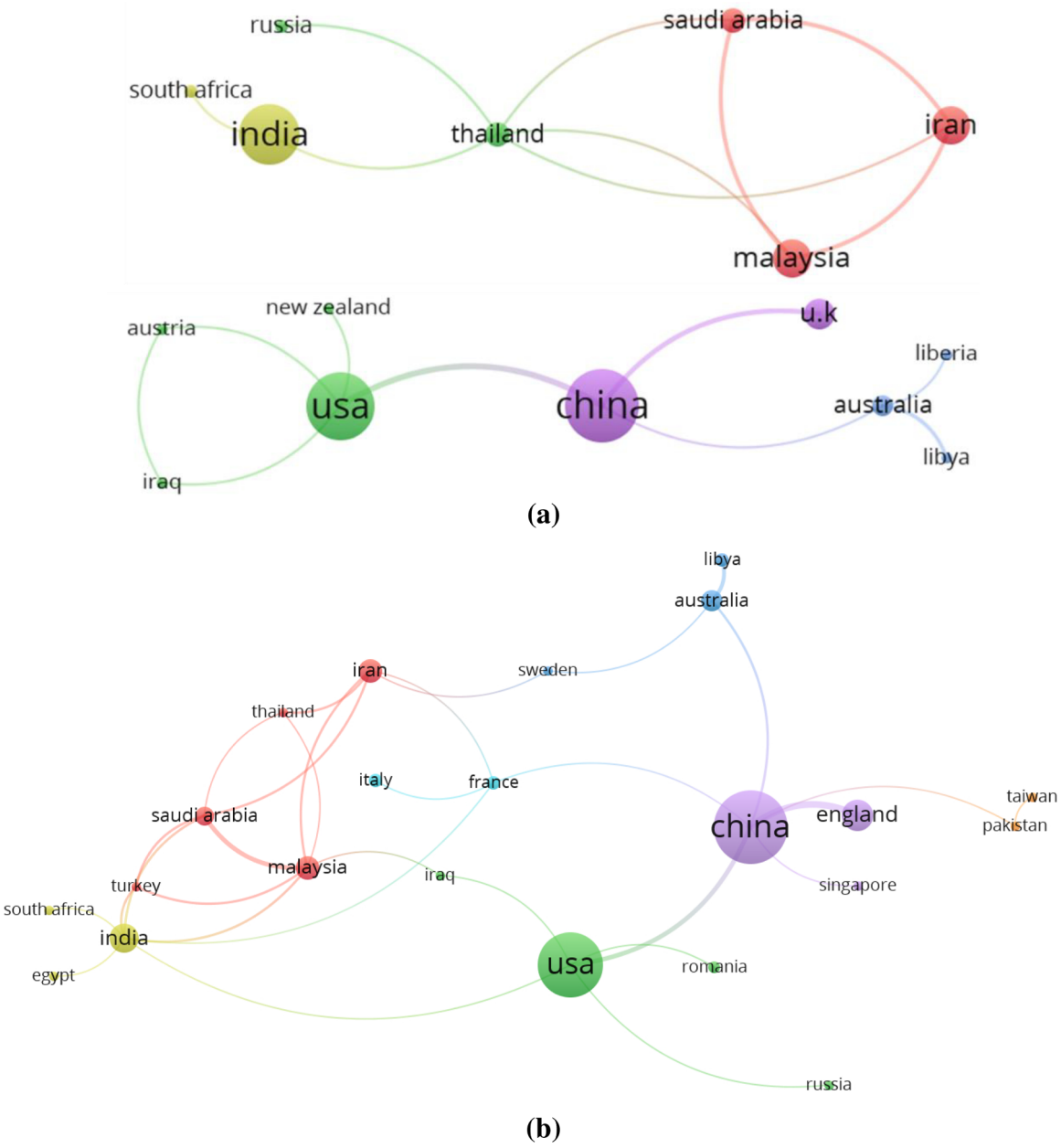

Fig. 5. Cooperation network map by countries or regions according to (a) Scopus, and (b) Web of Science.

LHTES, “latent thermal storage”, allowing in the latter three words between thermal and storage, when using Scopus, it was written as “latent thermal /w3 storage” (Fig. 2). Along the screening process, an exclusion to make was discovered. Because of PCM also stands for phase change memory, regarding a non-volatile RAM memory to store data by changing the state of the material (it changes back and forth between amorphous and crystalline) the word “memory” was added to the query as exclusion. Therefore, on the obtained results, a deeper screening process was carried out to check if all the documents were related with the topic. Finally, 200 and 144 publications from Scopus and WoS focusing in the use of heat pipes coupled with latent TES were identified. Therefore, all the documents were compared to check if both databases retrieved the publications. As a result of this process, 232 publications were identified in one or the other databases.

3. Bibliometric analysis

Prior to analyse every collected document from the query (Fig. 1) a bibliometric analysis of the publications within the reviewed topic was carried out. Providing a global overview of the topic and its tendency along the past years. The analysis was performed for the different results of the two used databases, Scopus (200 documents) and Web of Science or WoS (144 documents).

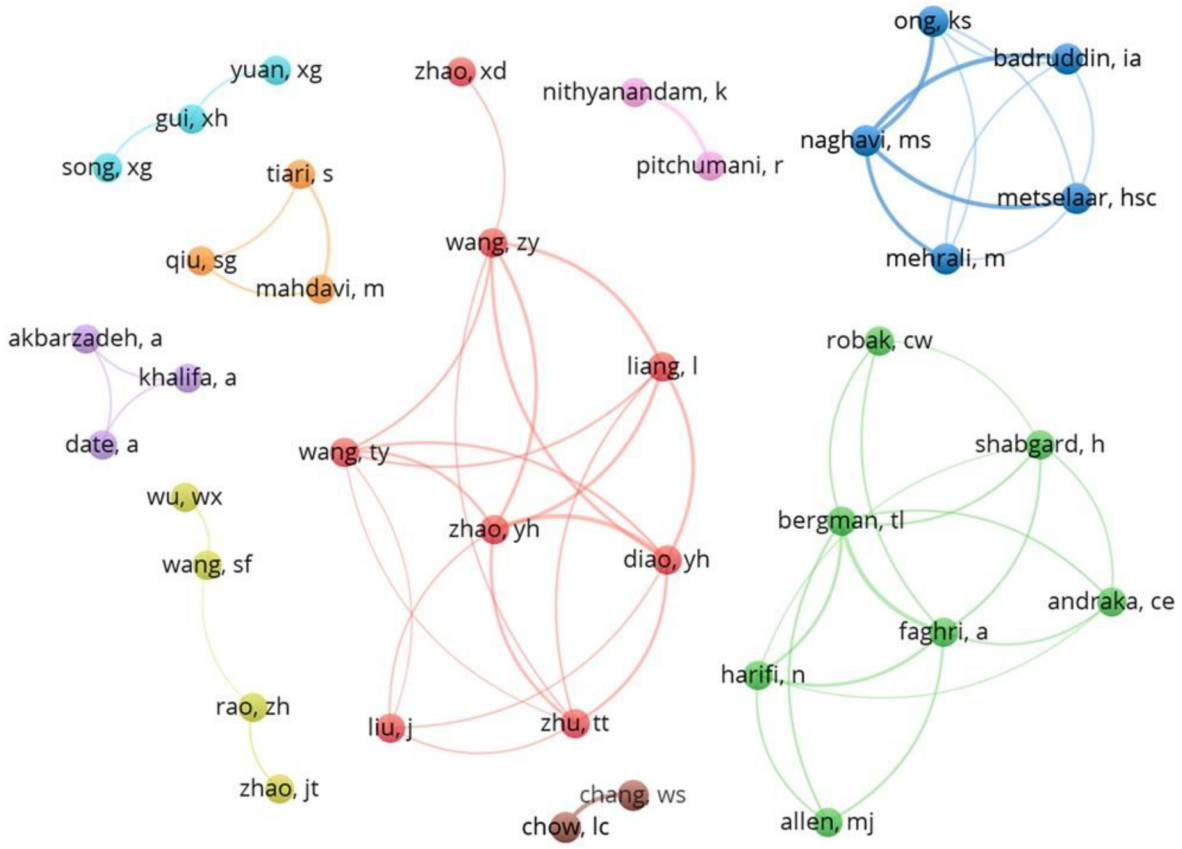

Fig. 6. Co-authorship network on heat pipes and latent TES.

3.1. Yearly distribution and growth trends

The number of publications along time is an indicator of the trends regarding the topic, and it can be seen in Fig. 3, also with the accumulative publication number. The topic got on fashion from 2014, having increased its publications over the last years. After a review of the total documents regarding this topic, it was found that the aforementioned increase was due to the portable computer technology and its necessity of high performance refrigeration in small devices, and the coupling of this hybrid technology with solar energy systems.

3.2. Distribution of publications by country

The 232 retrieved publications on the topic PCM plus heat pipes were distributed along 36 countries, when considering both databases. Analysing Scopus and WoS separately, the studied topic was present in 32 and 29 different countries or regions. Fig. 4 shows a world map, highlighting the countries where at least one document related with the topic was published. Fig. 4a shows the countries which have published some document according to Scopus, in blue colour, and Fig. 4b those which occur just in WoS, in red. By comparing both maps it can be observed that Canada, Oman, Russia, and Sweden were present just in Fig. 4b. Otherwise, Italy, Egypt, Liberia, New Zealand, Pakistan, Turkey, and United Arab Emirates were present just in Scopus database (Fig. 4a). When matching the number of publications per country in both databases, some differences were found for the same country. It can be observed in Fig. 4 that within countries such as Australia, Libya, Iraq, South Korea, Sweden, Canada, Oman, and Russia there is a mismatch in favour to WoS (this mismatch means 10 publications). However, when performing a deeper study on the documents retrieved by Scopus, the total amount of publications was 224 instead of 200, because some documents have more than one affiliation. Also, there are some documents retrieved by Scopus which were conference reviews, those add an extra document to the search but they are not a publication itself (those documents were discarded when performing the review). Additionally, the query in Scopus retrieved 19 publications classify as “undefined” country or region. All in all, the distribution of publications by country, although it is relevant because it shows a global picture of the research topic, it is not 100% accurate. Fig. 4 shows that, between China and USA the majority of the total publications was covered. However, this was because USA and China were the first and the second countries in the rank regarding the global GDP, respectively, and they both had a huge population. Therefore, it did not mean that they are specially focused on this topic.

The cooperation network among the countries was studied by using VOSviewer, it was done separately with data retrieved from Scopus and from WoS. When analysing the data from Scopus, the results showed that there were two groups of countries which work together; the first one gathered China, USA, U.K, Australia, Liberia, Libya, New Zealand, Austria, and Iraq; the second group was formed by Iran, Malaysia, Saudi Arabia, Thailand, Russia, India, and South Africa. Fig. 5a shows the network among the different countries. On the other side, the data from WoS show that all countries were indirectly connected being China and USA the main participants (Fig. 5b). On Fig. 5, the label is sized by the

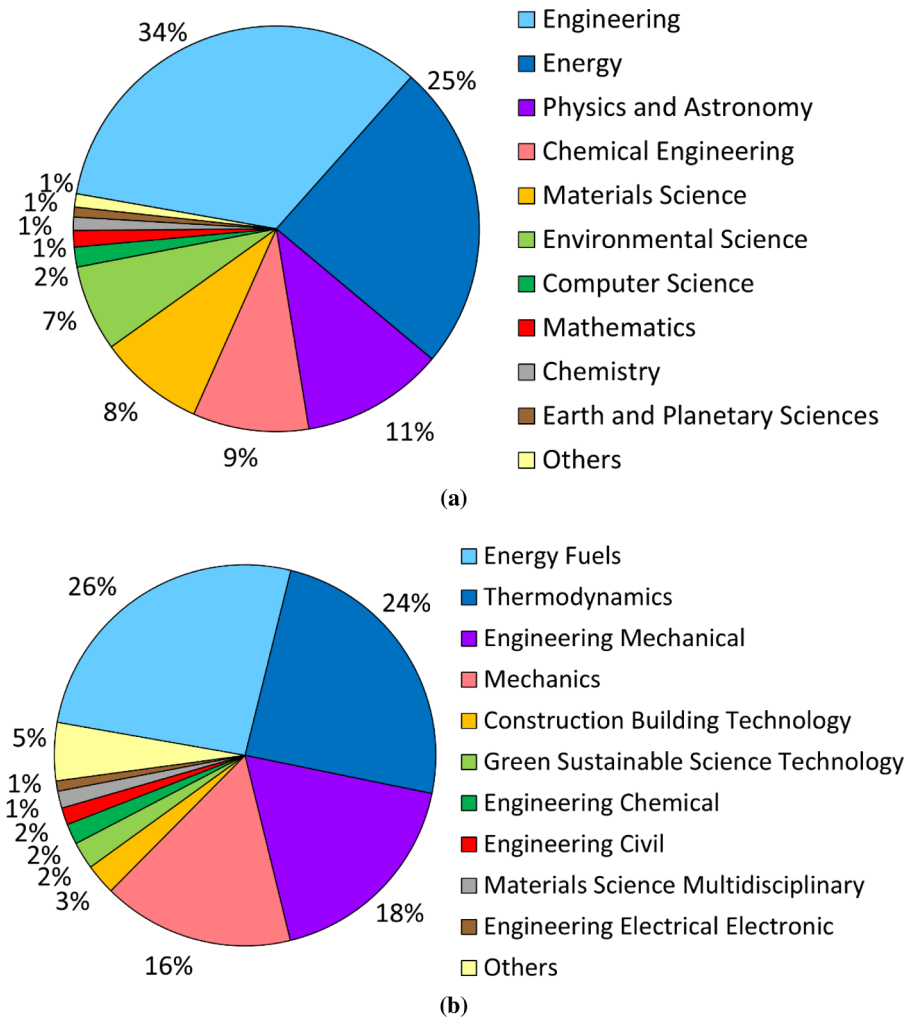

Fig. 7. Documents distribution by subject categories in (a) Scopus, and (b) Web of Science.

number of publications in each country, and the line thickness between nodes represents how strong the cooperation between those countries was. The colours represent the collaboration clusters, which in this case were arranged by countries in direct connection. It has to be pointed out the fact that despite the great amount of publications by China and USA, both countries developed just eight documents with other entities from different regions, four out of those eight were carried out between these two countries.

3.3. Distribution of research institutions

Similarly as the analysis performed regarding the publications by country, the documents by institution were analysed. However, the approach in this case was just to know which institutions were more productive regarding the studied topic. There were 33 universities, higher education, and research institutions which published at least three documents in this topic. From this rank, the top two were the Beijing University of Technology and the Chinese Academy of Sciences, followed by University of Connecticut, and Virginia Polytechnic Institute and State University. Chinese and US institutions were at the top of this research topic, as expected after the analysis by country. Just two USA companies, Advanced Cooling Technologies, Inc. and The Energy Group, were among the institutions with three or more published documents.

3.4. Relationship by authors and co-authorship

The relationship among the different authors who had at least two publications on the topic heat pipe and latent TES topic was mapped (Fig. 6). This mapping analysis allows to identify the most productive authors and their group. This kind of study is useful for future researchers to seek a possible collaboration with others authors. Also, knowing the leading authors on the studied topic gives to future researchers a good starting point when performing the state-of-the-art before carrying out their own research. From the total 200 documents retrieved by Scopus, there were 162 different authors. Out of those, 53 authors contributed just with one document, 59 authors at least with two documents, and 50 authors published three or more documents. The most productive authors, who published 10 documents each, were T. L. Bergman (USA), A. Faghri (USA), L. Liang (China), K. Nithyanandam (USA), and R. Pitchumani (USA). From these five authors, Faghri and Bergman directly collaborated together and Liang was

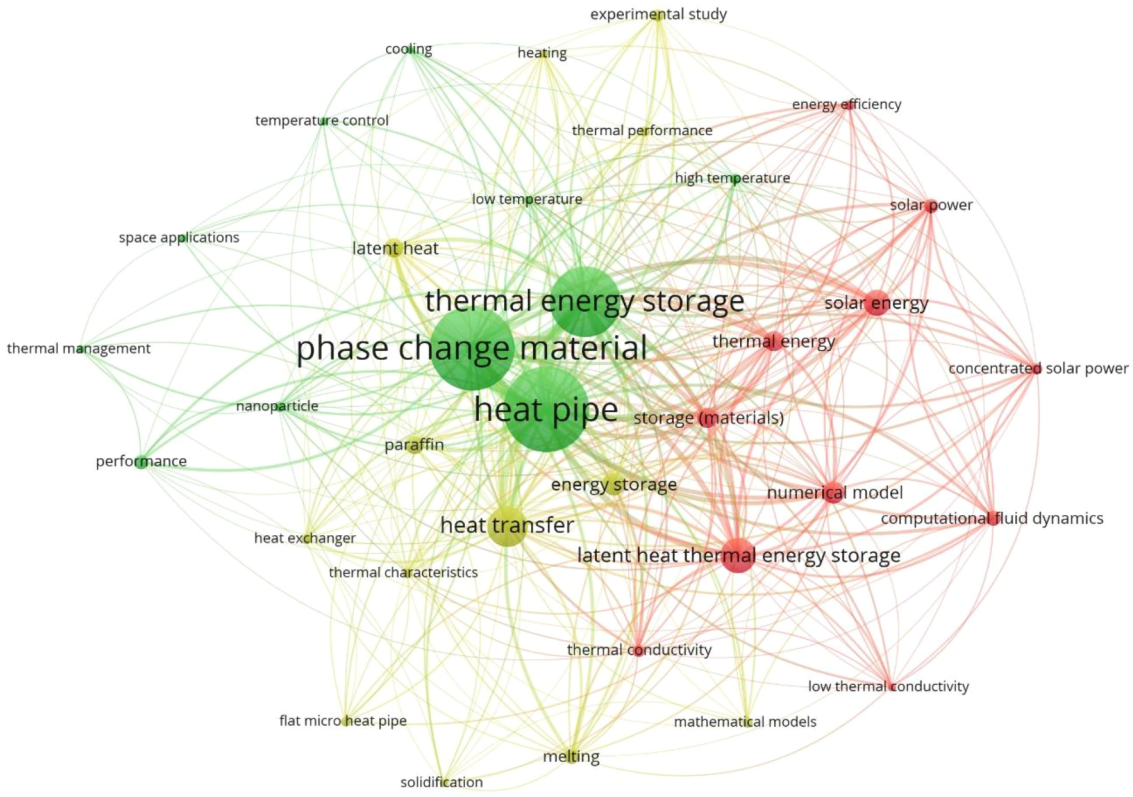

Fig. 8. Keywords co-occurrence related with heat pipes and TES systems.

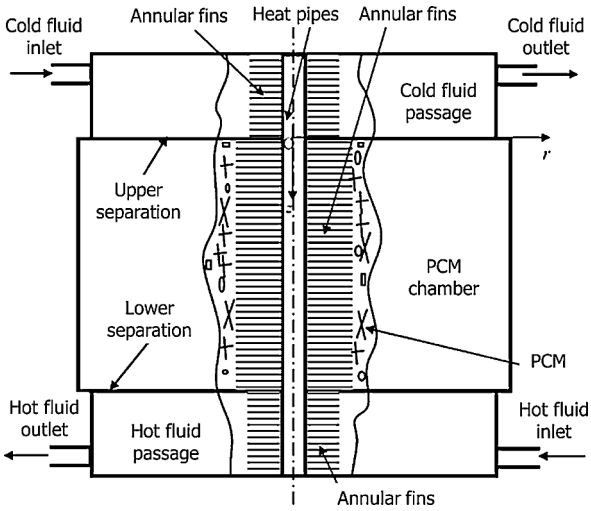

Fig. 9. Liu et al. [14] hybrid heat exchanger design with heat pipes and PCM. Adapted from Liu et al. [14].

indirectly connected with them. However, K. Nithyanandam, and R. Pitchumani had no cooperation at all with others authors. Finally, it has to be taken into account that the most cited author was A. Faghri (291 citations for his most cited paper) followed by Bergman (180 citations for his most cited paper). All in all, the research work developed by these two authors was a good starting point for performing a review on the heat pipes in couple with latent TES topic.

3.5. Distribution of published documents by subject categories

The documents found by both databases were categorized by subject categories to check which was the most common field assigned to them. Fig. 7 shows the documents, in percentage, included in the different areas of knowledge. The categories considered by Scopus and Web of Science were different. According to Scopus, the majority of the documents were published in Engineering and Energy journals, 34% and 25% respectively (Fig. 7a); those areas were the expected ones. However, the third subject is Physics and Astronomy (11%), due to the use of the heat pipes for space applications. When analysing the data from Web of Science, the main areas of knowledge with heat pipes and PCM studies were Energy Fuels (26%), Thermodynamics (24%), and Engineering Mechanical (18%), the three areas were an expected field (Fig. 7b). It has to be taken into account that Web of Science was more specific within the subject categories which it considers. All in all, the documents retrieved for performing the review matched with the desired field of study.

3.6. Document keywords analysis

Finally, by using the aforementioned software tool VOSviewer, the co-occurrence of every document keywords could be spotted (Fig. 8). Fig. 8 shows the keywords used in the published documents, regarding that only the keywords which appear in three or more documents were considered. The circle size gives the times that a keyword has been

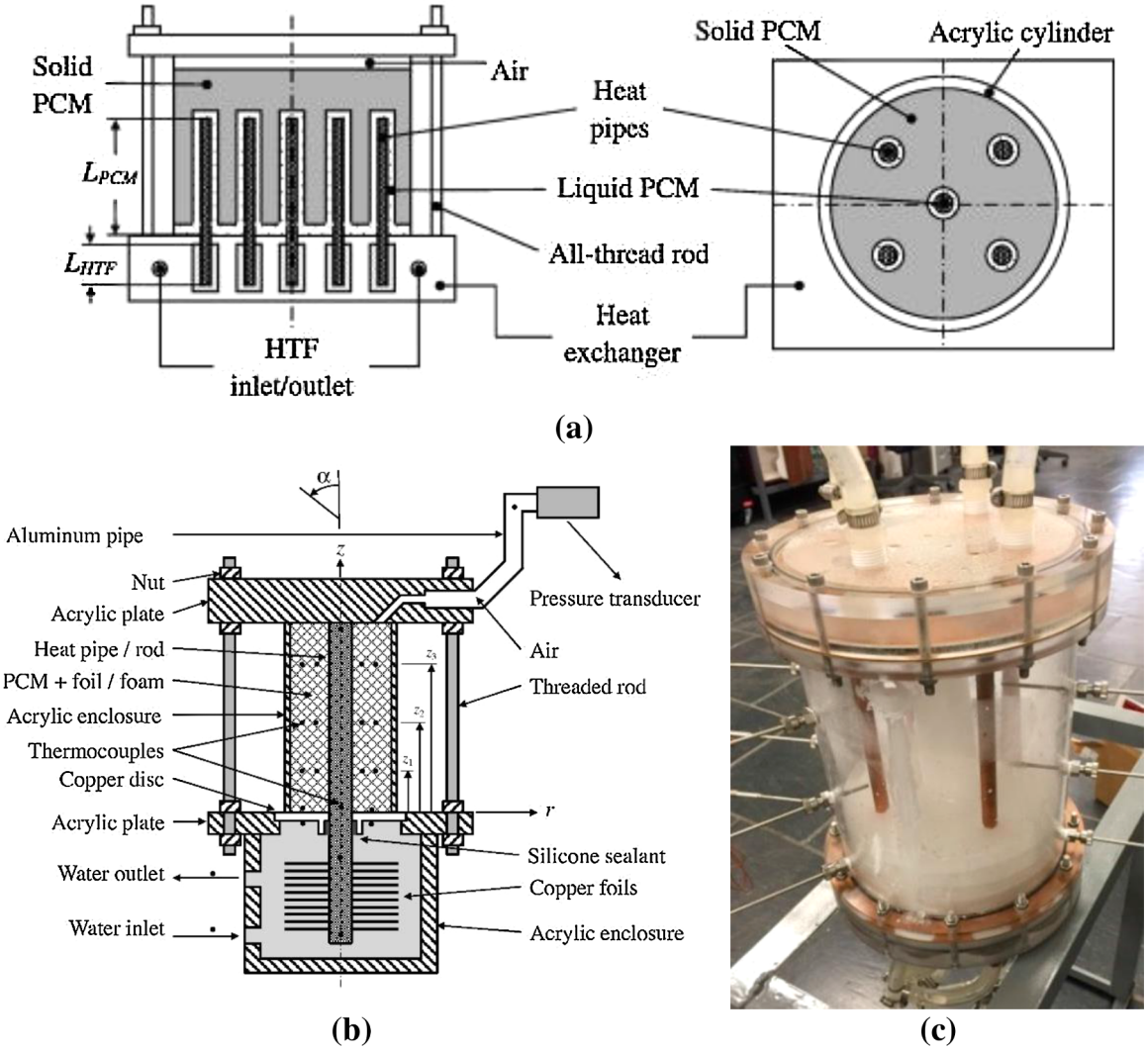

Fig. 10. Faghri et al. [16–19] design for a cylindrical latent TES with (a) several heat pipes and (b) with one heat pipe. (c) Tiari [20] latent TES with simplified heat pipes. Adapted from [16–20].

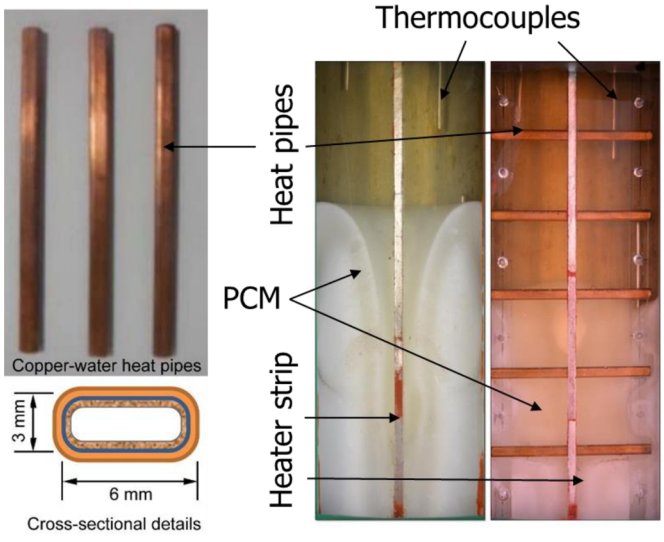

Fig. 11. Saraswat et al. [24] test rig description. Adapted from [24].

used, the links mean that the connected words share publications, the thicker the line is the more documents they appear together. As expected, the spotlight was on “heat pipe”, “phase change material”, “thermal energy storage”, “latent thermal energy storage”, and “heat transfer”. However, Fig. 8 relevance lays in its easiness to spot a non-related keyword. In this case, all keywords shown were connected with the studied topic, so the documents which were considered in this review were relevant at first sight. Some of the applications in which heat pipes and PCM were used can be seen on Fig. 8, such as concentrated solar power, energy efficiency, heat exchangers, cooling, heating, or space applications. The latter confirms Physics and Astronomy appearing as knowledge area in Section 2.5.

4. Review of hybrid systems applications

This section was categorized into three subsections, each of them related to a different temperature range in which the reviewed studies were performed. These subsections were low, medium, and high temperature, considering those below 150 °C, from 150 to 400 °C, and above 400 °C, respectively [11]. Also, the documents reviewed were

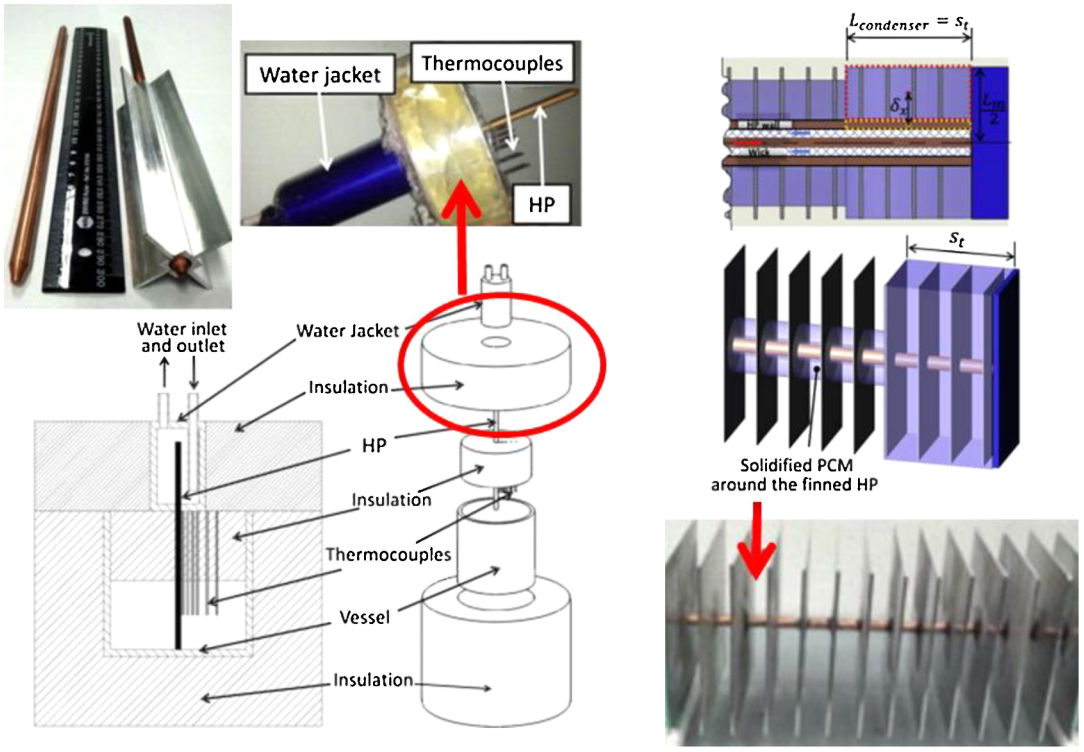

Fig. 12. (a) Khalifa et al. [25] latent TES with bare heat pipe and finned heat pipe. (b) Khalifa et al. [27] TES design for solar power plants thermal storages. Adapted from [25,27].

Table 1
Hybrid system for heat exchanger applications.

Year	PCM	$T_{melting}$ [°C]	Heat pipe	Outcomes	Ref
1978	Paraffin-white $H_{10}Na_2O_8S_2$	48 55	Aluminium (ammonia)	The charging time for a sodiumthiosulphate-pentahydrate TES was 2.6 times longer than paraffin-white, numerically. Paraffin-white was chosen to build the finned heat pipe heat exchanger.	[12]
1984	Myristic acid	53	-	Varying the inlet hot fluid temperature from 63 to 78 °C increased the heat transfer rate from 0.6 to 1.5 kW. Also if the HTF flow rate rose from 100 to 350 l/h, the heat transfer rate was doubled.	[13]
2006	Paraffin wax	52	Copper (acetone)	Increasing (lowering) the inlet hot (cold) fluid temperature from 70 °C to 90 °C (25 °C to 10 °C), shortened charging (discharging) time from 251 to 121 min (155 to 118 min) respectively, being a 52 % time reduction (24%). Same effect was produced by increasing the flow rate from 0.83 to 3.33 kg/min, the melting (solidification) time was reduced by 24% (17.5%).	[14]
2006	Paraffin wax	52	-	When simultaneous charging and discharging happens, the cold water loop took the majority of the heat input, due to the PCM thermal resistance. Therefore, to regulate the energy part store, the heat transfer between the heat pipe and the PCM had to be improved.	[15]
2014	Rubitherm RT82	82	Copper (water)	Numerical and experimental testing of using bare heat pipe or finned heat pipe. The addition of four (five) fins increased the overall effectiveness by around 24% (34%) when comparing with a bare heat pipe. The loss in TES capacity due to fin addition was 0.86% (1.07%).	[25]
2015	Paraffin wax RT60	60	Copper	The model was validated with experimental results and then used to simulate a storage tank at a CSP. The latent TES tank fed a 50 MWe turbine along 9 hours. In comparison with liquid and solid sensible TES, the proposed model required 81% and 51% less materials, respectively.	[27]
2016	Paraffin wax RT60	60	Copper	The numerical and experimental results were compared, showing a mismatch which overestimated the effective thermal conductivity. Three heat pipes volumes fractions were studied (1%, 2% and 3%), effective thermal conductivity gradually increased up to 2% and then ramped up. For simulations at higher temperature (280-390 °C), 10 % of heat pipes volume fraction was used. The improvement was measured in regards to HFT tube length required, being this reduced by 77%.	[28]
2018	Paraffin	52	Copper	Different heat pipe working fluid filling ratios were tested (50%, 25%, 12.5%, and 0%), showing the best results at 25%, regarding the equivalent thermal conductivity (2.05, 4.85, 1.53, and 1.49 W/(m.K)).	[29]
2017	Rubitherm RT3 Rubitherm RT4 Rubitherm RT5	2-5 2-4 1-6	Copper	The average temperature of the food on the self was reduced by 13.7-32%. The temperature was more uniform, reducing its fluctuation in 53.3-83.3%. RT4 showed better results, keeping the food 0.2-0.5 °C below the other PCM.	[31]
2017	Paraffin	60	Copper (water)	A semi cylindrical container, where the heat pipes were attached axially into a strip heater. The melting process time was compared with and without heat pipes, being 5.5 and 12 hours respectively. The vertical thermal gradient was reduced, lowering the effect of natural.	[24]

Table 2
A cylindrical latent TES assisted by heat pipes and its upgrades along the time [16–20].

Year	PCM	$T_{melting}$ [ºC]	Heat pipe	Outcomes								Ref
2011 -2014	N-octadecane ($C_{18}H_{38}$)	27.5	Copper (water)	Enhancement	Porosity	Pore density	Foil number	Melting Time [min]	Effectiveness	Solidification Time [min]	Effectiveness	[16–18]
				Rod	1	-	-	200	1	152	1	
				Heat pipe	1	-	-	126	1.4	102	1.5	
				Heat pipe - Foil	0.957	-	162	13	14.7	11	8.4	
				Heat pipe - Foil	0.987	-	49	31	6.4	21	5.2	
				Heat pipe - Foam	0.948	40	-	29	7.9	25	4.2	
				Heat pipe - Foam	0.949	20	-	29	7.6	23	4.5	
				Heat pipe - Foam	0.943	5	-	29	7.4	24	4.2	
				Heat pipe - Foam	0.870	20	-	21	11.2	14	6.4	
The effectiveness is calculated by comparing the thermal performance to the base case (rod). Heat pipe with 162 foils gave the best effectiveness, 14.7 (8.4) when melting (solidifying), outperforming the heat pipe-foam case which had 11.2 (6.4).												
2015	N-octadecane ($C_{18}H_{38}$)	27.5	Copper (water)	Enhancement	Melting at different orientation angles				Solidification at different orientation angles			[19]
					Time (min)		Effectiveness		Time (min)		Effectiveness	
					0º	90º	0º	90º	0º	90º	0º	90º
				None	136	172	1	1	398	428	1	1
				Foam	106	104	1.3	1.5	112	112	1.7	1.7
				Rod	96	118	2	1.9	102	98	1.9	2
				Heat pipe	78	106	2.2	2.3	84	72	2.3	2.1
				Heat pipe - Foil	16	18	7.2	5.4	13	11	3.7	3.8
				Heat pipe - Foam	34	38	11.9	9.4	26	28	5.7	5.3
The effectiveness was calculated by comparing the thermal performance to the base case. Taking into account that when the orientation angle is 0º (90º), the system was vertical (horizontal); the angle affected significantly the effectiveness of the configurations with heat pipe and foil or foam, and specifically during the melting process.												
2017	Rubitherm RT55	55	Copper (water) + Acrylic (water)	Charging	HTF inlet temperature 63 ˚C, 68.3 ˚C, and 73 ˚C, resulted in a charging time of 16, 10, and 7 hours respectively. Increasing the HTF flow rate 1.89, 3.79, and 7.57 l/min (at 68.3 ˚C) reduced the charging time from 14 to 12 and 10 hours respectively.								[20]
				Discharging	HTF inlet temperature 20 ˚C, 15 ˚C, and 10 ˚C, resulted in a discharging time of 17, 16.7, and 16.7 hours respectively. Increasing the HTF flow rate 1.89, 3.79, and 7.57 l/min (at20 ˚C) reduced the discharging time from 17 to 16.7 and 16 hours respectively.								
2016	N-octadecane ($C_{18}H_{38}$)	28	Copper (water)	The heat pipes into PCM reduced the melting (solidifying) time from 190 (800) to 16 (80) min. Increasing (reducing) the input temperature from 35 ˚C to 50 ˚C (from 15 ˚C to 5 ˚C) reduced the charging (discharging) time by 53% (49%).								[23]

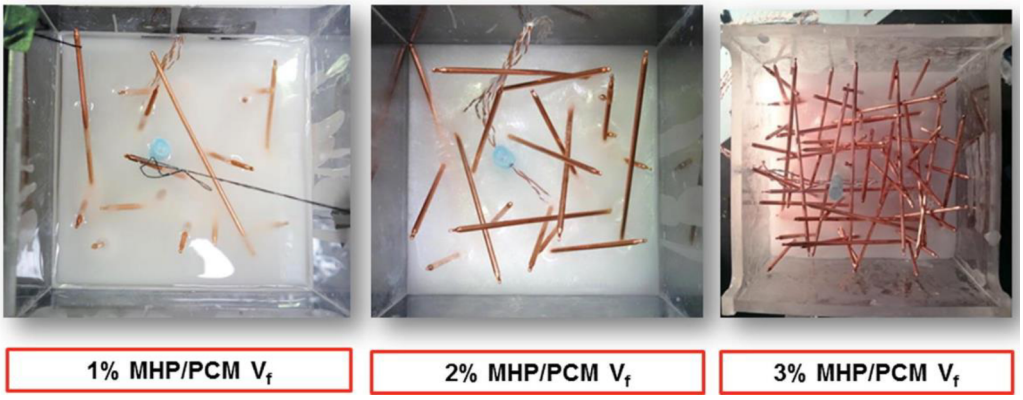

Fig. 13. Khalifa et al. [28] latent TES with heat pipes randomly spread within the PCM.

divided into several groups according to their final application. The main applications, in which this review was classified, were heat exchange, solar, electronics, battery, and spacecraft applications. Finally, they were also classified by the research methodology being experimental studies or numerical modelling.

4.1. Applications at low temperatures

Among all the reviewed experimental documents, the great majority of them were included within this section, hybrid applications at temperatures below 150 ˚C. So further categorization was made, according to the research application. Being those, heat exchangers, solar systems,

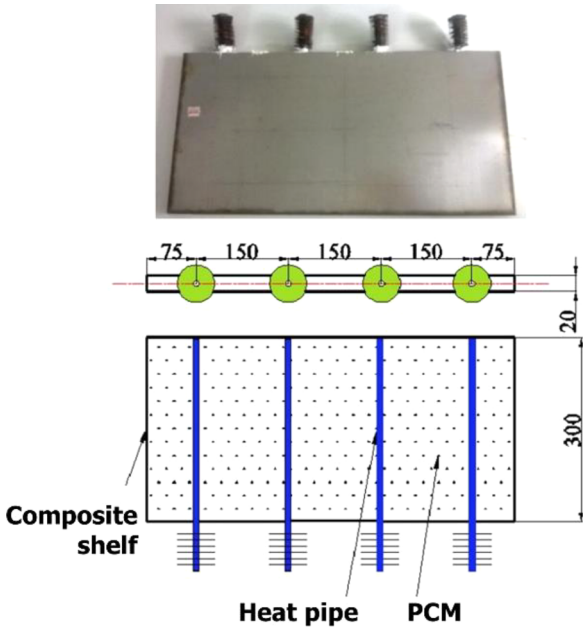

Fig. 14. Wu et al. [31] hybrid shelf design for cooling in vertical open refrigerated display cabinets. Adapted from [31].

cooling in electronics, batteries, and buildings.

4.1.1. Hybrid systems as heat exchangers

Although many of the next designs were thought to work in couple with solar applications, they were heat transfer devices between heat input and a heat sink, making them a proper heat exchanger solution. The first records of a hybrid PCM and heat pipe system to work as a heat exchanger was developed in 1978 by Abhat [12]. A six litres cylindrical glass container with a finned heat pipe in the middle was made with paraffin-white inside as PCM. The heat pipe could transport 100 W at 50 °C. A simple model of the design was developed, and it determined that the PCM used, fin geometry and heat flux input played an important role into the system performance. Following his previous research, Abhat [13] developed a modular finned heat pipe heat exchanger full of fatty acid as PCM (myristic acid). Charging, discharging, and both processes at the same time (By-pass mode) were carried out at different HTF flow rates and temperatures. The advantage of the modular configuration was that heat capacity could be increased and, as it was checked, heat transfer rate kept constant.

An annular finned gravity driven heat pipe heat exchanger with latent TES was designed and developed by Liu et al. [14,15]. There was a hot water loop and a cold one which flowed through the heat pipe evaporator and condenser, respectively (Fig. 9). The apparatus could operate for charging, discharging or simultaneously, making it suitable for weather dependant applications, such as solar thermal energy systems. The water temperature and flow from both loops, determined the operation mode. The influence of several parameters such as hot and cold fluid inlet temperature, fluid flow rate, and PCM initial temperature, was experimentally tested.

A cylindrical latent heat TES coupled with heat pipes was designed and developed by Faghri et al. [16–19] (Fig. 10a and b). They added fins and then heat pipes as heat transfer enhancement method. The use of heat pipes improved the melting ratio over 70% and 50% in regards to the control case and the fin scenario, respectively. When solidifying the PCM, heat pipes almost two-folded the rate over the standard design. The use of foil and foam in couple with a heat pipe was also tested, where the control design was a copper rod with PCM tank. All configurations with heat pipes: just heat pipe, heat pipe plus foil, and heat pipe with foam, enhanced the melting (solidifying) time, by 37% (33%), 93.5% (92.8%), and 89.5% (90.8%) respectively. The effect of foil thickness and foam pore density was found to be insignificant in comparison to the influence of porosity (Table 2). Additionally, six different configurations (heat pipe with foil or foam, just heat pipe, just a copper rod, just foam, and none enhancement) were tested under different inclination angles. As solidification was mainly driven by conduction, the system orientation hardly affected the process. However, the angle influenced the heat pipe performance due to the capillary limit of the wick. Table 2 gives more details about this research. Faghri study was kept on by Tiari et al. [20] who manufactured a design previously modelled [21,22] (see hybrid systems numerical models Section 5.3). The device consists of cylindrical latent TES with a heat pipe network (a primary heat pipe and four secondary ones) embedded in PCM (Fig. 10c). The secondary heat pipes transferred heat excess to the PCM. The heat pipes were simulated by common pipes through where HTF flows. Therefore, the HTF entered through the main acrylic pipe and then the stream split, some runs towards the secondary copper pipes and some flows back to the heater water tank. The influence of HTF flow rate and inlet temperature were assessed. A flow rate increase from 1.89 to 7.57 l/min, reduced the charging process time by 30%. However, this parameter hardly affected the discharging process (mainly driven by heat conduction), when rising the flow rate by 300%, a 6.5% improvement in solidifying time was achieved. Higher inlet HTF temperature (from 63 °C to 73 °C) also accelerated the charging process by 55% (see Table 2). Motahar et al. [23] also designed a cylindrical latent TES assisted with a heat pipe, and like Faghri et al. [16–19] used n-octadecane as PCM. Their goal was to check the effect of input temperature and the use of heat pipes. As expected, higher temperature input (from 35 °C to 50 °C) reduced the charging time (by 53%) and colder temperature (from 15 °C to 5ºC) accelerated the discharging time (by 49%).

A similar design, but semi cylindrical container, was developed by Saraswat et al. [24]. The main difference was that the heat pipes were attached axially into a strip, as seen in Fig. 11. As the strip was connected to a power supply, it worked as a heater. The addition of heat pipes reduced the melting time from 12 to 5.5 hours. Natural convection influence was reduced, since melting was localized at each heat pipe, the vertical thermal gradients were lowered.

Khalifa et al. [25] took a design modelled by Shabgard et al. [26], which is described in hybrid systems numerical models Section 5.2, and used the same approach for the paper numerical part and also to build the prototype. Bare heat pipe and finned heat pipe as heat transfer enhancement were numerically and experimentally tested (Fig. 12a). By adding an aluminium cover with four fins around the heat pipe, the system effectiveness improved by 24%, in regards to the bare heat pipe option. Khalifa et al. [27] followed the same procedure, they modelled, built and experimentally studied a design at low temperature (60 °C) applying later the model to high temperature solar applications (Fig. 12b). More details about Khalifa et al. [27] outcomes are in Table 1. Khalifa et al. [28] repeated the same procedure (numerical and experimental tests) with a different design (Fig. 13). The authors added miniature heat pipes randomly into a square box full of PCM. This configuration improved the heat transfer performance, but random distribution of heat pipes could disappear due to natural convection when the PCM was melted. Then the model was used to simulate a medium/high temperature (280 °C - 390 °C) storage for a concentrated solar power plant. A similar latent TES with heat pipes block was built

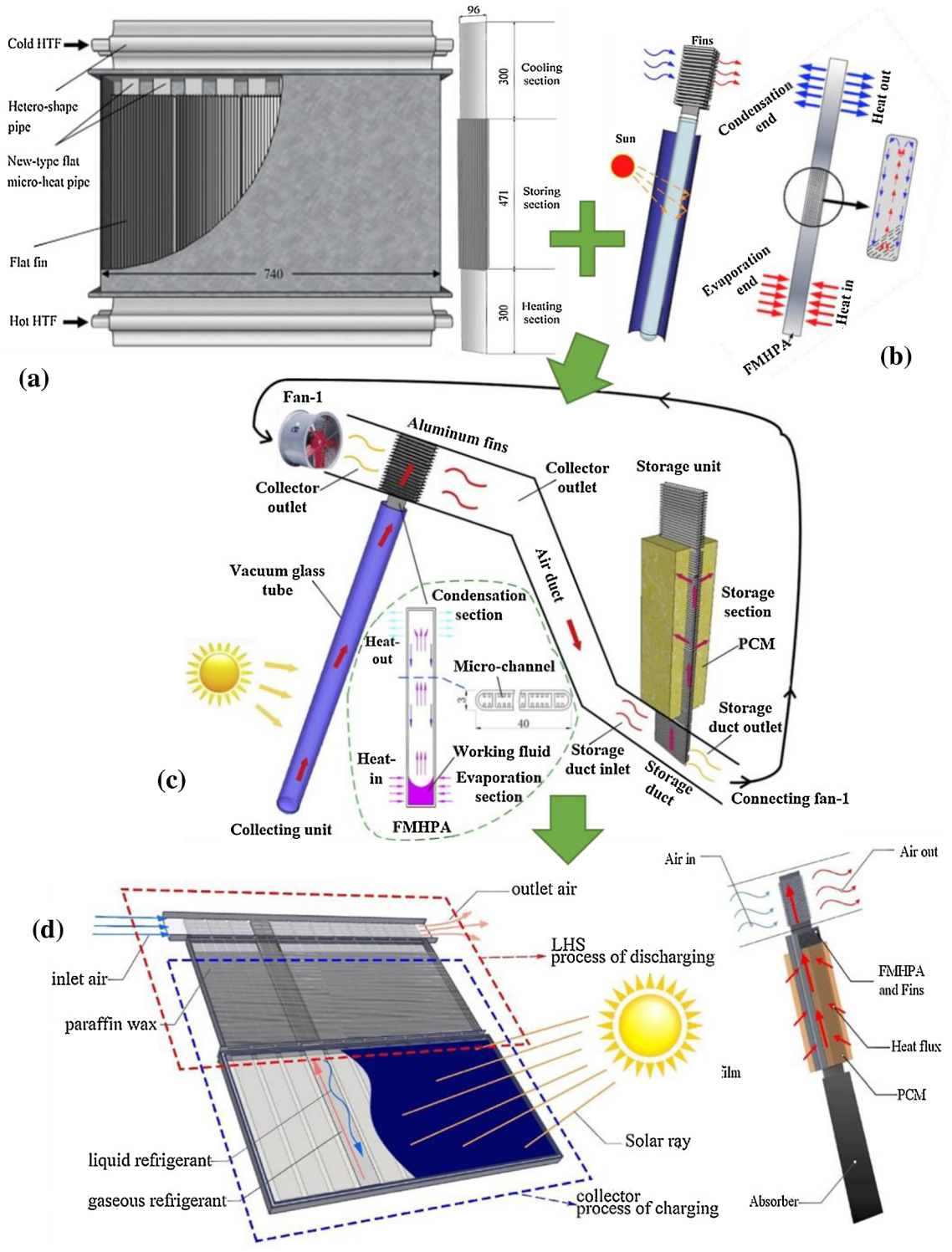

Fig. 15. Diao design along their research, (a) first latent TES system with flat micro heat pipes [33], (b) flat micro heat pipe in couple with a solar collector [44], (c) designs (a) and (b) combined through an air duct [35], (d) upgrade of design (c), the air duct is suppressed [37]. Adapted from Diao et al. [33,35,37,44].

by Weiss et al. [29], where a hot plate transferred the heat towards a cold plate passing through the TES block. Jouhara et al. [30] built a heat exchanger in which the charging channel were made by stainless steel heat pipes. The heat pipes transferred heat from a steam flow. Then cold water flowed through a stainless steel coil inserted into the latent TES tank too. The experiments showed the feasibility of this concept for waste heating recovery.

Among all the experimental studies considered, just one was focused

Table 3
Diao et al. [33–41] studies about flat-micro heat pipes arrays system.

Year	HTF	Heat pipe working fluid	PCM	$T_{melting}$ [ºC]	Outcomes	Ref
2015	Water	Acetone	Paraffin wax	58	At certain working conditions, the charging and discharging took 150 and 115 min, respectively. Being their average thermal power approximately 658 and 894 W, respectively.	[33]
2016	Air	Acetone	Lauric acid	43.5	The TES average thermal power was approximately 447.3 and 376.9 W, for charging and discharging processes, respectively. Rising (lowering) the inlet HTF temperature from 60 °C to 70 °C (25 °C to 15 °C), shortened the melting (solidifying) process about 40% (38%).	[34]
2017	Air	Acetone	Lauric acid	43.5	Different air volume flow rates were tested. At 240 m^3/h the shortest charging and discharging times were achieved, 134 and 153 min respectively. The air side thermal resistance was a key parameter to take into account.	[35]
2017	Water	Acetone	Lauric acid	43.5	Different working conditions were tested, at standard ones (2 l/min as flow rate, hot loop at 70 °C and cold loop at 15 °C) the systems reached 1299 and 1120 thermal W power for charging and discharging, respectively. Also, the system efficiency was 91.9%. The PCM thermal resistance ruled the processes.	[36]
2017	Air	Refrigerant R141b	Paraffin wax	52	The TES systems were integrated into a solar collector for air heating. Charging and discharging power (and efficiency) were 393 (56.6-65.5%) and 344 W (91.6%), respectively. Three air flow volume ratios were tested, 100, 150 and 200 m^3/h, the heat extracted from the device rose by 10% and 26%, respectively.	[37]
2018	Air	-	Paraffin wax	52	A rise on the heating power (from 0.2 to 2.04 kW) reduced the charging time from 806 to 59 min, increasing the efficiency from 71.16 to 96.97%. Higher air flow rate (40 to 120 m^3/h) increased the discharging power from 0.51 to 1.3 kW. If the inlet air temperature was risen from 15 to 24 °C, the discharging process took longer (39 extra min).	[38]
2018	Air	-	Paraffin wax	52	Different influence factors were tested, the heating power, the external temperature, the air flow rate and the HTF inlet temperature. Having the same effect as aforementioned. The outdoor temperature decreased from 35.4 °C to 6.5 °C reducing the charging power by 48.6% (from 531.2 to 272.9 W).	[39]
2019	Water	Acetone	Paraffin wax	52	The effect on the heating power due to variation of ambient temperatures, water flow rates and HTF inlet temperature were analysed. Those parameters had the same effect as seen before. The highest efficiency was 61.5%, the average device power 1323.3 W with 42.1 °C average outlet temperature.	[40]
2019	Air	-	Paraffin wax	52	Simultaneous charging and discharging process of an integrated solar air collector heater was tested. Reaching maximum power of 573.4 W and 4 hour of energy supply when sun was gone.	[41]
Common outcomes	Natural convection played an important role within charging processes. However, its effect was much weaker when discharging, since conduction was the main heat transfer driver. Moreover, the hot/cold HTF temperatures significantly influenced the charging/discharging processes. The increase (reduce) of the hot (cold) HTF temperature resulted in significantly fast melting (solidification), being this influence greater in the hot loop. The hot/cold HTF flow rate also influenced the charging/discharging processes, but this influence was not obvious. Greater heating power, no matter if it was an electrical heater, the solar irradiation or a hot fluid flowing, reduced the charging time.					

Table 4
Hybrid systems in couple with solar panels for solar applications.

Year	PCM	$T_{melting}$ [ºC]	Heat pipe	Outcomes	Filling ratio [%]	Time [min]	Evaporator/ condenser	Time [min]	Heat pipe diameter [mm]	Time [min]	Ref
2017	Paraffin	50	Copper	A 18 mm diameter heat pipe with 80% filling, and 1.1 evaporator/ condenser length ratio was chosen. The comparison against the copper pipe storage tank led to an enhancement of 187% in charging time.	120	120	0.9	105	14	120	[49,50]
					100	120	1	90	16	90	
					80	105	1.1	80	18	85	
2017	Tritriacontane	72	Copper	The solar collector in couple with PCM and heat pipes, improved the efficiency over the standard solar collector on 26% (for normal operation) and 66% (on demand operation).							[50]
	Erythritol	118									
2016 2017	Paraffin	51.24	Copper	The addition of paraffin into the evacuated tube collector increased the total heat obtained from the system by 45%-79%. Then including a parabolic concentrator to the evacuated tubes, the aforementioned heat increased by 8%.							[56,64]
2017	Paraffin	57-57	Cooper Water	The system thermal efficiency varied from sunny days to cloudy-rainy ones, from 38-42% to 34-36%, respectively. The feasibility of this prototype was confirmed and a validated model developed.							[49]
2017	Erythritol	119	-	Expanded graphite was spread into the PCM regarding the mass fraction (0%, 1%, 2%, 3% and 4%). The thermal conductivities of the composite PCM were 0.700, 0.844, 1.264, 2.400 and 2.674 W/(m•K) respectively. Expanded graphite at 3 wt% was selected for the tests.							[54]
2018	Paraffin	40-60	Copper (water)	The system gave back 10401, 8936, and 7082 kJ when the ambient temperature was 18 °C, 25 °C, and 28 °C respectively. The solar collector could achieve 414, 321, and 249 W, respectively. The air flow was kept constant at 6 m/s.							[55]
2016	GR52	52.09	-	Efficiencies	PV/T + heat pipes		PV/T		PV/T + PCM with heat pipes		[58]
					Solar collector	PV					
				Electrical %	-	12.75	4.4	9.4	7.7		
				Thermal %	57.04	-	63.1	41.9	61.1		
				Total %	57.04	12.75	67.5	51.3	68.8		
2019	$CaCl_2$•$6H_2O$	29	Aluminium	The proposed system showed an improvement over a conventional PV/T. An air source heat pump and a solar energy heat pump were compared. The solar collector hosted the latent TES with embedded flat heat pipes. The COP of both systems were 1.88 and 3.23; and their heating capacity were 370 and 740 W, respectively. The latent TES solar collector improved the COP in 72%, and 100% regarding the heating capacity. The water heating time from 15 to 50 °C was shorten 50%.							[56]

in hybrid, heat pipes and PCM, system for refrigeration [31]. Wu et al. [31] developed a shelf for food vertical open refrigerated display cabinets (Fig. 14). The shelf itself was the PCM tank and heat pipes were inserted in it by the evaporator part. Three different PCM were compared against themselves and against a normal shelf. The food average temperature was reduced by 13.7-32%, and the temperature fluctuation decreased by 53.3-83.3% (see Table 1).

4.1.2. Solar applications at low temperatures

Diao et al. [32] designed, manufactured, and patented a flat micro-heat pipe arrays TES unit (Fig. 15a), which was deeply analysed along several experimental [33–41] and numerical [42,43] studies. The latter will be explained in hybrid systems numerical model Section 5. The flat micro-heat pipes evaporator section was in contact with the heat supply, which could be a hot fluid [33–36], an electrical heater [38] or directly a solar collector [37,39–41]. The condenser part of heat pipes was inserted into a cold loop. The heat pipes had fins attached and were embedded into a container with PCM. They used acetone and refrigerant R141b as heat pipe working fluid, and the chosen PCM was paraffin wax (melting temperature 52-53 °C) or lauric acid (melting temperature 43 °C) (Table 3). From the experiments, it was realised that the effect of natural convection played a significant role when melting the PCM. However, natural convection effect was weaker during the discharging process.

Diao et al. [35,37,39–41] combined the previously developed flat micro-heat pipe energy storage device directly (Fig. 15d) and indirectly (Fig. 15c) with a solar collector. The solar collector included another heat pipe module into the absorber panel [44] (Fig. 15b). As in previous experiments the influence of the heating input power (solar irradiance), and HTF volume flow rate was tested. Two studies used the same test rig [36,39], PCM, and working modes (alternative charging and discharging processes) but changing the HTF, being first air [37] and then water [40]. Within both studies the system stored more or less the same energy (around 11 MJ), and the PCM temperature rose up to 60 °C; but the water system achieved it in four hours, unlike the air one which took eight hours. Therefore, the HTF meant a significant power difference, being 1323,3 W the water system and 393 W the air one, when loading.

Ladekar et al. [45,46] also made a prototype with a solar collector in couple with a latent TES with embedded heat pipes, connected by a HTF loop. A latent TES with heat pipes was compared against a latent TES with copper pipes. The heat pipes were optimized by studying the heat pipe working fluid filling, the ratio between evaporator and condenser, and the heat pipe diameter (see Table 4). They achieved a 187% improvement against the copper pipe storage tank, regarding charging and discharging times. Shinde et al. [47] built a similar system, solar collector in couple with latent TES, for solar drying. Faegh and Shafii [48] designed and developed a solar system for drying purposes too. Their systems stored the excessed heat from desalination in the latent TES. When the solar input was gone, the stored heat was transferred back for desalination through the heat pipes.

As Diao et al. did [35], Naghavi et al. [49] also inserted the heat pipes into the evacuated tubes, the condenser section was into the TES module (Fig. 16). However, Naghavi et al. [49] storage was directly connected with the evacuated tubes and the discharging was made by a water pipe loop, unlike Diao et al. [35] which used air. Anyways, in terms of efficiency a comparison can be done since the PCM used is similar. Naghavi et al. [49] prototype reached a thermal efficiency of 38-42% along sunny days, while Diao et al. [35] got up to 53.3%.

Many authors developed solar collectors in which the PCM as well as the heat pipes were inserted into absorber tubes (Fig. 17a), or solar panels. Papadimitratos et al. [50,51] built a solar collector that included the PCM with embedded heat pipes into the absorber tubes (Fig. 17b). They tested the viability of the technology at large scale with two different PCM, tritriacontane (72ºC) and erythritol (118 °C). Same concept was scaled up by Feliński and Sekret [52,53] and, as

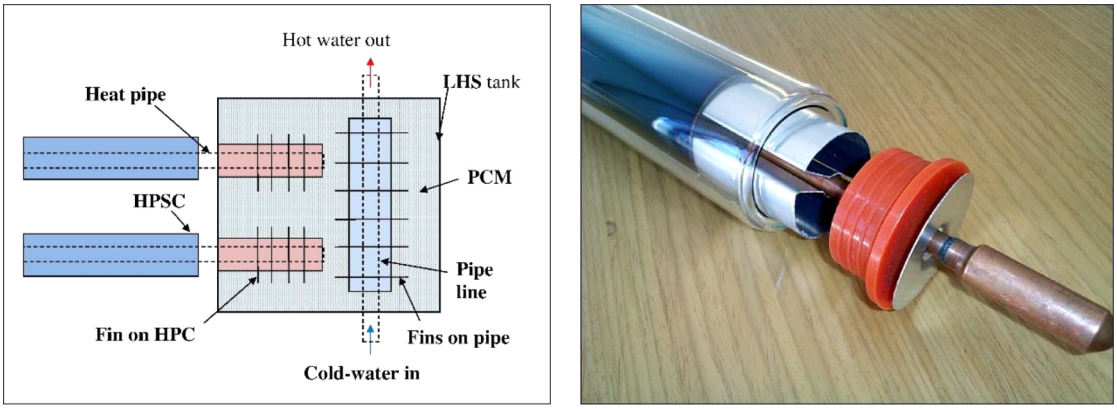

Fig. 16. Naghavi et al. [49] solar evacuated tubes collector with heat pipes and latent TES. (a) Concept design, (b) evacuated tube with a heat pipe inserted. Adapted from [49].

Papadimitratos et al. [50,51], compared it against a solar collector with no PCM, but with heat pipes. They managed to reduce the heat losses, due to temperature difference between the collector and ambient air, by 32% compared with the conventional system. The addition of the PCM achieved to supply 45-79% more useful heat than the normal solar collector. Then they added a compound parabolic concentrator (Fig. 17c) to enhance the thermal efficiency of the prototype. The parabolic concentrator allowed the solar radiation to hit the shaded absorber tube area, increasing the heat stored in the system by 8%. Li et al. [54] also poured erythritol into the evacuated solar tubes (Fig. 17d), but they added expanded graphite for heat transfer enhancement (3 wt%). Compared to pure erythritol, 3 wt% and 97 wt% increased the thermal conductivity by 241.4%. The solar collector showed 40.17% average storage efficiency. Bai et al. [55] built similar concept, assembling a heat pipe into an evacuated solar tube with PCM in it. The heat pipe condenser section was finned, and air flows along them. The system overall solar energy efficiency was 55% (when the solar radiation was 997 W/m^2, average). Wu et al. [56] developed a PCM storage integrated into a solar collector with flat heat pipes too, where water served as HTF (see Table 4 for details). The PCM was within the solar panel part with embedded heat pipes (Fig. 17e and f). Unlike Diao et al. [40], Wu et al. [56] inserted both, the heat pipes and PCM in the solar panel, both solar collectors had same area, but the PCM was difference. When comparing these two studies in terms of power, since the concept is similar, Diao et al. [40] system provided 1323,3W while Wu et al. [56] 740 W. Also, Wu et al. [57] built a solar collector with integrated PCM, but this time the flat heat pipes were replaced by oscillating heat pipes, proving its use as solar energy application for domestic hot water (DHW).

The research carried out by Wang et al. [58] and Modjinou et al. [59] studied the combination of a photovoltaic thermal (PV/T) solar panel with PCM. Wang et al. [58] compared their proposed system with a solar collector, a PV, a conventional PV/T, and a PV/T with heat pipes. Their system succeeded in terms of total efficiency (electrical and thermal) but just by almost 2%. Table 4 shows the details. Modjinou et al. [59] inserted macro-encapsulated PCM, and micro-channel heat pipes within the solar PV/T. Although both technologies were considered within this paper (heat pipes and PCM), they did not work coupled but were compared. Three PV/T panels were built: a conventional PV/T, a PV/T with macro-encapsulated PCM, and a PV/T with micro-channel heat pipes. Their thermal (electrical) efficiencies were 23.9% (7.88%), 28.76% (7.95%), and 27.7% (7.78%), respectively.

4.1.3. Cooling in electronics

Weng et al. [60] developed the same concept (Fig. 18a) as Abhat [13], a heat pipe heat exchanger with PCM (Fig. 18b), for electronics cooling purposes, and compared the use of two storing materials, tricosane, and water, against system without TES material. Usually a computer microprocessor could produce 70-100 W thermal power and reach even 104 °C (at 95 °C the microprocessor integrity is at risk), when in mobiles 45 °C is limit that should be exceed. Comparing the use of tricosane against no PCM at all, tricosane reduced the fan energy demand by 46%, keeping the heater 12.3 °C lower. Same design and PCM but with the addition of Al_2O_3 was tested by Krishna et al. [61,62]. An air fan refrigerated the heat pipe condenser section. The PCM module automatically managed the heat transfer rate, regarding the PCM mass, fan voltage, and heater temperature. The heater could be an electronic device which needed to be cooled such as a processing unit. Both research managed to reduce the evaporator section temperature, and up to 53% of fan power consumption (Table 5).

Similar set-up was used by Chougule and Sahu [63,64] (Fig. 18c). They tested several heat pipe working fluids, water and nanofluid (water with carbon nanotube), and also different energy storage materials; water (sensible range), paraffin, and paraffin with carbon nanotubes (CNT). When comparing water and PCM as storing option, PCM stored more energy at each heat pipe configuration. The heat pipe charged with nanofluid enhanced the module performance, but when the carbon nanotubes concentration exceeded 2 wt.%, the performance decreased. Combining the PCM and CNT (2 wt.%) charged heat pipe, the system saved 66% of heating power, reducing the voltage and consumption of the refrigeration fan. For that reason, Chougule and Sahu [64] took 2 wt.% carbon nanotubes as heat pipe working fluid for their next study where they analysed paraffin with carbon nanotubes as PCM. Also, paraffin with carbon nanotubes as TES performed better than just paraffin, and the latter better than water (Table 5). Paraffin was also chosen by Zhuang et al. [65] who developed a similar design but the PCM container was a cylinder this time. Different paraffin filling ratio were studied, when 75% of the chamber was full of PCM, the temperature dropped by 9.31% compared to no PCM at all. As shown on the aforementioned documents, the cooling power was decreased

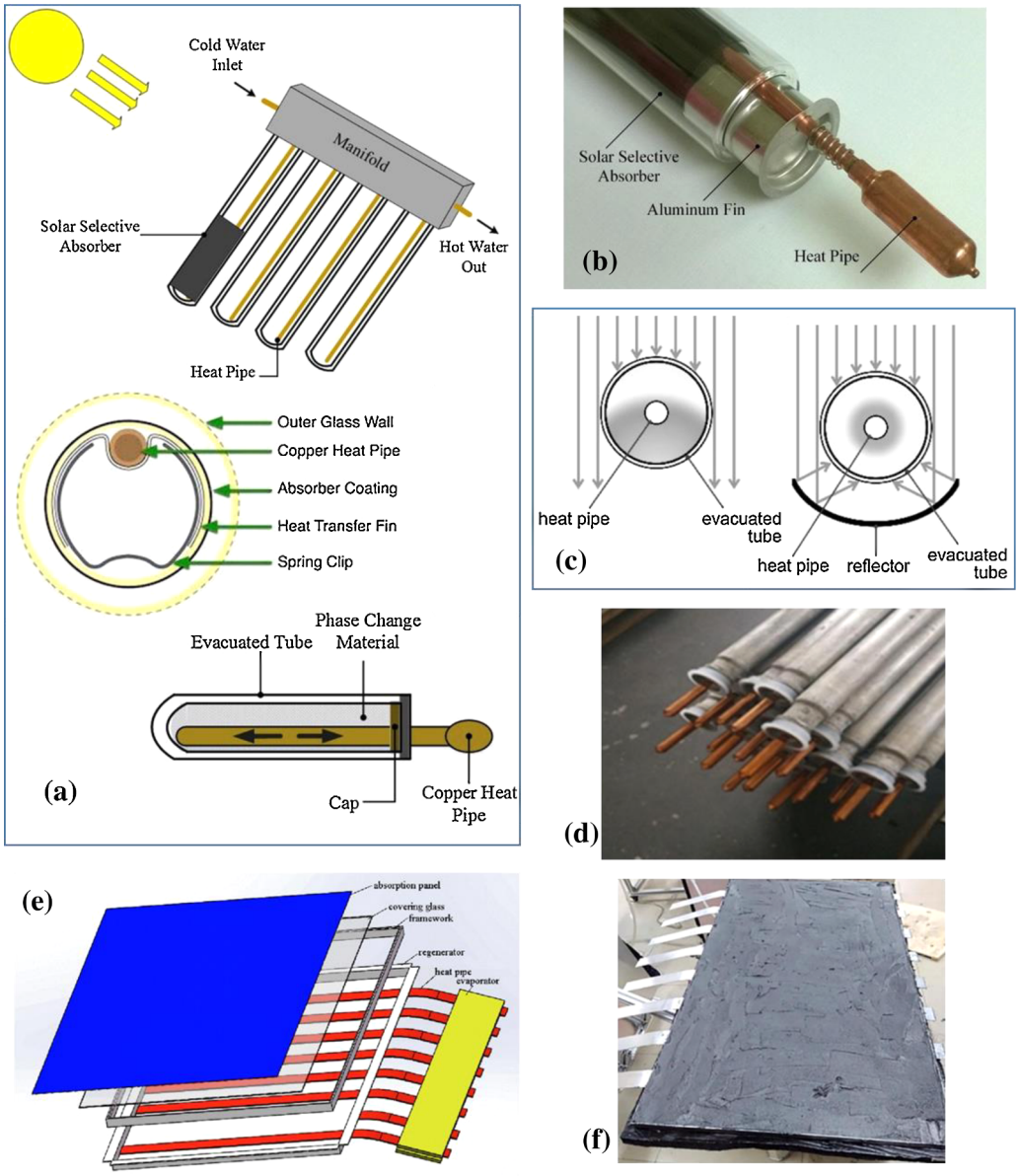

Fig. 17. Solar collectors with heat pipes and PCM into the evacuated tubes or panel. (a) Evacuated tubes concept [50], (b) Papadimitratos et al. [50] evacuated tube with PCM, (c) Feliński and Sekret [53] addition of a parabolic concentrator, (d) Li et al. [54] manufactured solar tube with heat pipes and erythritol. (e) Solar panel concept [56], (f) Wu et al. [56] solar panel with PCM and expanded graphite. Adapted from [50,53,54,56].

because of the PCM storage (see Table 8 for details), also temperature shocks were avoided, protecting the attached device. Wu et al. [66] used the PCM and heat pipe combination for cooling high-power LEDs, they compared the use of air, water and PCM as heat sink. PCM heat sink kept the high-power LEDs temperature below 75 °C (critical operation temperature) longer than 100 min, when water reached 60 min and air heat sink hold for less than 30 min.

The heat pipe with PCM for cooling electronic devices concept was scaled up by Yang et al. [67]. The heater (the electronic heated part) was located below a cooling block were 20 heat pipes (10 per side) were connected. The heat pipe condenser part was embedded into a PCM container (Fig. 18f). The thermal behaviour of a low melting point metal (E-BiInSn) and octadecanol as PCM was studied under different thermal inputs (from 200 to 1000W). The metal PCM could keep the cooling block below 100 °C between 1.4 and 2.4 times longer than octadecanol (Table 5). Li et al. [68] also chose a liquid-metal PCM as storing material, in couple with a flat heat pipe to refrigerate high power portable electronic devices. They compared the use of liquid-metal PCM, flat heat pipes, and the combination of both, to keep the surface temperature below 45 °C (temperature considered uncomfortable for the user). The hybrid prototype proved its value to thermal manage high power portable electronics, since kept it lower than 45 °C for around 3600 seconds, the other options failed at 600 seconds (just PCM) and at 1200 seconds (just flat heat pipes).

Hybrid prototype was also used to refrigerate the electronics components of a downhole well drill [69]. Keeping the electronic

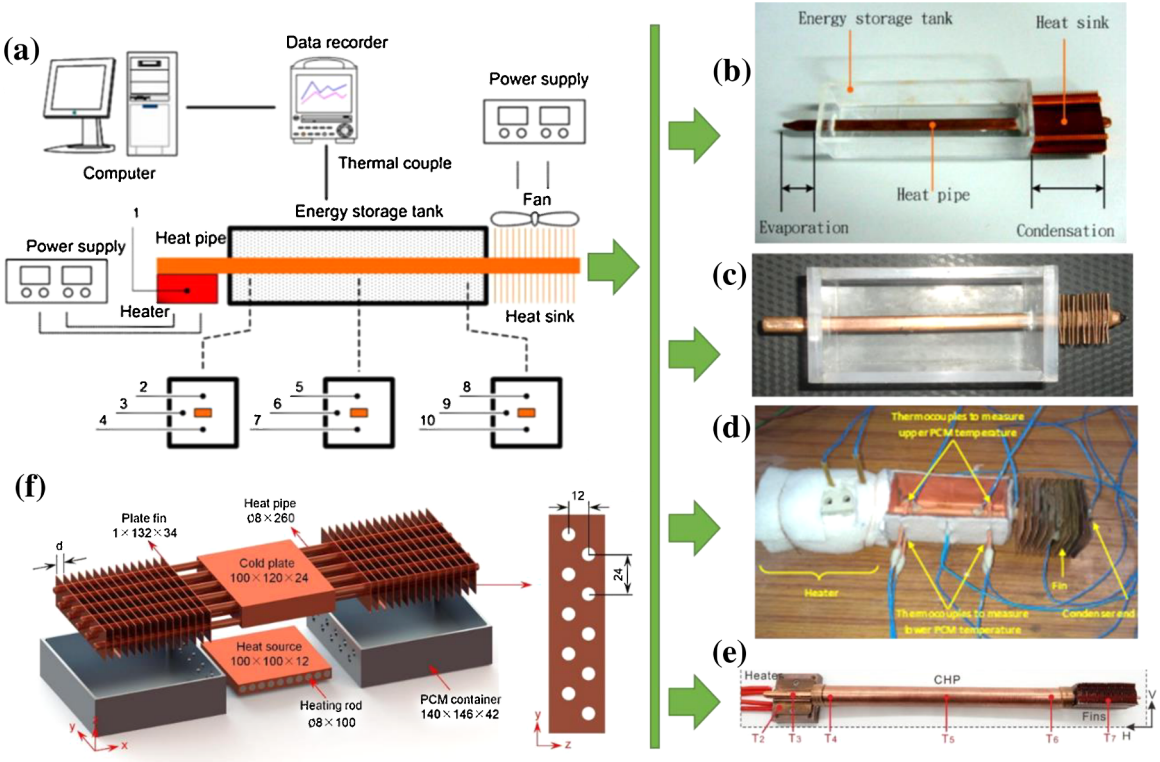

Fig. 18. Heat pipe with latent TES cooling device (a) concept [60], (b) Weng et al. set up [60], (c) Krishna et al. test rig [61], (d) Chougule and Sahu system [63], (e) Zhuang et al. cylindrical PCM container configuration [65], (f) Yang et al. cooling application design [67]. Adapted from [60,61,63–65,67,72].

equipment cooler than 125 ˚C for six working hours at 200 ˚C. Behi et al. [70] slightly changed the design by using water as refrigeration fluid at the heat pipe condenser section, but keeping the concept. All experiments were perfumed with the same PCM (Rubitherm RT42) and applying different heat input powers. Tso et al. [71] built a cooling unit consisting in an aluminium block with PCM, connected to a mobile battery and chip, which was the heat source. They checked the improvement due to the heat pipe by comparing it with a copper rod. They realised that the heat pipe, with an effective thermal conductivity of 10.000 W/(m•K), and the copper rod (400 W/(m•K)), performed similarly. Concluding that the heat pipe either malfunctioned or was not properly chosen.

4.1.4. Electric batteries applications

In 2013 Rao et al. [73] started coupling heat pipes with electric vehicle batteries to manage them thermally. In 2014, Rao et al. [74] took the oscillating heat pipe designed by Akachi [9] in the middle 1990s to replace the cylindrical heat pipes of his previous design and finally in 2016 they coupled their design with a PCM storage [75,76]. The battery cell, and heating input, was experimentally simulated as an aluminium block, with the PCM inside (Fig. 19a). Different number of turns in the oscillating heat pipe were tested, heating powers (from 10 to 80 W), and heat pipe orientations (see Table 6 for details). The heating power and the cold loop worked at the same time, making the PCM a “shock absorber” taking the extra heat that the refrigeration loop could not remove. It was observed that while the oscillation in the heat pipe worked and was stable the system kept the temperature. However, the PCM thermal conductivity and the heat pipe heat transfer ratio limited the heating power threshold which could be maintained. The number affected the start-up temperature of the heat pipe and the close loop oscillating heat pipe stability (less turns made it unstable). When comparing the results with previous research [77], they concluded that the addition of PCM made the system more efficient in cooling. The maximum temperature reached was higher if the module was horizontal then when it was vertical at the same power. Gravity had a great influence backing the heat pipe flow. Then the system was slightly modified, the PCM was installed between a heating aluminium block and a water-cooled block (Fig. 19d), also expanded graphite was added to paraffin wax [78,79]. The inclination was again tested, resulting that when the angle was larger than 30º its influence was negligible. While charging, the average PCM temperature rose faster if expanded graphite was added to paraffin. Also, the discharging process took about half the time when expanded graphite was used (Table 6). This set-up kept being improved and tested with different heat pipe working fluids (water, ethanol and a self-rewetting fluid), heat loads, and filling ratios [79,80]. The working fluids were compared regarding their thermal resistance, concluding that for high heat flux applications, self-rewetting fluid was better (Table 6 shows more details). Thermal efficiency increased as the heat power input did but it remained stable at high heat load. The oscillating heat pipe can hold larger heating power if the filling ratio was greater than 30% (from 40 to 80%). Their last research with oscillating heat pipes consisted in tested the use of a 3D-oscillating heat pipe (Fig. 19d) versus several 2D-oscillating heat pipes (Fig. 19e), within the same volume [81]. They concluded that the use of several layers of 2D-oscillating reduced the solidification time about 48% while the 3D-oscillating heat pipe 29%, in regards to the just paraffin case. From their previous research with cylindrical heat pipes [73] and their expertise with heat pipes and paraffin with expanded graphite, in 2017

Table 5
Hybrid systems for electronics apparatus.

Year	PCM	$T_{melting}$ [ºC]	Outcomes	Ref
2011	Tricosane	48	Heater temperature [ºC] at different cooling options Material used: No material / Water / Tricosane Lowest [ºC]: 64.3 / 60.5 / 55.5 Highest [ºC]: 85.3 / 79 / 69 To keep the same heater temperature, water option required 1.12 W fan power, unlike tricosane case that needed 0.6 W. The use of tricosane reduced the fan energy consumption up to 46% and kept the heater at 12.3ºC lower than if no PCM were used.	[60]
2017	Tricosane	47	Al_2O_3 nanoparticles was dispersed among the PCM at different volume ratios (0, 0.5, 1, and 2 %). Al_2O_3 in 1% volume showed the best results, reducing the evaporator temperature about 25.75 %. Saving 53 % of the fan power consumption.	[61]
2015, 2018	Paraffin	65	The use of nanofluid with 2 wt% of carbon nanotubes as working fluid improved the thermal performance, as well as, the addition of carbon nanotubes (at 3 wt %) into the PCM. Time required to reach 80 °C in the TES part per storage material Heat pipe working fluid: None / Water / Paraffin with carbon nanotubes (0 wt% / 1 wt% / 2 wt% / 3 wt%) Water: 460 / 2600 / 1000 / 970 / 940 / 900 Nanofluid 1 wt%: 390 / 2300 / 850 / - / - / - Nanofluid 2 wt%: 250 / 2000 / 750 / 720 / 700 / 630 Nanofluid 3 wt%: 325 / 2200 / 800 / - / - / -	[67,68]
2019	Paraffin	55	Several PCM filling ratio in the container were tested (0%, 25%, 50%, and 75%); as well as, different heat inputs (10, 15, and 20 W), and various wind speed within the refrigerator fan (0.5, 1, 1.5, 2, 2.5, and 3 m/s). Higher PCM ratio kept the temperature lower than other case. When wind speed was 3 m/s there were no phase change.	[65]
2016	Paraffin	52	The PCM/heat pipe as refrigeration system for high-power LEDs, showed a temperature reduction on the device of 16 and 32 °C in comparison with water or air base refrigerators respectively (heat input 30W).	[66]
2018	Octadecanol	55.6	The low melting point metal showed better performance when thermal shocks were applied to the cooling device. Time required to reach 100 °C at the cooling block [minutes] TES material / Heating power input [W]: 200 / 400 / 600 / 800 / 1000 None: 24 / 8.7 / 5.6 / 4.4 / 3.6 Octadecanol: 64.5 / 21 / 10.5 / 6.5 / 4.5 (E-BiInSn): 88.7 / 32 / 19.4 / 14 / 9.3	[67]
	$Bi_{31.6}In_{48.8}Sn_{19.6}$ (E-BiInSn)	60.2		
2016	Liquid-metal gallium	30	A flat heat pipe with liquid-metal as PCM kept the electronics surface temperature below 45 °C for 3500 seconds (at 3.65 W) and for 600 seconds (at 7.25 W) approximately.	[68]
2017	Eutectic salts	61.1	The PCM reduced the electronics temperature from 154 °C to 124 °C. The use of heat pipes reduced the temperature difference between the electronics and the PCM from 17.5 °C to 5.5 °C.	[69]
2017	Rubitherm RT42	38-43	The heat pipe in couple with PCM supplied the 86.7% of the cooling requirements when the input was from 50 to 80 W.	[70]
2015	N-eicosane	36.5	The PCM kept the mobile chip 20 °C cooler than a non-PCM cooling unit. From the PCM finned container performed better,	[71]

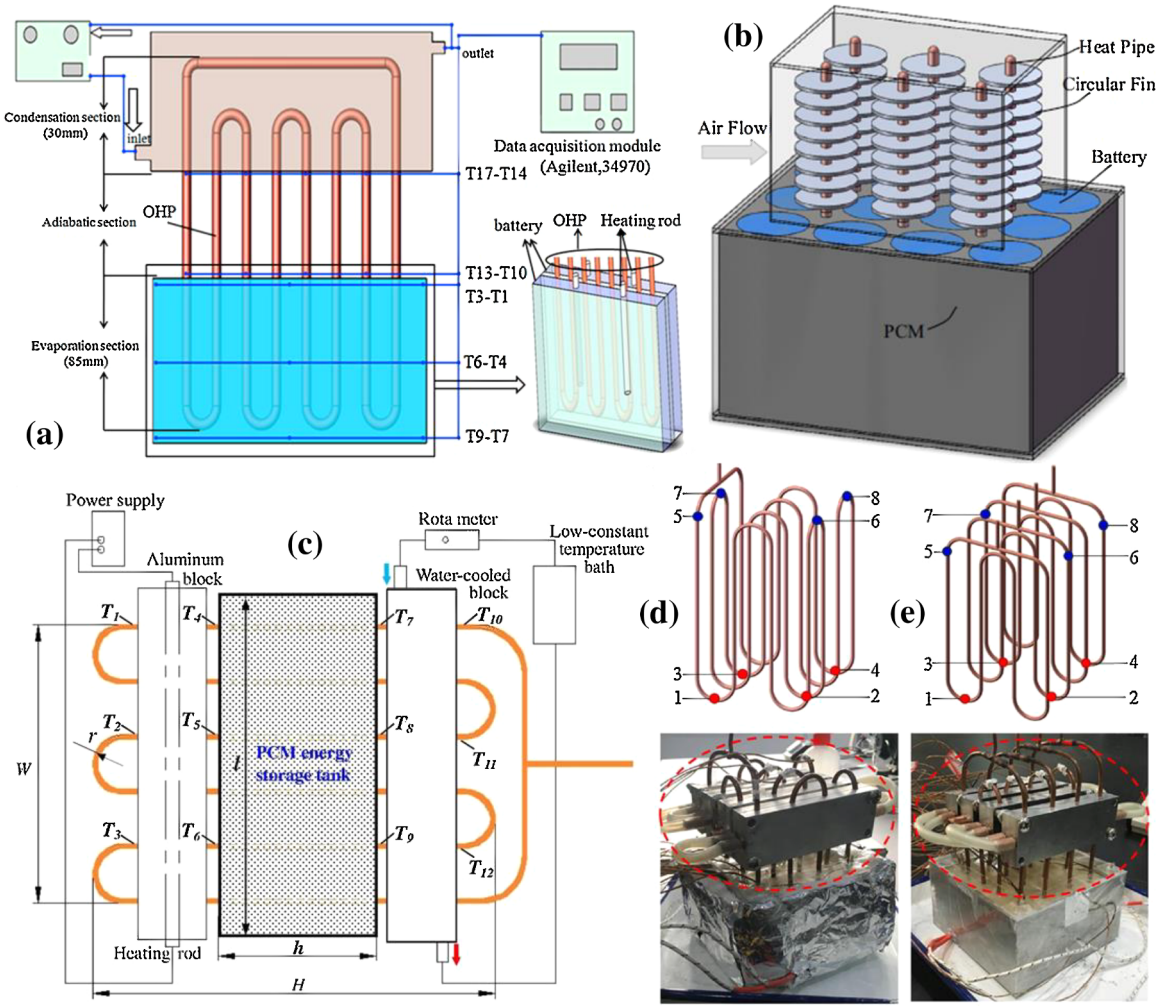

Fig. 19. Rao design along their research, (a) battery with latent TES system and oscillating heat pipes, (b) power battery embedded into a PCM block with finned heat pipes, (c) modification of design (a) to host the TES in between heating and cooling section, (d) 3D-oscillating heat pipe design, (e) four layers of 2D-oscillating heat pipe. Adapted from Rao et al. [75,76,78–82].

Rao et al. designed and manufactured a battery substitute (Fig. 19b) [82]. The PCM block hosted the battery cylindrical blocks as well as the heat pipes (the evaporator section); around the finned heat pipe condenser air flowed. They compared the use of PCM with and without heat pipes against the battery just refrigerated by air flow. The hybrid solution performed better, being able to control the maximum temperature below 50 °C longer than the other options. The temperature difference between maximum and minimum temperature in the battery was reduced by 33.6% by adding PCM and 62.5% when heat pipes were included. So, temperature along the power battery was more uniform. Huang et al. [83] designed a similar battery pack, a PCM block hosted the cylindrical batteries, but the block was split in cell modules. Between the cell modules, flat heat pipes were placed. They compared three systems, just PCM, PCM with heat pipes and air cooled, and PCM with heat pipes and water cooled, (Table 7 shares the details). Same concept but now pouring the PCM into the cylinder inner part was developed by Gou et al. [84]. A comparison among, natural convection cooling, PCM internal cooling, and PCM and heat pipe cooling battery was made; being the latter, the one that showed the best results.

In parallel, and from Rao [73] first research coupling heat pipes and PCM, Yamada et al. [85] developed a cooling system also for electric vehicles batteries. As Rao, they built simulated battery cells, and between them PCM with embedded heat pipes was placed (Fig. 20). They tested four systems: just battery cells, four batteries with PCM, four cells with heat pipe, and the batteries with PCM plus heat pipes. They achieved to keep the battery temperature below 100 °C for 30 minutes. The system could maintain the battery temperature below 50 °C. Table 7 shares more details about Yamada et al. [85] research. Wu et al. [86] and Zhang et al. [87] also designed a cooling device with PCM and heat pipes for electrical batteries. A block with a mixture of paraffin with expanded graphite, hosted the heat pipes evaporator section, and was in contact with the battery cell. The addition of expanded graphite had a significant effect on the device.

4.1.5. *Hybrid system for cooling in buildings*

In 2000, Turnpenny, Etheridge and Reay [88,89] designed, developed, and tested, numerically and experimentally, a ventilation system to reduce energy consumption for space cooling in buildings. The system used the night-time for freezing the PCM, then the hot day-time air was forced to flow through the storing device to cool it. In this

Table 6
Rao et al. studies of coupling heat pipes with PCM storage for thermal managing electric vehicles batteries.

Year	PCM	$T_{melting}$ [ºC]	Outcomes												Ref
2016	Paraffin	64	Time needed to enter the phase change temperature [seconds]												[75,76]
			Configuration	Heating power [W]							Cooling				
				10		20		40							
			PCM	3333		1333		635			3111				
			PCM/heat pipes	5174		1587		730			1334				
2016	Paraffin	41	Time that the battery surrogate was below 50 ˚C [seconds]												
			Heat input [W]	Air cooled	Heat pipe cooled				Heat pipes/PCM cooled						
				20	Horizontal	Vertical			45º tilted		Vertical				
			20	359	565	637			1075		1162				
			30	206	296	317			491		511				
Using heat pipes implied a better refrigeration. The PCM reached the melting temperature later and when the heat input was gone it solidified faster. The hybrid design extended the time the battery was below 50 ˚C longer than just oscillating heat pipe.															
2018, 2017	Paraffin	40	Heat input [W]	Thermal resistance (ºC/W)					Effective thermal conductivity [W/(m•ºC)]						[79,80]
				Water	Ethanol	Self-rewetting fluid			Self-rewetting fluid filling ratio						
									30 %	40 %	50 %	60 %	70 %	80 %	
			100	0.96	1.2	1.09			173	173	173	190	225	208	
			200	0.52	0.4	0.46			572	347	485	485	468	555	
			300	0.21	0.2	0.27			1127	624	832	850	832	954	
			400	0.12	0.11	0.22			1179	1110	1040	1283	1196	1283	
			500	0.35	0.26	0.18			763	2046	1318	1890	1682	1803	
			600	0.28	0.39	0.13			780	3988	1734	2116	2220	2306	
Self-rewetting fluid was a better choice for high heat flux applications since it had lower capillary resistance than water, and the ethanol evaporator section can be dried out easily. The effective thermal conductivity evolved similarly at every filling ratio until 500 W, when the 30% option fell down.															
2017	Paraffin	40					Air cooled	PCM cooled	PCM with heat pipes						[82]
			Flow rate [m/s]				6.3	0	0	2.3	6.3				
			Temperature difference is below 5ºC for: [s]				148	430	524	562	545				
The hybrid solution performed better, being able to control the maximum temperature below 50 ˚C longer than the other options. The temperature difference between the maximum and minimum temperature in the battery was reduced by 33.6% by adding PCM and by 62.5% if heat pipes were included.															

Table 7
Electric vehicles batteries cooling systems with heat pipes and PCM.

Year	PCM	$T_{melting}$ [ºC]	Outcomes	Ref
2015	Paraffin Rubitherm RT50	46-50	Surface battery temperature [ºC] by cooling configuration Time [min] / Just battery / PCM / Heat pipes / PCM + heat pipes 0 / 25.7 / 26.5 / 26.2 / 25.8 1 / 58.9 / 50.5 / 51.4 / 44.3 2 / 88.2 / 65.4 / 66.2 / 53.4 4 / 131.4 / 91.2 / 82.9 / 60.7 5 / 143.9 / 100.6 / 88.8 / 63.9 15 / - / 124.8 / 132.2 / 85.5 25 / - / 141.5 / 135.4 / 96.1 60 / - / - / 147.2 / 118.8 The thermal runaway of the mimic battery was extended from 104 seconds to 708 seconds by adding a cooling device based on PCM and heat pipes.	[85]
2018	Paraffin	50	Cooling system / System temperature [ºC] along time 5000 s / 10000 s / 15000 s / 20000 s / 25000 s PCM: 14.5 / 52.4 / 63.2 / 71.4 / 78.3 PCM/heat pipe-air: 46.1 / 47.9 / 51.6 / 52.1 / 52.8 PCM/heat pipe-water: 46.3 / 47.7 / 48 / 48.1 / 47.9 Flat heat pipes with 10.000 W/(m•K) thermal conductivity were installed between battery cells.	[83]
2017	Paraffin	42	The highest temperature of the battery block could be controlled below 50 ˚C.	[86]
2019	Paraffin	41-43	Just the hybrid cooling device / Maximum temperature [ºC] Expanded graphite [%] / Heating power [W]: 22.7 / 37.6 / 56.1 / 80.7 0 / 53 / 60.6 / 61 / 60 5 / 46.5 / - / - / - 10 / - / 52.7 / 52.2 / 56.3 20 / - / 48.8 / 47.3 / 52.4 Combined with a thermoelectric cooling / Maximum temperature [ºC] Expanded graphite [%] / Heating power [W]: 37.6 / 80.7 15 / 52 / 52.3 20 / 45.6 / 46.3 When the additional thermoelectric cooling device was also used, an increase in the heating power did not have much effect on the battery temperature.	[87]
2019	Paraffin	31.5	Natural convection, PCM, and PCM with heat pipe as battery cooling systems were compared. Their peaks temperatures were, 45.7 ˚C, 35.5 ˚C, and 31.5 ˚C, respectively.	[84]

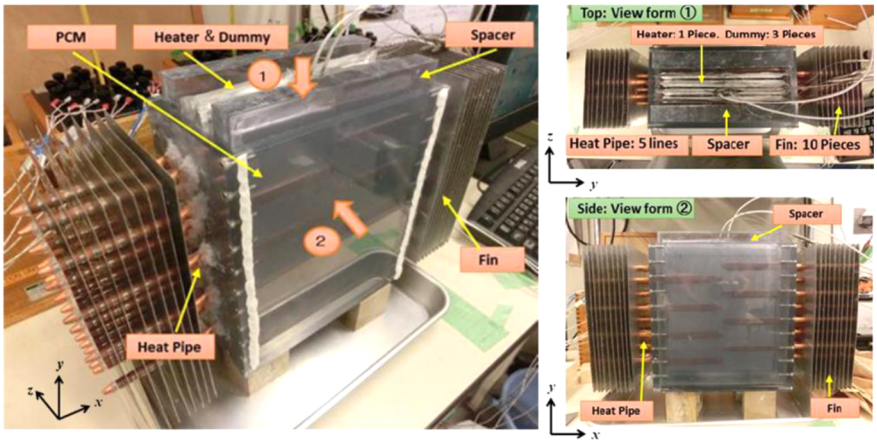

Fig. 20. Yamada et al. vehicle electric battery mimic with PCM with heat pipes cooling system. Adapted from [85].

Table 8
Hybrid system for cooling in buildings.

Year	PCM	$T_{melting}$ [ºC]	Outcomes	Ref
2000	Na2SO4.10H2O + borax nucleating agents (1.5%)	21	The system achieved 40 W heat transfer rate along 19 hours. The numerical simulations showed that by adding fins to the heat pipe would reduce the melting/freezing time up to 7-10 hours.	[88]
2001			The previous numerical results were used to design the prototype, reaching 200 W heat transfer rate. The prototype was compared against a conventional air conditioning, and the cost savings were from 100 to 1050£ regarding the production and 30£ per year in terms of operation.	[89]
2006	Hydrated Glauberis salt + Borax	21	The system proved its worth to reduce or even eliminate the use of conventional air conditioning. As the above studies, the prototype used the night time to freeze the PCM and then release the stored cold into the room.	[90]

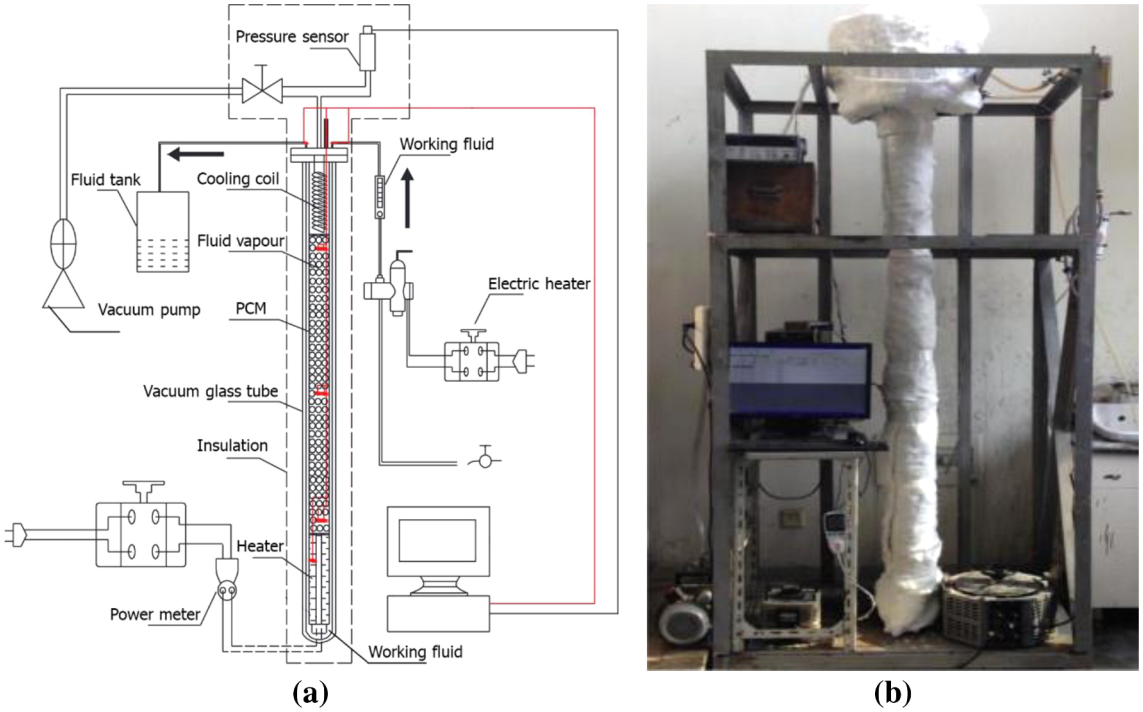

Fig. 21. Liu et al. [91,92] (a) test rig scheme, (b) prototype. Adapted from [91,92].

Table 9
Liu et al. research of a thermal latent storage heat pipe type at medium temperature.

Year	PCM	$T_{melting}$ [ºC]	Outcomes							Ref
2015	RT100 High-density polyethylene 102	142	Temperature inside the unit [ºC] at different heating power inputs							[96,97]
			RT100 + polyethylene			Sodium nitrate with potassium nitrate, and bentotite				
			Time [min]	300 W	400 W	Time [min]	300 W	Time [min]	600 W	900 W
			0	23.1	20.25	0	7.4	0	7.1	7.7
			5	46.9	49.5	10	7.4	5	8.3	8.9
			10	55.4	58.8	20	10.8	10	11.9	157.4
	Sodium nitrate and Potassium nitrate, and bentotite	206-247	15	63.8	70.5	30	156	15	156.7	185.7
			20	72.6	77.6	40	172.4	20	179.1	221
			30	84.7	93	50	201.7	25	203.8	243.4
			35	90.3	99.4	60	223.9	30	227.4	-
			40	93.945	108.7	70	237.9	35	241.6	-
			50	107.5	-	80	-	40	251	-
The experimental results showed the potential of this technology for medium temperature applications. Higher heat input made the system to melt faster, as expected. However, it was also an indicator of the good thermal conductivity performance.										

system, the heat pipes were embedded in the PCM and the air moved along them. The heat pipes condenser and the evaporator sections reversed regarding if the PCM was being charged or discharged. The system provided cost and energy savings in comparison with conventional cooling systems such as cooled beams under UK summer conditions. Later, Etheridge and Reay [90] kept going forwards into the prototype to develop a hybrid heat pipe and PCM cooling system for air conditioning in buildings. Table 8 gives more details about this research.

4.2. Applications at medium temperatures

Just two documents carried out their experimental research at medium temperatures (from 150 ˚C to 400 ˚C), both developed by Liu et al. [91,92]. They designed a gravity-assisted wickless heat pipe thermal storage. The storage unit itself was the heat pipe, since the granular PCM was into the heat pipe, the electric heating device was the evaporator, and the cooling unit the condenser section of the heat pipe; as shown in Fig. 21. The heat pipe had no wick and it was made of stainless steel, then hosted into a vacuum glass tube and wrapped by an insulation layer. The working fluid (water first and then naphthalene) was evaporated at the bottom by a heating rod, flowing upwards along the PCM. Then, at the top, it condensed in the cooling unit and went back down by gravity. As thermal storage material they tested a composite granular solid-liquid PCM mixture of RT100 and high density polyethylene (HDPE), and a mixture of metal salt and bentonite. The

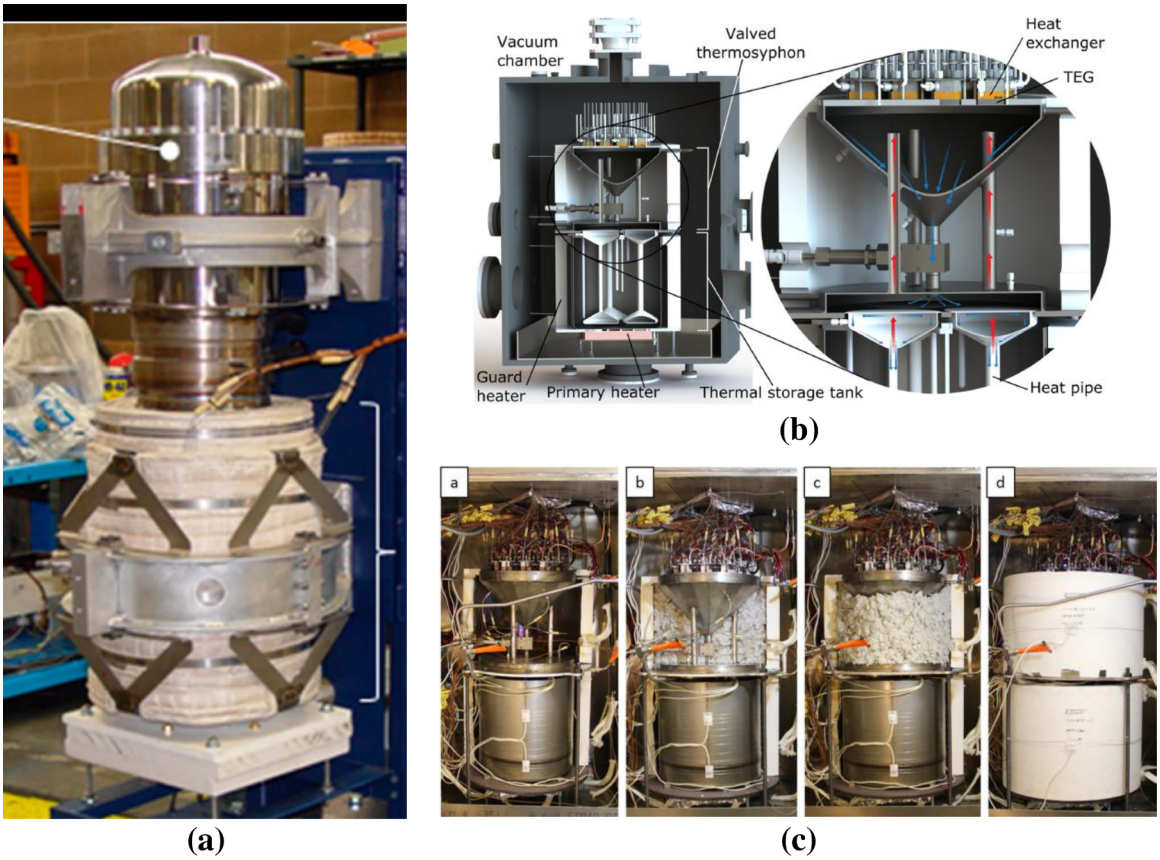

Fig. 22. Experimental test rigs at high temperature. (a) Qiu et al. [94,98] latent TES with heat pipes in couple with a Stirling engine. Oshman et al. [95–97] set up, (b) concept design, (c) prototype.

Table 10
Research carried out at high temperatures.

Year	PCM	$T_{melting}$ [ºC]	Outcomes	Ref
2017	NaF-NaCl	680	A novel hybrid system at high temperature, based on previous design at low temperatures, was built. Its feasibility was successfully tested. This technology had potential to work in couple with concentrated solar power plants. The latent TES with heat pipes was experimentally assessed in vertical and horizontal position. The device supplied 2.8 thermal kW at 750 ˚C when vertical. At horizontal position the system provided 5.7 thermal kW at 800ºC.	[94,98]
2017-2018	Aluminium-silicon	577	A hybrid solution to transfer heat from a latent TES towards a power block was developed. The system included a thermosiphon connecting both parts, which could work as control thermal valve. Also, within the storage block there were heat pipes embedded. The thermosiphon valve provided a heat flux of 26900 W/m^2 and its effective conductivity was 316 W/(m•K). The higher heat losses between interfaces were found across the power block, from 525 to 560 ˚C.	[95–97]

melting temperature of the two first tested PCM was 100 ˚C, and the mixture melted from 200 ˚C to 250 ˚C. The composite granular PCM was made by mixing three parts of RT100 per one part of polyethylene, 3:1 in mass ratio. The authors managed to build and test the viability of a heat pipe TES unit at medium temperature with potential for solar applications. The whole system worked almost isothermally, and the low thermal conductivity of PCM was not longer a limitation (Table 9).

4.3. Applications at high temperatures

Qiu et al. [93,94] took Tiari et al. [20] design for a cylindrical heat exchanger with PCM and heat pipes described in Section 4.1.1 (Fig. 10c), to develop a high temperature (above 400 ˚C) latent TES. Tiari et al. device incorporated two heat pipes lines, a primary one and several secondary heat pipes (Fig. 31a). The new system had as goal to be coupled with a 3 kW free-piston Stirling convertor (Fig. 22a). The PCM used was a eutectic mixture, NaF (mole 34%)-NaCl (mole 66%), which melted at 680 ˚C. The system was tested at vertical and horizontal positions, performing better the latter one. The storage supplied 5.7 thermal kW at 800 ˚C. The engine was able to supply 1 kW from the energy storage (Table 10).

Oshman et al. [95–97] designed, modelled, and experimentally tested a high temperature thermosiphon to connect the latent TES (Fig. 22b and c) and the power block of solar power plant. The

Table 11
Latent TES with heat pipes modelling, where the heat pipe is modelled as a highly thermal conductivity solid.

Year	Heat Pipe conductivity	PCM	$T_{melting}$ [°C]	Main conclusions	Ref
2015 2018	3.8·10^4 W/(m·K)	KNO_3	335	A square latent TES assisted with finned heat pipes was modelled. Enthalpy-porosity method was used to develop a 2D transient finite volume model of PCM. The heat pipe spacing (heat pipe number) influence was tested 122 (1), 74 (2), and 41 (3) mm between them. At the three heat pipes configuration, the influence of fin length (15, 25, and 35 mm), and the fin number (10 or 20) was analysed. Finally, two nanoparticles were studied, CuO and Al_2O_3, as well as, their volume fraction (0%, 5%,and 10%).	[100,102]
2015		$NaNO_3$-KNO_3	220	A transient 3D finite volume model of a cylindrical latent TES with heat pipes was made, employing a finite volume based model and enthalpy-porosity technique for the phase change. Heat pipe spacing, 31 and 17.4 mm (5 and 9 heat pipes and different heat pipes configurations was analysed. The heat pipes were finned (ten fins of 8 mm per each one). Also, the effect of natural convection was modelled.	[101]
Common outcomes	Natural convection affected notably the melting process, as heat convection was the main driver, reducing the melting time by 30%. The fins number hardly affected the system performance, but larger fins made the PCM temperature more uniform. The number of heat pipes, as well as a proper distribution of them increased the melting rate. Al_2O_3 nanoparticles, and higher volume fraction (10%) performed faster charging process.				
2018	3.8·10^4 W/(m·K)	RT55 Rubitherm	55	A cylindrical latent TES with heat pipes embedded within the PCM was modelled. The heat source was fluid flowing through a tube in the container centre, where the heat pipes were attached. Nanoparticles (CuO and Al_2O_3) were spread in the PCM. Velocity-pressure was modelled with SIMPLE algorithm. Increasing the number of heat pipes to 2, 3, and 4, reduced the charging time by 40.86%, 63.70%, and 75.16%, respectively. Higher nanoparticles volume fraction to 5% and 10%, decreased the process time by 15% and 25% respectively.	[103]
2019	9250 W/(m·K) 30381 W/(m·K)	Lauric acid	43.5	The enthalpy-porosity technique, based on finite volume method, was used to model a latent TES with flat miniature heat pipes arrays, with rectangular fins. Different HTF temperatures and flow rates were compared, realising that those parameters affected the melting process. Outlet temperature and charging power increased linearly with the inlet temperature. The device geometry was studied with the aim of optimizing the design. As expected, less fin spacing meant less thermal storage capacity. Fin thickness hardly affects the charging power.	[42,43]
2013	30769 W/(m·K)	n-eicosane	37	A heat storage unit with PCM for mobile phone cooling was numerically modelled. The heat pipe connected the cooling unit with the mobile chip, which was the heater. Different unit configurations were tested. The simulations showed that the cooling design could not refrigerate the mobile when being used intensively.	[99]
2019	-	Rubitherm RT35	29	Enthalpy-porosity method was used to model the phase change in a heat storage enhanced with heat pipes. The heat source was a hot water flowing along a U-shaped tube. The influence of heat pipes, number of tubes and their angle was studied. The addition of heat pipes reduced the melting time by 91%. Also, it was realised that as angle of the HTF plate increases, the melting process became faster.	[104]

thermosiphon had a valve to control or shut down the working fluid (sodium) return. Firstly, the thermosiphon was tested at lab scale showing a heat flux of 26900 W/m^2. The effective conductivity of the device was 316 W/(m•K). Later, the thermosiphon was tested in couple with a latent TES, proving its feasibility. It has to be pointed out that the thermal storage system had heat pipes embedded too. However, the thermal efficiency was lower than expected, but the authors considered that scaling up the prototype would solve that issue. The PCM used was aluminium-silicon eutectic mixture.

5. Hybrid systems numerical models

When going deeper into the modelling done about heat pipes and PCM, three different main methodologies came up. The first option considered the heat pipe as a highly thermal conductive solid. In the second, the model was based on the simplified thermal resistance network model. The third methodology described the heat pipe in detail, applying the continuity, momentum and energy equation to the fluid inside the heat pipe. Therefore, this section is divided regarding how the authors modelled the heat pipes.

5.1. Heat pipes as high thermal conduction element

This assumption to simplify the heat pipe was suggested used by Faghri [9], there were three different methods to do it: assigning a constant high conductivity to the heat pipe, simulating the heat pipe as a constant heat flux input, and considering a constant temperature along the het pipe outer wall. It has to be pointed out that the other elements apart from the heat pipe were modelled either following an approach called layered thermal resistance (LTR) or by applying the fluid dynamics equations as in heat pipe modelled by using CFD Section 5.3. Hence, the three different heat pipe modelling ways have as goal to set the boundary conditions, which are used later within the latent heat TES model. Out of those three the simplest are to consider a constant outer heat pipe wall temperature or a constant heat flux input, because the heat pipe becomes directly a boundary condition for the PCM model. Giving the heat pipe a constant high conductivity includes the heat pipe within the model, since the heat pipe still is considered as a heat transfer device, having a heat input and output.

5.1.1. Heat pipes are modelled as a solid with high thermal conductivity

Dealing with heat pipes as high thermal conductive solid was first used by Faghri [9], who described the heat pipes as a device which thermal conductivity is 90 times greater than a same size copper rod. Eight studies followed this approximation, assigning to the heat pipe a constant thermal conductivity value [42,43,99–104]. Table 11 shows every study which considers just the heat pipe conductivity, also the PCM properties.

This method simplified the heat pipe energy equation, which for a 2D situation was Eq. 1 [100]. Thus, despite the fact that it was a hybrid device, the model was actually a PCM physical model.

$$(\rho.\ c_p)_{eff}.\ \frac{\partial T}{\partial \tau} = k_{eff}.\left[\frac{\partial^2 T}{\partial x^2} + \frac{\partial^2 T}{\partial y^2}\right] \quad (1)$$

being c_p, the specific heat [J/(kg•K)]; ρ, the density [kg/m^3]; τ, the time [s]; T, the temperature; and k the thermal conductivity [W/(m•K)].

In Diao et al. [42,43] research k_{eff} is given by Fourier heat conduction equation Eq. 2:

$$k_{eff} = Q.\ (L_{eff}/(A.\ \Delta T)) \quad (2)$$

being Q, the heat flux [W/m^2]; L, the heat pipe length [m]; and A, the area [m^2].

Tiari et al. [100] developed a transient two-dimensional high temperature squared PCM tank (Fig. 23a), and later a transient three-dimensional cylindrical PCM tank [101] (Fig. 23b). In both geometries

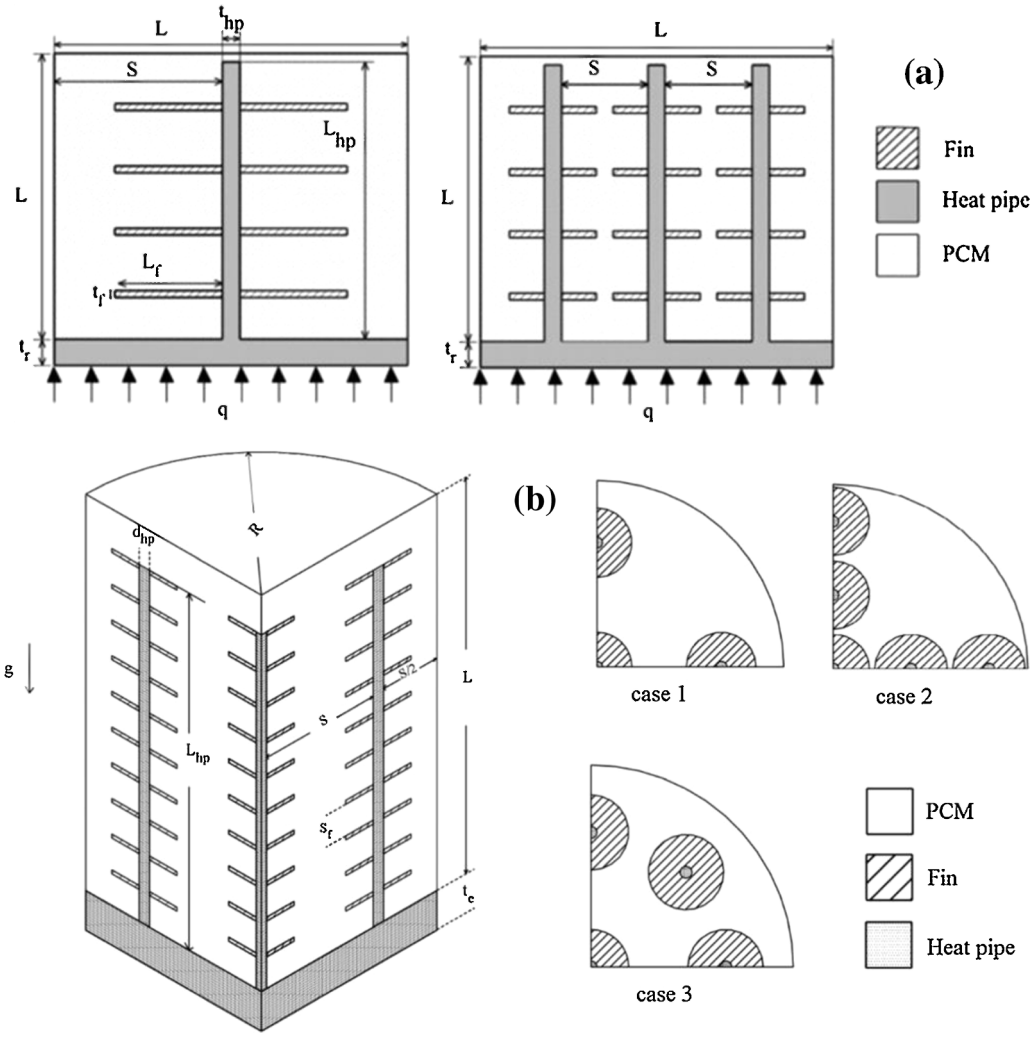

Fig. 23. Tiari et al. (a) 2D square latent TES [100,102], (b) 3D cylindrical latent TES [101], both with vertical finned heat pipes.

the heat pipe heat inlet was at the bottom tank surface (just charging process was analysed), and nickel fins were attached to the condenser section. Both models studied the influence of the heat pipe number, and effect of the natural convection. Adding more heat pipes increased the melting rate and lowered the bottom wall temperature, making the container stronger against overheating. Natural convection had the same effect as adding more heat pipes, decreasing the charging time, but natural convection also made the temperature distribution within the PCM more uniform. The 2D model also checked different fin length, and their number, that also helped to lower the base temperature and to decrease temperature difference in the PCM, and the number of attached fins. The 3D model allowed to test different heat pipes placements, showing that the optimal distribution could enhance the thermal performance. More recently, Tiari et al. [102] employed their 2D model to test the use of nanoparticles dispersed within the PCM as thermal conductivity enhancement method. They compared copper oxide and aluminium oxide nanoparticles at different nanoparticles volume fraction (0%, 5% and 10%). Concluding that as the volume fraction increased the faster the charging process was. Also, aluminium oxide nanoparticles reduced the charging time. A similar study was performed by Mahdavi et al. [103] in which nanoparticles (CuO and Al_2O_3) were dispersed within the PCM. Unlike the previous article, in this one the heat input came from a hot HTF which flowed through a pipe where heat pipes were attached. Same conclusions as in their foregoing work were achieved.

Diao et al. [42,43] modelled their LHTES with flat miniature heat pipe arrays (see section Solar applications at low temperatures 4.1.2) as well, basing the simulation of heat pipes as in the previously mentioned Tiari et al. studies [100,101]. However, the heat pipes thermal conductivity was based on their previous experimental studies. Along the first study (Fig. 15a), in which water was the HTF [42], the heat pipe effective conductivity was 30381 W/(m•K) according to their experimental studies [36] and using Fourier heat conduction equation Eq. 2. The effect of the fin size and their spacing was studied. The results showed that if fin spacing was larger than 6 mm the PCM melted from top to bottom, and the other way around if it was lesser than 6 mm. Also, if fin space was narrower than 4.14 mm the charging power basically did not improve any longer. The other numerical study performed by Diao et al. [43] simulated a similar device but with air as HTF, which was previously experimentally tested [34]. In this simulation the influence of the HTF inlet temperature and flow rate was analysed. The inlet temperature could vary the system efficiency from

Table 12
Latent TES with heat pipes modelling, where the heat pipe is modelled as a constant heat flux supplier.

Year	Heat flux	PCM	$T_{melting}$ [°C]	Main conclusions	Ref
2015	41000 W/m^2	KNO_3	335	A two-dimensional finite volume based numerical model along with enthalpy-porosity technique was employed to simulate the phase change of storage media during discharging mode. They studied the influence of heat pipe spacing, fin geometry and quantities, and natural convection, on the storage system thermal performance. The results indicated that the phase change material solidification process was hardly affected by natural convection. Decreasing heat pipe spacing resulted in faster discharging process. Increasing the fins length did not change the discharging time. Using more fins also accelerated the discharging process.	[105]
2018	6200 W/m^2 (100 W per heat pipe)	Solar salt $NaNO_3$ (60%) + KNO_3 (40%)	220	Configuration / Time [hours]: Common fins: Steel 4.2, Discharging 4.5, Charging at 218 °C 5, Charging at 210 °C 4.2; Aluminium 3.8, 3.8, 4.2; Perforated fins: Aluminium 4.1, 4.3, >6.2. Different fins configurations in couple with heat pipes embedded into a PCM tank were modelled and analysed.	[106]
2010,2011,2015,2017	-	LiF (80.5%) + CaF_2 (19.5%)	767	Model assumptions: (i) The temperature along the heat pipe wall was uniform, assumed symmetry in incident flux (ii) the initial thermal storage void volume was fixed, (iii) heat convection along liquid PCM was not considered, microgravity neglects natural convection, (iv) there was no contact resistance between the heat pipe wall and the PCM canister, (v) all void cavity surfaces were grey bodies with diffusion reflection. Results showed that void cavity thermal resistance was much higher than PCM's, therefore void cavity prevented the heat transfer from the canister wall to the PCM, lowering the PCM thermal storing capability, as the void ratio increased. The void distribution highly affected the phase change, an improved distribution increased the liquid fraction achieved during melting process (from 0.76 to 0.80).	[107–110]

74.55% to 88.47%, and the flow rate from 78.34% up to 88.47%. The heat pipes were modelled as before, but the experimental data determined their thermal conductivity to 9250 W/(m•K).

Ebrahimi et al. [104] also used Tiari et al. [100,101] numerical work as reference using the same approximation for their heat pipes model. Ebrahimi et al. [104] designed a single heat pipe as the cylindrical shell of the tank, reducing the melting time by 91% in comparison with a simple shell. Additionally, the effect of the number of HTF tubes was analysed; when this number was double and tripled the melting time was reduced by 13.2% and 19.4%, respectively. Kumaresh [99] also modelled the heat pipe as a rod which thermal conductivity was 30769 W/(m•K), for heat removal in mobile phones. They developed a case with PCM with nanoparticles and several fin configurations. The PCM mainly worked as a "shock absorber", taking the heat that the refrigeration system could not remove, which would be dissipated when the phone was not being used.

5.1.2. Heat pipes are modelled as a heat flux input

There were six studies in which despite the fact that they followed the same assumption as Faghri [9], the heat pipes were highly conductive elements, they were considered as constant heat flux supplier (Table 12). Tiari et al. [105] used the same design they modelled before (Fig. 23a) but this time they studied the discharging process. For doing so, the heat pipe removed a constant heat flux from the PCM, 40 W per second in this case. They investigated the same comparisons as in Tiari et al. [100]; the effect of natural convection, heat pipe spacing, and fin size. The difference was that the discharging process was mainly driven by conduction. Therefore, natural convection was not such influential as it was when charging.

Costa et al. [106] used this approximation as well, for modelling a latent heat TES tank with different fin geometries. In this case, each heat pipe supplied 100 W (40 heat pipes are attached to the system). They compared the use of steel, aluminium fins, and aluminium perforated fins. As expected, aluminium option was better than steel one (Table 12 shares the details).

A PCM canister with heat pipes receiver for space applications was modelled by Gui et al. [107–110], considering the heat pipes as a constant heat flux supplier, which wall temperature was uniform. The device was divided in two main parts the heat receiver and the TES part (Fig. 24). They performed a two-dimensional canister, axial and radial, model. The influence of void ratio on the PCM was analysed. They compared their numerical result against NASA simulation data [108,110] and the experimental data from NAL in Japan [109]. Concluding that, since the void cavity thermal resistance was so much higher than the PCM canister, the heat transfer was hampered between them. Thus, if void cavity existed the PCM latent heat could not be fully charged during sunlight time, either the PCM could not totally release the heat along eclipse periods.

5.1.3. Heat pipes are modelled as a wall with constant temperature

Pan et al. [111] developed a cylindrical coordinate model by layered thermal resistance method (LTR) (Fig. 25a). The design included finned heat pipes. However, the heat pipe in particular was a high conductive solid which external wall temperature was assumed constant, and its other boundaries with no heat fluxes (Table 13). The model was used to optimize the finned heat pipe dimensions under minimizing the cost condition. The results showed that the thinner the fins were the cheaper the system was. Also, if the fins were thicker than 2 mm, it was better to use more than heat pipes than welding fins. Taking into account that the heat pipe cost was the same as attaching the fins. This model was later implemented in a PCM cooling unit [112], concluding the same as before in terms of cost.

Lohrasbi et al. [113,114] designed a finned heat pipe inserted in a cylindrical latent heat TES system (Fig. 25b). As the previous studies the heat pipe was a high thermal conductivity element with a constant temperature (306 K and 240 K in this study for charging and

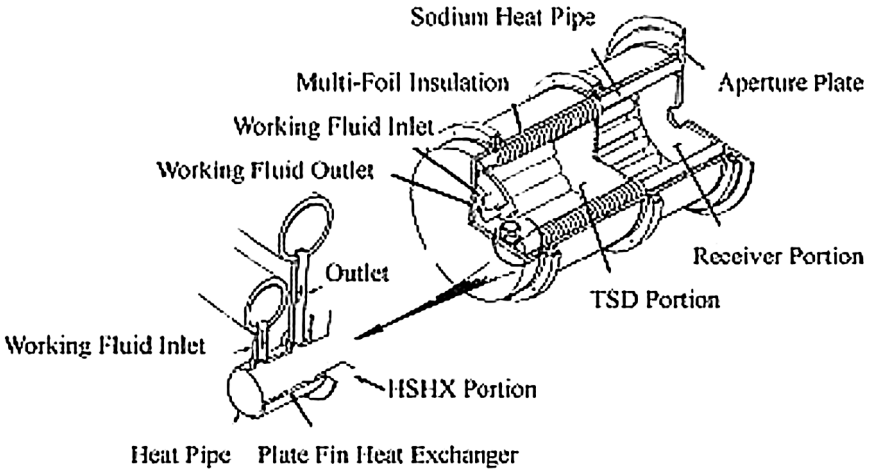

Fig. 24. Latent TES canister with heat pipe receiver design for solar spacecraft purposes [108–110].

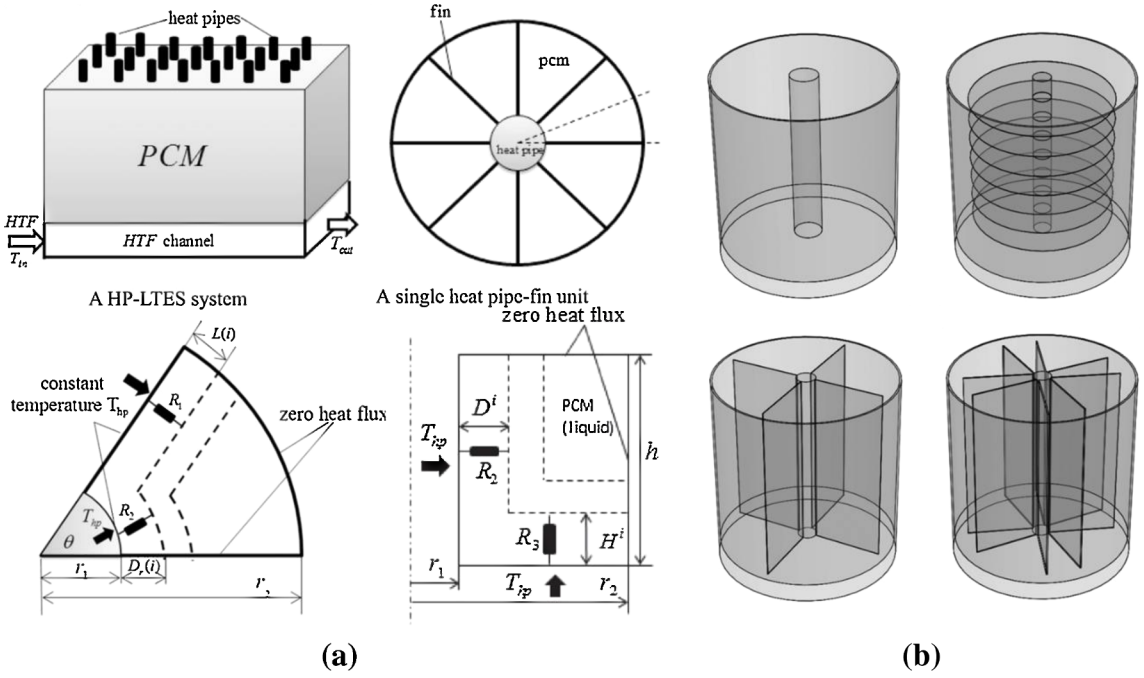

Fig. 25. (a) Pan et al. hybrid concept for batteries [111,112]. (b) Lohrasbi et al. latent TES tank model with different fin geometries [113,114].

discharging respectively), thus the liquid-vapour phase change during the heat pipe simulation was not considered. Four configurations were modelled: a heat pipe assisted LHTES tank with no fins, with radial fins, with longitudinal fins, and with a V-shaped fin. Being the V-shaped fin the best option, increasing the discharging ratio by 4.214 times (Table 13) about the no fin configuration. If the angle of the V-shaped fin was optimized, the increase aforesaid rose up to 4.28 times. Also, the fin size (thickness and length) and the use of nanoparticles within the PCM were also analysed. Regarding fin sizing, as they grew thicker and longer the discharging rate improved but also the energy storage capacity was lowered. Although thicker fins improved the heat transfer, it did not compensate the energy storage capacity lost, so they were kept as thin as possible. In regard with fin length, a trade-off had to be achieved between both thermal characteristics. The addition of 2.5% and 5.0% volume copper nanoparticles increased the discharging rate by 1.099 and 1.208 times, respectively.

Ren et al. [115] also assumed a constant temperature for the heat pipe to simulate a PCM (Li_2CO_3-K_2CO_3 mole ratio 62/38) squared tank enhanced with nanoparticles and metal foam. Different nanoparticles volume fraction, metal foam porosity and pore size, and heat pipe radius were analysed. Roughly speaking, if the heat enhancement technique was larger (more nanoparticles, lower foam porosity and pore size, and larger heat pipe radius) the melting process was faster, as expected. However, the energy storage capacity was lower; so a trade-off between these parameters had to be reached. Among the several studied cases in the paper, an optimum combination could be achieved to get the best energy storage efficiency. It had to be pointed out that when keeping the same PCM volume, metal foam gave better results

Table 13
Latent TES with heat pipes modelling, where the heat pipe is modelled as a surface at a constant temperature.

Year	Heat Pipe temperature [°C]	PCM	$T_{melting}$ [°C]	Main conclusions	Ref
2017,2018	-	$CaCl_2$•$6H_2O$	29.5	A cylindrical latent TES with finned heat pipes was modelled as supplementary cooling system for air cooled condensers. The heat pipe was at a constant temperature and the other elements following the layered thermal resistance (LTR) model. The system was optimized regarding cost, concluding that thinner fins lowered the costs. Also, the use of carbon-steel was cheaper than aluminium. It was found that the PCM energy capacity was a first-order factor on the system cost.	[111,112]
2017	Charging at 33 °C Discharging at -33 °C	Water	0	A 2D model of a cylindrical latent TES with nano enhanced PCM was made by finite element method. Novel V-shaped finned heat pipe was assessed. The design was optimized by a response surface method (RSM). Configuration / Optimizing discharging Time [s] / Enhancement [n-time faster] / Optimizing charging and discharging Enhancement [n-time faster] No fins / 29500 / - / - Radial fins / 8915 / 3.582 / 3.55 Longitudinal fins / 8236 / 3.309 / 3.26 V-shaped fins / 7000 / 4.241 / 4.28	[113,114]
2018	516	Li_2CO3-K_2CO_3Mole ratio 62/38	486	The melting performance of a latent TES unit with heat pipes, enhanced by nanoparticle metal foam was modelled. The foam porosity, pore size, volume fraction of nanoparticle, and the heat pipe radius was studied. The melting time was reduced by decreasing the metal foam porosity or rising the nanoparticles volume fraction. Reducing the pore size at a determined porosity, accelerated the meting ratio. Heat pipe radius affected greatly the melting speed.	[115]
2019				The circular heat pipe was replaced by a novel sinusoidal heat pipe in a nanoparticle-enhanced PCM tank, without affecting the TES capacity of system. The results suggested that as the sinusoidal heat pipe enlarges the heat transfer area, the system was highly improved.	[116]

than nanoparticles. Later Ren [116] modified his previous model by replacing the circular heat pipe by a sinusoidal heat pipe (the heat pipe temperature was constant too). The sinusoidal heat pipe accelerated the PCM melting even though the heat pipe wall temperature was considered 10 °C lower than the circular one.

5.2. Heat pipe modelled by using the simplified thermal resistance network model

This sections presents the scientific contributions that used a simplified thermal resistance network model to investigate a hybrid TES with heat pipe [26,117–131]. This concept represents the thermal transfer as a thermal circuit (Fig. 26b), an analogy of an electrical circuit (Fig. 26a). The thermal circuit is solved with the electrical equations (Fig. 26b), but using their thermal equals (Fig. 26d). Each element of the thermal circuit is like an electrical resistor (Fig. 26d), and the heat transfer is the electric current. Fig. 26e shows an example of a heat pipe modelled by this method [122].

Shabgard et al. [26] developed a thermal network model to analyse the transient behaviour of a LHTES system with embedded heat pipes. They designed two different modules; the first one, four heat pipes were attached to a tube through which the HTF flows, and PCM was around the pipe (Fig. 27a and c). The second design swapped the HTF and the PCM (Fig. 27b and c). The assumptions made for the lumped model followed a previous Faghri et al. study [132]. The thermal network was made of coupled thermal elements, every element included both the thermal resistance and capacitance (Fig. 27d). The study assessed the effect of the heat pipes orientation and the number of heat pipes by evaluating the heat pipe effectiveness. Inserting more heat pipes speeded up the charging and discharging rates, for either arrangement. When module 1, heat pipe orientation barely affected the thermal behaviour of the system. However, module 2 was highly affected, for instance, two vertical heat pipes performed better that two horizontal heat pipes plus a vertical one (Table 15 shares more details about their research). Shabgard et al. [127] performed a model following the same method from previous research [26], with gravity assisted heat pipes (Fig. 28). The study compared three different PCM materials (Table 14). Additionally, the coupling of three modules, each one with each PCM, as a cascaded latent heat TES system was analysed. An exergy analyse was performed, concluding that for solar power working temperatures (from 280 °C to 390 °C), the best exergy efficiency was given by the LHTES system with the lowest melting temperature. However, the latent heat TES cascade arrangement recovered around 10% more exergy than the best non-cascaded LHTES system during a 24 hours charging-discharging cycle.

Nithyanandam and Pitchumani [124–126] followed Shabgard et al. model [26], developing in 2010 a transient heat pipe in couple with a LHTES model by the simplified resistance network method. The same two configurations were used. Later, this model but varying the heat pipes number and distribution was used several times by the authors [119,121,128–131]. The heat pipes effectiveness while charging and discharging processes was studied, as well as the energy store. In both configurations, increasing the HTF mass flow rate, the tube radius and the module length, reduced heat pipes effectiveness. Regarding heat pipe parameters, lengthening condenser and evaporator sections, and enlarging inner heat pipe radius improved heat pipe effectiveness. After the parametric study, an optimum design for both modules were developed, showing that heat pipes effectiveness was higher for module 1, but the effective charging and discharging PCM rates were better for optimal configuration 2. Regardless the HTF mass flow was, the energy transfer rate during PCM phase changes were higher for module 2 [125].

Then a parametric analysis was performed comparing both modules with no heat pipes, two vertical heat pipes or two horizontal ones [124]. Horizontal heat pipes showed the better effectiveness at both configurations, and module 1 provided more energy storage but module

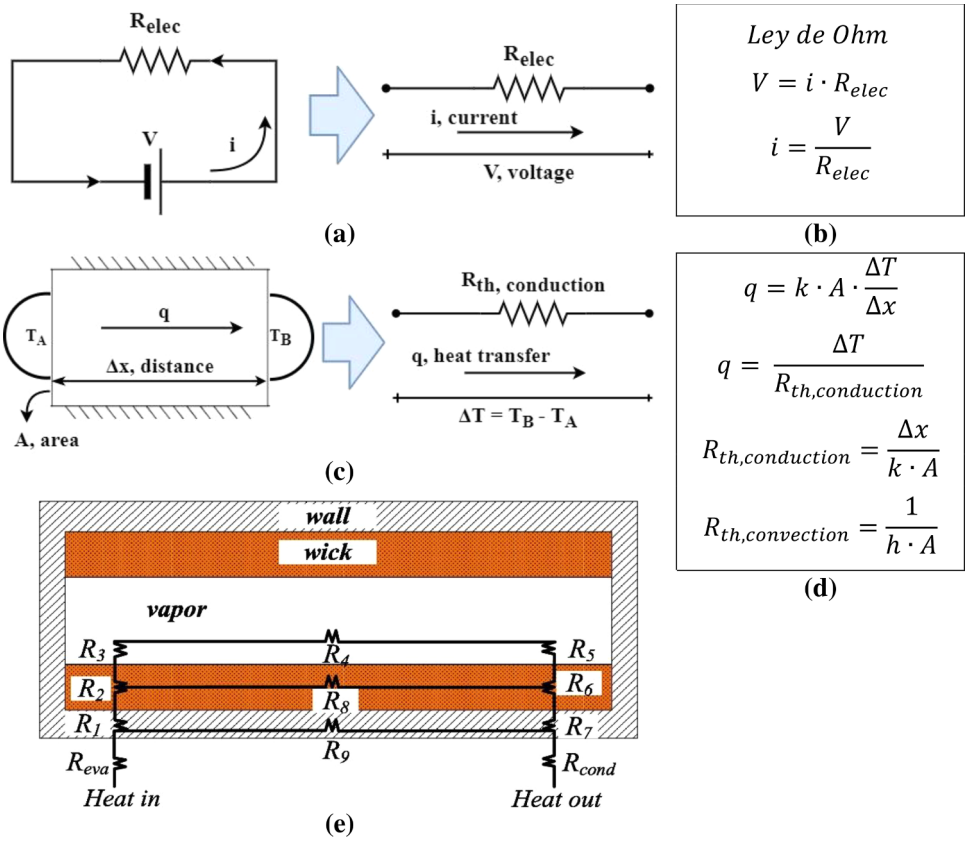

Fig. 26. Thermal resistance network model concept. (a) Electric circuit, (b) electric circuit equations, (c) thermal circuit, (d) thermal circuit equations, (e) heat pipe thermal circuit [122].

2 had higher melting fractions. The heat pipe performance was highly influenced by natural convection, and thermal stratification appeared in module 2. Module 2 with two horizontal heat pipes embedded was analysed deeper [126], aiming to test the effect of several cycle (charging and discharging) ratios on a cyclic LHTES operation mode. Finding that equal charging and discharging time periods made a more efficient latent heat TES performance. Later, the authors used the same model to evaluate the use of three or four heat pipes at different angles (Fig. 27e) [129]. As expected, four heat pipe configurations provided higher effectiveness. However, regarding power density per heat pipe unit, the best combination was module 2 with two vertical heat pipes. In general, module 1 presented substantially better effectiveness results at every heat pipe arrangement, and higher energy storage capacity. Nonetheless, module 2 showed higher melting fraction. Same study was performed but using thermosiphons instead of heat pipes [128]. Additionally, a new arrangement was included Fig. 27e heat pipe arrangement 4-X shaped. The results revealed thermosiphons inefficiency when the evaporator section was above the condenser; making thermosiphons no better than common fins, if the heat transfer direction was same as gravity. Also, the model served to parametrically check the use of metal foams within the PCM to enhance the heat transfer [119,121]. In this case just module 2 was studied. Due to the metal foam, the effective heat transfer surface increases, improving the discharging rate. The results showed that increasing the foam pore density, reduced the heat transfer rate; due to the hampering of convection currents because of the buoyancy. More details about the results from this design studied, can be found in Table 15.

The same technique was used to model a latent TES with embedded heat pipes, although the geometry was different from the above mentioned research, but following one of Shabgard concepts too [127] (Fig. 28). The storage design factors were studied, so it could be attached to a 200 MW_e concentrated solar power plant, being the TES levelized cost of electricity less than 6 cents per kWh, and the total storage cost less than 87.95 million USD [130,131]. The hybrid latent TES was compared against an encapsulated PCM TES system. Among other results, they concluded that the maximum cost of the heat pipes to satisfy their goals was 4 USD/unit heat pipe.

Nithyanandam and Pitchumani module 2 [125] was also developed following the lumped resistance network method by Yang et al. [122] to check the effect of flow conditions, the heat pipe condenser length and two heat transfer fluids (Therminol/VP-1 and air). Charging process was 10 times faster if the HTF flow was turbulent; also, Therminol/VP-1 reduced the charging time. Charging time was not significantly affected by larger heat pipe condenser section.

Shabgard et al. [26] module 1 was improved and numerically tested by Almsater et al. [120]. They attached fins to the heat pipes, in the condenser section what was in contact with the PCM. This time, they fixed a charging and discharging time (3 hours) and analysed the energy stored by then, instead of fully charging and discharging time. The finned heat pipe double the energy stored after 3 hours, and the discharging was improved by 79%, when comparing with bare heat pipes.

Jung and Boo [118] designed and modelled a latent heat TES system with embedded finned heat pipes. The heat pipes evaporator section was in contact with the charging hot HTF and a cold HTF flows along

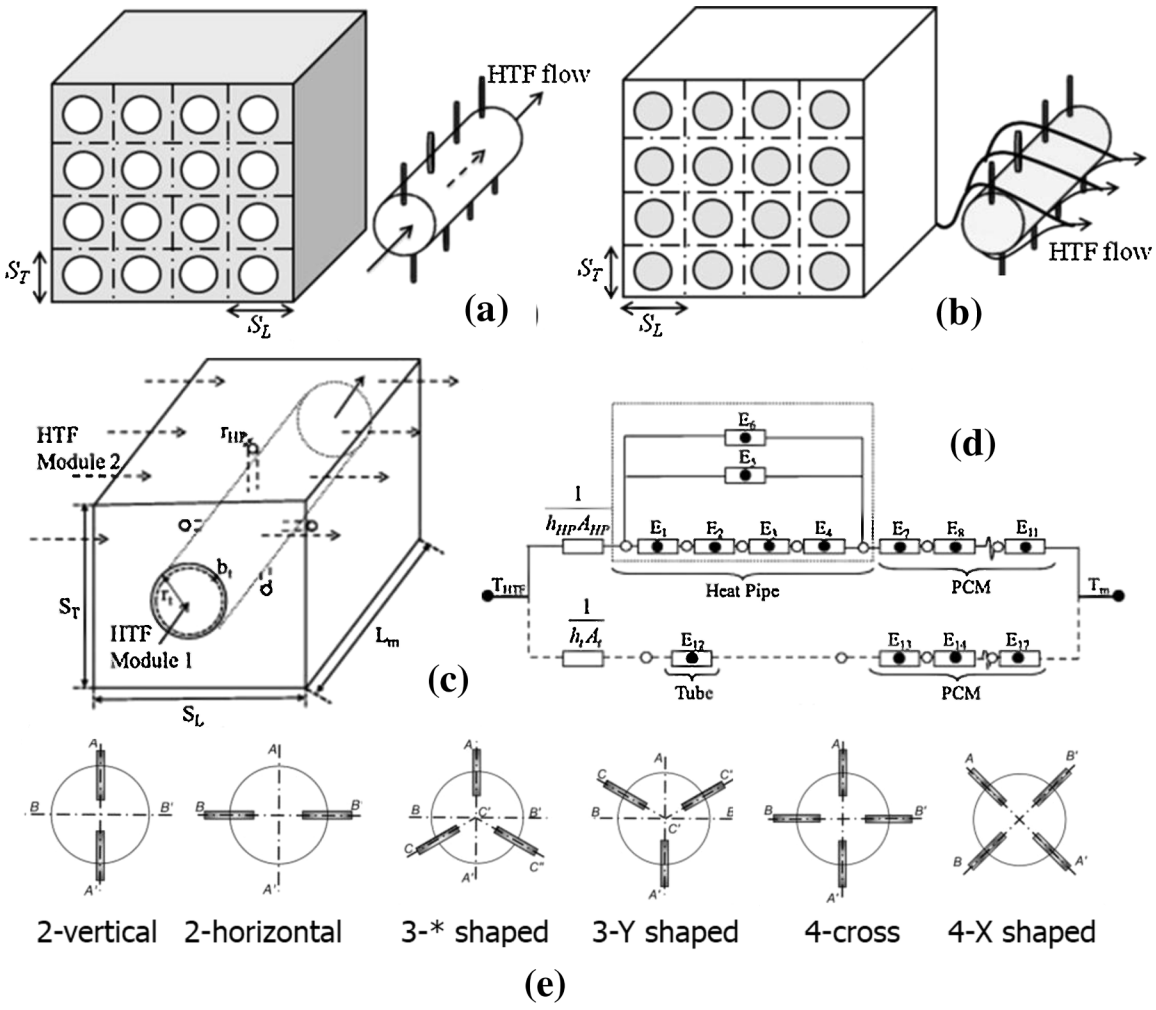

Fig. 27. Latent TES design modelled by thermal resistance network method. (a) Module 1, the PCM is around the pipe through where the HTF flows [129], (b) module 2, the PCM is encapsulated in tubes, and the HFT flows around them [129], (c) modules 1 and 2 scheme [125], (c) design thermal resistance network [125], (e) different heat pipes arrangement [128,129]. Adapted from [125,128,129].

the heat pipes condenser part. The model based on Shabgard et al. [26] for developing the thermal resistance network. However, they neglected the heat pipe internal thermal resistance due to heat pipes work at almost isothermal way [133]; so the paper mainly modelled, a LHTES. The fin pitch was studied as design parameter, concluding that as the fin pitch increased, its effect in the system performance became minimal. The models showed a mismatch of 8% when compared against the experimental data [14]. A new solar collector concept with a PCM storage, both connected by six heat pipes, was designed by Bilardo et al. [123]. The prototype was modelled following an electrical analogy and manufactured, so the model could be experimentally validated.

Chang et al. [117] used the lumped-heat-capacity method to model their previous design [134] (explained within the next section Heat pipe modelled by using CFD 5.3). The study compared three heat pipes configurations: a heat pipe with a hollow cylinder in the vapour channel, a heat pipe with a PCM encapsulated in a cylinder, and a heat pipe with six small PCM cylinders arranged around the vapour core (Fig. 29). They included the heat pipe wick and wall, considering also the liquid in the grooves. However, the heat transfer driver thorough the wick and working fluid was just conduction, because the speed flow was very low and the liquid thermal conductivity very high. It was concluded that PCM was an effective way to absorb the pulsed heat loads when operating the heat pipe. The most efficient configuration was the six small PCM cylinders arrangement.

5.3. Heat pipe modelled by using CFD

The research described in this section comprises scientific contributions which have used the descriptive equations for the heat pipe and the PCM [21,22,117,134–141]. Those fluid dynamics equations, when discretized, allow to perform a detailed model of the system. However, they require high computational cost to run the simulations (Table 16).

Chang et al. [117,134] were the first to model and discretize the fluid dynamics equations of a hybrid systems with PCM and heat pipes. Heat pipe wick and wall, and the liquid within the grooves were considered. Just conduction was assumed to be the only heat transfer driver through the wick and working fluid; since the liquid thermal conductivity was very high, and the speed flow was very low. Three configurations were compared: a heat pipe with a hollow cylinder in the

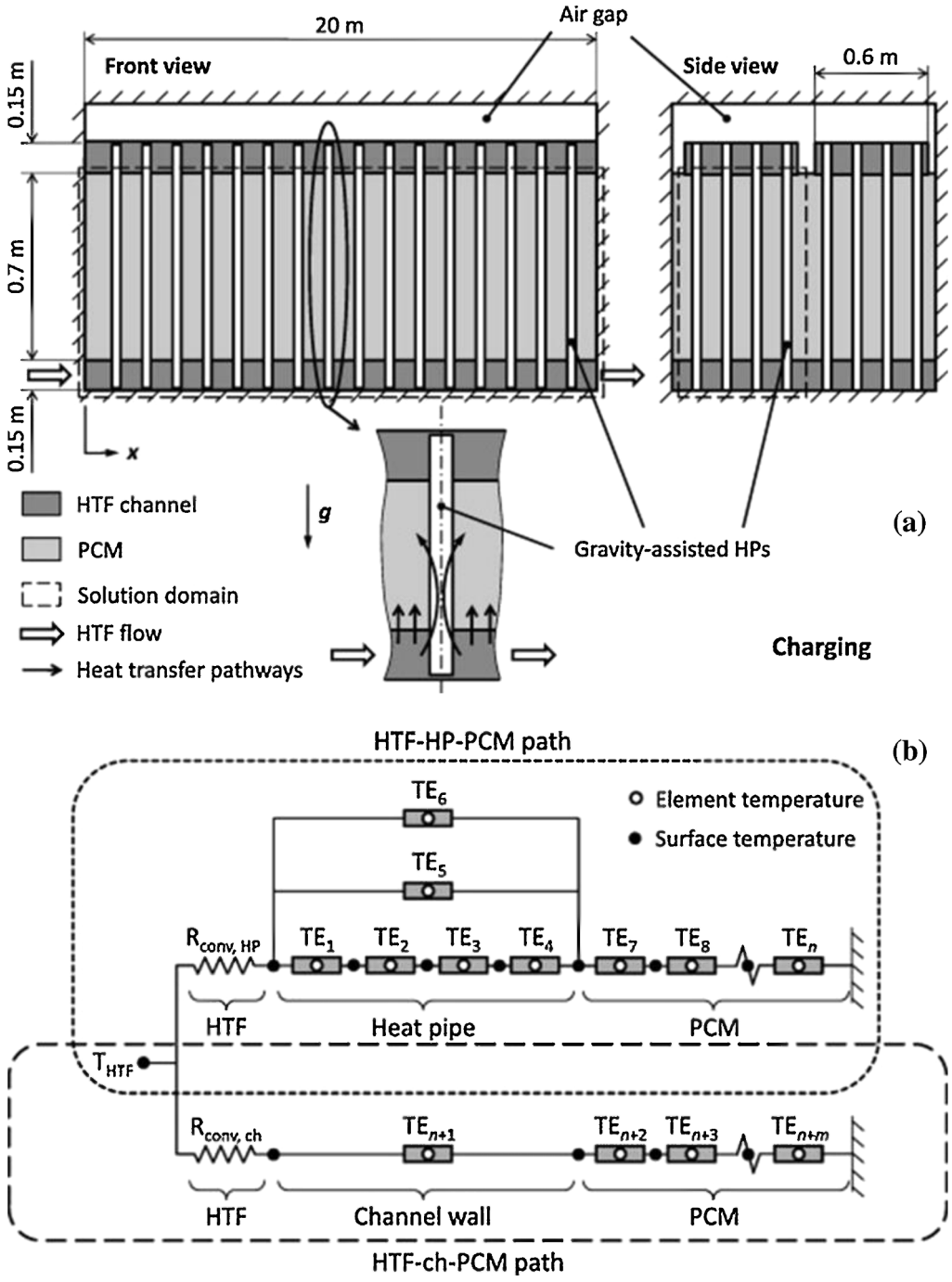

Fig. 28. Shabgard et al. [127] latent TES with gravity assisted heat pipes design. (a) Concept, (b) thermal resistance network.

vapour channel, a heat pipe with a PCM encapsulated in a cylinder, and a heat pipe with six small PCM cylinders attached around the vapour core (Fig. 29). It was concluded that the PCM was like a capacitor, absorbing the pulsed heat loads when the heat pipe was working.

Sharifi et al. [137] developed a numerical model of a hybrid design, which geometry corresponded to a cylindrical PCM container (Fig. 30a). The simulations compared a heat pipe against a solid rod or a hollow tube as heat input, also the difference between heating coming from below or from above was analysed. The heat pipe working fluid was potassium and the wick and wall were made of stainless steel, as the rod and the tube. The flow inside the heat pipe was a two-dimensional laminar compressible flow, being the potassium vapour considered as an ideal gas. The vapour was saturated at the wick surface and the wick was fully saturated. The liquid flow in the porous wick was neglected [142]. Also, the wick was able to provide enough capillary force to drive the liquid through the wick itself. Regarding the

Table 14
Latent TES with heat pipes modelling, modelled with the thermal resistance network method.

Year	PCM	$T_{melting}$ [°C]	Main conclusions	Ref
1991	Lithium hydride	683	A heat pipe with encapsulated PCM cylinder in the evaporator was modelled. The transient behaviour of the system was modelled by a lumped-heat-capacity method. One heat pipe included a hollow inner tube in the evaporator section, the second had a tube filled with PCM, and the last one had six PCM tube. The six tube geometry performed better, and they solidified faster.	[117]
2012	NaOH•NaCL (73.3/26.7 wt.%)	370	A latent TES with embedded gravity assisted heat pipes was modelled by thermal resistance network method. The model included different latent TES tanks working in cascade, with different PCM.	[127]
	$KCl•MnCl_2•NaCl$ (22.9/60.6/16.5 wt.%)	350	Storage Material: NaOH•NaCL (73.3/26.7 wt.%); $KCl•MnCl_2•NaCl$ (22.9/60.6/16.5 wt.%); $NaOH•NaCl•Na_2CO_3$ (65.2/20/14.8 wt.%); Cascade	
	$NaOH•NaCl•Na_2CO_3$ (65.2/20/14.8 wt.%)	318	Time [h]: 4 8 4 8 4 8 4 8 Energy stored [GJ]: 8 10 9.5 13 14.5 19 12.5 16	
2014	-	503	A latent TES with embedded gravity assisted heat pipes was modelled by thermal resistance network method. The storage tank was dimensioned to match a 200 MWe concentrated solar power plant. The unit was optimized so the TES levelized cost of electricity less than 6 cents per kWh, and the total storage cost less than 87.95 million USD. The results provided guidelines for designing latent TES for CSP plants.	[130,131]
2014	KNO_3	335	A latent TES tank with finned heat pipes was modelled by using a thermal resistance network. The tank was considered for a concentrated solar power plant. Reducing the number of circular fins, by rising the pitch from 4 to 16 mm, increased the heat transfer rate by 18.4 %	[118]
2019	$NaNO_3$	307	A cylindrical encapsulated PCM heat pipe assisted was simulated by employing the thermal resistance network method. Turbulent flow on the HTF made the charging process 10 times faster. Larger heat pipe condenser length hardly affected the charging process.	[123]
2019	Polyethylene glycol 6000	52-66	The modelling of heat pipe followed the simplified thermal resistance network model as an electrical analogy. The temperature of the evaporator section was constant and got from experimental results, also the conductance resistance was constant chosen after the experimental results. The model was experimentally validated.	[122]

PCM model, molten PCM was Boussinesq fluid, natural convection was a two-dimensional laminar incompressible flow. PCM density did not change with its phase. The results showed that the heat pipe was the best enhancement in comparison with either the rod or tube. When comparing an up to bottom heat income against bottom up, the rod and tube poorly performed if heat input was coming from above. The study inferred that the melting rate was governed by conduction in the heat pipe wall, rod and tube; condensation, vaporization and compressible flow of the heat pipe working fluid; and natural convection within the molten PCM. Later they added foils to their design [17] (Fig. 30b), improving the phase change rate by adding 1.21% foil volume. Sharifi et al. [140] continued their previous model with some modifications. This time the PCM was attached to the adiabatic section of the heat pipe (Fig. 30c), also the working fluid was sodium instead of potassium. Three working modes were tested, charging only, just discharging, and charging and discharging at the same time. The results showed that a larger PCM enclosure (keeping the same PCM mass) decreased the average heat pipe temperature at the bottom wall. Additionally, due to a larger heat transfer surface and narrower conduction length (the PCM container radius was smaller) melting was improved when simultaneous operation mode.

A similar model to Sharifi et al. [140] was developed by Song et al. [135], the same geometry was considered and same model assumptions. However, as it was an energy storage system for a space station application, there was no gravity and so heat convection was not considered, just conduction was the heat transfer driver. Based on an exergy efficiency analysis the system was optimized with a genetic algorithm, by modifying the different heat pipe sections length. The exergy efficiency achieved its maximum when the evaporator, adiabatic and condenser length were 0.36, 0.41 and 0.43 m, respectively.

Shabgard et al. [138] developed a numerical model of a latent heat TES assisted by heat pipes coupled with a dish/Stirling solar receiver. The two-dimensional model included two heat pipes, one was the heat input and the other the one was the output. The concept modelled within this study was later used to economically modelling the system levelized cost of energy, simplified though [143]. Shabgard et al. [140,144] followed the same assumptions as the aforementioned study. However, they included the liquid flow through the wick. The system transferred the solar irradiation to a Stirling engine. As the unit had separated input and output heat channels, three scenarios were simulated: charging only, discharging only, and both simultaneously. The system worked as a capacitor, absorbing the excess heat input and smoothing the Stirling heat input. The space between heat pipes was identified as a key parameter, providing better stability in the heat supplied to the engine if reduced. However, it has to be pointed out that lesser heat pipe spacing means more heat pipes, instead of a smaller unit.

Mahdavi et al. [21,22,139] also developed a two-dimensional axisymmetric model for a device which transfer solar irradiation towards a Stirling engine. The system included a complex heat pipe network, where there was a primary heat pipe and a secondary heat pipe array (Fig. 31a). The main heat pipe was the thermal energy carrier from solar power to the engine; the secondary heat pipe network charged the PCM with the heat excess. Sodium vapour flow within the heat pipe chamber, heat conduction in the heat pipe wall and wick were modelled. The wick-vapour interface temperature followed Clausius-Clapyron equation (Eq. 3) [145]. Usually, the boundary conditions at the condenser define a uniform mass flux, meaning a uniform heat removal at the condenser wall. However, this design implied that some vapour goes towards the secondary heat pipe network, discarding the latter assumption. Thus, porous layer was attached to the condenser wall and continuity and momentum equations were solved in this situation but not the energy equation (Fig. 31b). Five different locations and secondary heat pipe number in the network were studied (Fig. 31c). The results showed that the secondary heat pipe temperature was higher if it was placed away from the primary one [139]. Also, the effect due to

Table 15
Hybrid systems modelled following Shabgard et al. [26] design with thermal resistance network method.

Year	PCM	$T_{melting}$ [°C]	Main conclusions
Common design			A square TES with embedded heat pipes was modelled by using the simplified thermal resistance network method. Two designs were modelled: (i) the HTF flows into a tube were heat pipes are attached and PCM is around them, (ii) the HTF flowed around the tube full of PCM.
2011	Rubitherm RT82	82	Latent TES design Heat pipe arrangement
2010	KNO_3	335	2-horizontal
			2-vertical
			3-* shaped
2013			3-Y shaped
			4-cross shaped
			4-X shaped
2010	KNO_3	335	Geometry
			Module 1
			Charging
			Discharging
			Module 2
			Charging
			Discharging
2016	KNO_3	335	Effectiveness at the end of the process. Four finned heat pipes in Module 1 geometry.
			Charging
			Evaporator length [m]
			0.05 0.175 0.227 0.2
			2.9 4.2 4.6 4.2
2011	KNO_3	335	The model geometry and HFT mass flow rate was optimized, maximizing different parameters such as, charging (discharging) effectiveness, effective charging (discharging) rate, energy stored, and overall energy transfer rate.
			Flow rate [kg/s] Energy [MJ]
			Maximize: A - energy stored (discharged); B - charging (discharging) effectiveness; C - charging (discharging) rate
			Module (i) A - 2.8 (2.8)B - 2.8 (2.8)C - 2.8 (2.8) A - 5.021 (5.414)B - 1.027 (1.496)C - 1.027 (1.496)
			Module (ii) A - 2.8 (2.8)B - 2.8 (2.8)C - 2.8 (2.8) A - 4.096 (4.418)B - 1.174 (0.898)C - 4.096 (0.898)
2013 2014	Li_2CO_3 (56%)-Na_2CO_3 (44%)	497	A square TES with embedded heat pipes was modelled by using the simplified thermal resistance network method. The PCM with was contained into tubes, where the heat pipes were attached and the HTF flows around them. Different heat pipes configurations, and metal foam pore density and porosity were studied. The results showed that 2-vertical heat pipe arrangement with 40 pore per square inch (PPI) pore density, and 0.9 porosity gave the highest discharging power, and effectiveness (0.925). When charging the best configuration was 2-vertical heat pipes as well, 0.8 porosity, and 10 PPI, yielded 1.393 charging effectiveness.

Year	Main conclusions
Common design	A square TES with embedded heat pipes was modelled by using the simplified thermal resistance network method. Two designs were modelled: (i) the HTF flows into a tube were heat pipes are attached and PCM is around them, (ii) the HTF flowed around the tube full of PCM.
2011	Effectiveness at the end of the process
	Module (i) Module (ii)
	Heat pipes Thermosiphons Heat pipes
	Discharging Charging Discharging Charging
2010	1.14 - - 1.09
	1.79 1.59 1.59 1.32
	1.76 1.51 1.51 1.25
2013	1.76 1.62 1.63 1.37
	2.05 1.62 1.63 1.44
	1.68 1.43 1.42 1.48

(*continued on next page*)

Table 15 (*continued*)

Year	Main conclusions
2010	Effectiveness at the end of the process
	2-Hor. / 2-Vert. / 1-Hor.1-Vert. / 2-Hor.1-Vert.
	1.28 / 1.28 / 1.3 / 1.43
	1.19 / 1.19 / 1.28 / 1.28
	2-Hor. / 2-Vert. / 1-Hor.1-Vert. / 2-Hor.1-Vert.
	1.14 / 1.44 / 1.29 / 1.36
	1.12 / 1.21 / 1.17 / 1.23
2016	Effectiveness at the end of the process. Four finned heat pipes in Module 1 geometry.
	Charging / Discharging
	HTF pipe radius [m] / Evaporator length [m]
	0.2 / 0.275 / 0.3 / 0.05 / 0.175
	4.2 / 3.5 / 3.3 / 1.1 / 1.5
2011	The model geometry and HFT mass flow rate was optimized, maximizing different parameters such as, charging (discharging) effectiveness, effective charging (discharging) rate, energy stored, and overall energy transfer rate.
	Energy [MJ] / Effectiveness
	Maximize: A - energy stored (discharged); B - charging (discharging) effectiveness; C - charging (discharging) rate
	A - 5.021 (5.414)B - 1.027 (1.496)C - 1.027 (1.496) / A - 1.179 (1.188)B - 1.926 (1.981)C - 1.926 (1.981)
	A - 4.096 (4.418)B - 1.174 (0.898)C - 4.096 (0.898) / A - 1.079 (1.157)B - 1.449 (1.635)C - 1.079 (1.635)
2013	A square TES with embedded heat pipes was modelled by using the simplified thermal resistance network method. The PCM with was contained into tubes, where the heat pipes were attached and the HTF flows around them.
2014	Different heat pipes configurations, and metal foam pore density and porosity were studied. The results showed that 2-vertical heat pipe arrangement with 40 pore per square inch (PPI) pore density, and 0.9 porosity gave the highest discharging power, and effectiveness (0.925). When charging the best configuration was 2-vertical heat pipes as well, 0.8 porosity, and 10 PPI, yielded 1.393 charging effectiveness.

Year	Main conclusions	Ref
Common design	A square TES with embedded heat pipes was modelled by using the simplified thermal resistance network method. Two designs were modelled: (i) the HTF flows into a tube were heat pipes are attached and PCM is around them, (ii) the HTF flowed around the tube full of PCM.	
2011	Effectiveness at the end of the process	[126]
	Module (ii)	
	Heat pipes / Thermosiphons	
	Charging / Discharging / Charging / Discharging	
2010	1.09 / 1.07 / - / -	[124]
	1.32 / 1.34 / 1.23 / 1.26	
	1.25 / 1.26 / 1.2 / 1.2	
2013	1.37 / 1.36 / 1.2 / 1.2	[128,129]
	1.44 / 1.43 / 1.27 / 1.28	
	1.48 / 1.49 / 1.41 / 1.36	
2010	Effectiveness at the end of the process	[26]
	2-Hor.1-Vert. / 1-Hor.2-Vert. / 2-Hor.2-Vert.	
	1.43 / 1.43 / 1.58	
	1.28 / 1.28 / 1.38	
	2-Hor.1-Vert. / 1-Hor.2-Vert. / 2-Hor.2-Vert.	
	1.36 / 1.5 / 1.57	
	1.23 / 1.28 / 1.34	
2016	Effectiveness at the end of the process. Four finned heat pipes in Module 1 geometry.	[120]
	Discharging	
	Evaporator length [m] / HTF mass flow rate [kg/s]	
	0.175 / 0.227 / 0.2 / 0.275 / 0.3	
	1.5 / 1.7 / 2.2 / 1.9 / 1.8	
2011	The model geometry and HFT mass flow rate was optimized, maximizing different parameters such as, charging (discharging) effectiveness, effective charging (discharging) rate, energy stored, and overall energy transfer rate.	[125]
	Time [h] / Heat transfer rate [MJ/h]	
	Maximize: A - energy stored (discharged); B - charging (discharging) effectiveness; C - charging (discharging) rate	
	A - 2.156 (7.614)B - 0.445 (1.293)C - 0.445 (1.293) / A - 2.746 (0.845)B - 4.446 (2.292)C - 4.446 (2.292)	
	A - 0.586 (4.564)B - 0.284 (0.392)C - 0.586 (0.392) / A - 7.542 (1.120)B - 5.981 (3.745)C - 7.542 (3.745)	
2013	A square TES with embedded heat pipes was modelled by using the simplified thermal resistance network method. The PCM with was contained into tubes, where the heat pipes were attached and the HTF	[121]
2014	flows around them. Different heat pipes configurations, and metal foam pore density and porosity were studied. The results showed that 2-vertical heat pipe arrangement with 40 pore per square inch (PPI) pore density, and 0.9 porosity gave the highest discharging power, and effectiveness (0.925). When charging the best configuration was 2-vertical heat pipes as well, 0.8 porosity, and 10 PPI, yielded 1.393 charging effectiveness.	[119]

Fig. 29. Chang et al. [117,134], different geometries modelled, heat pipe with a hollow cylinder in the vapour channel (left), heat pipe with a cylinder full of PCM in the vapour core (middle), and a heat pipe with six small PCM cylinders distributed around the vapour core (right).

heat pipe geometry, working fluid, wick structure, and operational temperature were investigated by evaluating the heat pipe thermal resistance [21]. It could be concluded that heat pipe thermal resistance increased with the heat input and decreased if the vapour radius and operating temperature were risen. Also, a 15 mm radius of adiabatic section was enough, and a larger one did not improve the design. Within the last research with this model done by Mahdavi et al. [22] the heat pipe geometrical features were analysed. Three different configurations when the main heat pipe falls into the condenser (straight, rounded, and tapered), and two geometries from the condenser to the secondary heat pipe network (straight and tapered) were studied (Fig. 31d and e respectively). The geometry changes in the secondary heat pipe inlet hardly had any effect on either temperature or pressure distribution at the condenser section. However, when main heat pipe condenser inlet, the tapered corner had lower thermal resistances (14% lower) and higher temperatures were achieved.

$$T_{int} = \frac{1}{\frac{1}{T_o} - \frac{R_g}{h_{fg}} ln\left(\frac{P}{P_o}\right)} \quad (3)$$

Clausius-Clapyron equation, where T_{int} is the interface temperature [K], h_{fg} is the latent heat of evaporation [J/kg], R_g is the gas constant [J/(kg•K)], P is the relative pressure ($P_{absolute}$-P_o) [Pa], T_o and P_o are the operating temperature and pressure.

After considering all studies which deeply model hybrid latent heat TES and heat pipes by using CFD, the assumptions that would lead new numerical studies towards more accurate models (also more complex) but computationally affordable are as follow. The heat pipe is two-dimensional and axisymmetric; liquid and vapour flow in the heat pipe are steady and laminar; gravitational force is negligible; the wick is homogeneous, isotropic (the wick porosity and permeability are constant and uniform), completely saturated with liquid (the heat pipe cannot be dried out), and liquid flow in the porous wick is neglected; heat pipe working fluid evaporation and condensation only occur at the vapour-liquid interface; the vapour energy equation includes the pressure work and viscous dissipation; the saturation temperature at the wick-vapour interface follows Clausius-Clapyron equation (Eq. 3); all working fluid properties are calculated at the heat pipe operating temperature and assumed constant, except the vapour density, which is determined by the ideal gas equation. Common assumptions in regards to the PCM are that pure molten PCM density is the same as solid one, and the molten PCM is a Boussinesq fluid.

6. Conclusions

This paper presents a comprehensive review of the experimental and numerical research performed about heat pipes and latent TES hybrid applications. From the bibliometric study performed and posterior assessment of the retrieved documents from the query, we realised that despite of the concise query, many of the documents were not related to hybrid systems. The review provides details of the studies,

Table 16
Physical model of latent TES with heat pipes.

Year	Heat pipe	PCM	$T_{melting}$ [°C]	Main conclusions	Ref
1990	Stainless steel (sodium)	Lithium hydride	683	A heat pipe with encapsulated PCM cylinder in the evaporator was modelled. Three design were made, (i) the inner cylinder was hollow, (ii) the cylinder was full with PCM, (iii) there were six cylinders with PCM. The transient behaviour of the system was simulated with a numerical model based on finite-difference approximations.	[117][134]
2012	Stainless steel (potasium)	Sodium nitrate	307	A cylindrical latent TES tank with embedded heat pipes was modelled. They compared a heat pipe, a solid rod and a hollow tube. The heat pipe performed better than the others. Then, just with the heat pipe design, the effect of the PCM container height and heat input (output) rate on melting (solidification) was analysed. A longer container showed better melting when charging and discharging happened at the same rate. Increasing the input (output) heat transfer rate, highly affected the bottom (top) temperatures.	[137]
2015	Stainless steel (sodium)	Cu-Si (0.35)	803		[140]
2014	Stainless steel (sodium)	NaCL	800	A latent heat thermal storage with heat pipes was modelled. The unit connected a solar receiver with a Stirling engine. Two heat pipe networks were, the first between the solar receiver and the PCM, and the second between the later and the engine. Three working modes were studied: (i) charging only, (ii) simultaneous charging and discharging, and (iii) discharging only. The further the heat pipes were form each other, the higher were the temperature drops along the TES unit.	[138]
2015	Stainless steel (sodium)	-	-	A latent TES with two sets of heat pipes (main and an array of secondary ones) was modelled. The unit worked coupled with a Stirling engine. With one secondary heat pipe, either main and secondary heat pipes had higher temperature. With two or three secondary heat pipes, the secondary heat pipes temperatures depended on their position. The heat transfer performance was analysed regarding heat pipe geometry, working fluid, wick structure, and operational temperature, by calculating the thermal resistance. Observing that it decreased when the operating temperature and vapour radius rose. Then, the effect of heat pipe geometry when spliting towards the secondary heat pipes was studied. Among different shapes analysed at the main condenser inlet (straight, rounded, and tapered) tapered inlet resulted into the lowest thermal resistances.	[139] [21] [22]
2016					
2017	Stainless steel (sodium)	LiF•CaF_2 (80.5%/19.5%)	307	A physical model of a heat pipe receiver integrated with a latent TES was developed. The system exergy efficiency was analysed regarding several parameters. The model was optimized with a genetic algorithm. The exergy efficiency was maximized when the heat pipe evaporator, adiabatic and condenser sections length were 0.36, 0.41, and 0.43 m respectively.	[135]

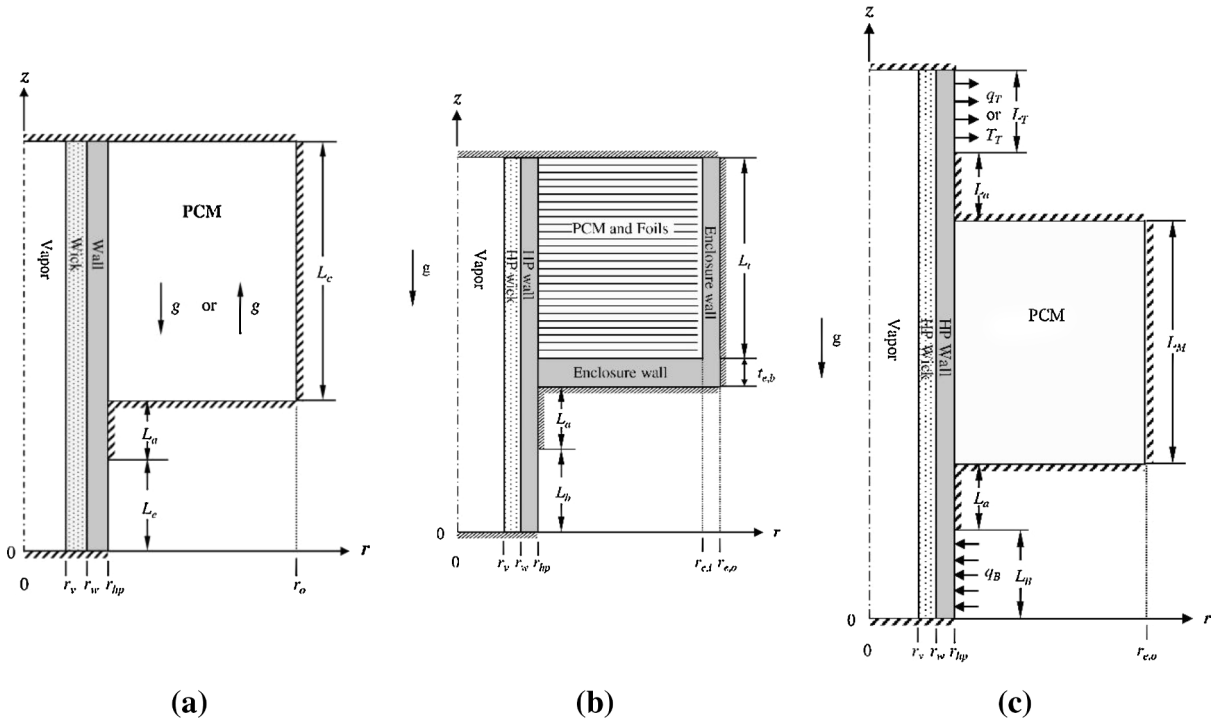

Fig. 30. Sharifi et al. physical model and computational domain. (a) Design for charging and discharging alternately [137], (b) foil addition [17] (c) system able to charge and discharge simultaneously [140].

helping new researchers to find paths to be further explored in regards to this technology.

It was observed that the main goal for these hybrid systems was to work in couple with solar applications. However, this solar experimental research was mainly dedicated to low temperatures applications. The other interested fields regarding coupling of latent TES and heat pipes were cooling for electronics or electric batteries. But the latter two the PCM usually worked as a thermal shock absorber, avoiding overheating of electric equipment.

While most of experimental works were dedicated to low temperature applications (mainly around 55ºC), efforts using numerical modelling were focused on high temperature applications. The procedure followed by many was first to develop a model of the design, second to validate it with experiments at low temperature and third, to apply the model to higher temperature applications. However, when escalating up the device, slight differences between model and experimental could be also scaled up. Therefore, further experimental research needs to be done to validate the models at high temperature before jumping to real scale facilities.

Also, regarding the research on modelling, many documents simulated the heat pipe as high thermal conductive solid (e.g. the heat pipe is modelled as a copper pipe which conductivity is 90 times higher). Those models although performing well when being validated with experimental tests at low temperatures, they did not describe the working principle of the heat pipe as good as solving Navier-Stokes equations, as described in heat pipe modelled by using CFD Section 5.3. It was true that the computational cost was highly reduced, so they were a good starting point when modelling a hybrid latent TES system. However, a detailed CFD modelling should be used in case that the model precedes a new equipment design, especially at high temperatures, to ensure a proper and safer approximation.

All in all, from the assessment performed in this review, some guidelines for future research about hybrid systems (latent heat TES and heat pipes) can be drawn. Taking into account that one of this hybrid technology biggest potential is found within solar applications, but just a few were performed at high temperature range (> 150 °C), contributing to this gap experimentally would be the main advice. Also, this hypothetically future research will fill the gap found into numerical research, which necessity to be validated at higher temperatures with experimental data is yet to be done.

CRediT authorship contribution statement

José Miguel Maldonado: Conceptualization, Investigation, Writing - original draft, Writing - review & editing. **Alvaro de Gracia:** Conceptualization, Methodology, Resources, Writing - review & editing, Visualization, Supervision, Project administration. **Luisa F. Cabeza:** Conceptualization, Methodology, Resources, Writing - review & editing, Visualization, Supervision, Project administration, Funding acquisition.

Declaration of Competing Interest

The authors declare that they have no known competing financial interests or personal relationships that could have appeared to influence the work reported in this paper.

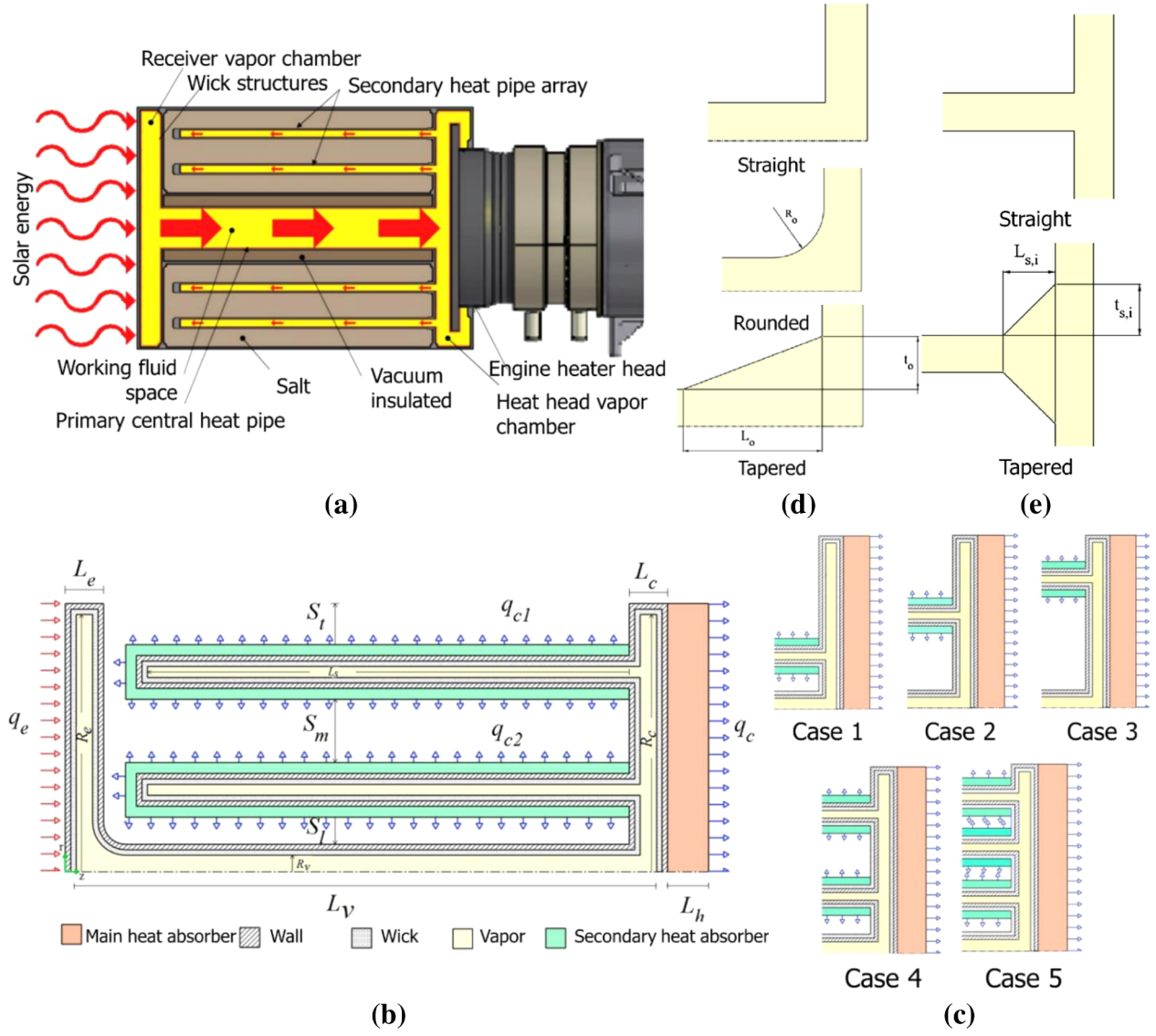

Fig. 31. Mahdavi et al. latent TES unit with two heat pipe network model. (a) Unit concept, (b) addition of porous wall to the model, (c) heat pipe studied locations, (d) different heat pipe network geometries studied. Adapted from [21,22,139].

Acknowledgements

This work was partially funded by the European Union's Horizon 2020 Research & Innovation Programme under Grant Agreement 723596 with reference name Innova MicroSolar. This work was partially funded by the Ministerio de Ciencia, Innovación y Universidades de España (RTI2018-093849-B-C31 - MCIU/AEI/FEDER, UE) and by the Agencia Estatal de Investigación (AEI), of the Ministerio de Ciencia, Innovación y Universidades (RED2018-102431-T). José Miguel Maldonado would like to thank the Spanish Government for his research fellowship (BES-2016-076554). The authors would like to thank the Catalan Government for the quality accreditation given to their research group (2017 SGR 1537). GREiA is a certified TECNIO agent in the category of technology developers from the Government of Catalonia. This work is partially supported by ICREA under the ICREA Academia programme.

References

[1] MR Gilpin, DB Scharfe, MP Young, RN Webb, High Energy Advanced Thermal Storage (HEATS) - Final Report, High Energy Advanced Thermal Storage (HEATS) - Final Report 33 (2018) https://apps.dtic.mil/sti/citations/AD1063579 (accessed June 12, 2020).

[2] A. Faghri, Heat pipes: review, opportunities and challenges, Front Heat Pipes 5 (2014), https://doi.org/10.5098/fhp.5.1.

[3] J Gasia, L Miró, LF Cabeza, Review on system and materials requirements for high temperature thermal energy storage. Part 1: General requirements, Renew. Sustain. Energy Rev. 75 (2017) 1320–1338, https://doi.org/10.1016/j.rser.2016.11.119.

[4] B Zalba, JM Marín, LF Cabeza, H Mehling, Review on thermal energy storage with phase change: materials, heat transfer analysis and applications, Appl. Therm. Eng. 23 (2003) 251–283, https://doi.org/10.1016/S1359-4311(02)00192-8.

[5] MS Naghavi, KS Ong, M Mehrali, IA Badruddin, HSC Metselaar, A state-of-the-art review on hybrid heat pipe latent heat storage systems, Energy Convers. Manag. 105 (2015) 1178–1204, https://doi.org/10.1016/j.enconman.2015.08.044.

[6] J Gasia, L Miró, LF Cabeza, Materials and system requirements of high temperature thermal energy storage systems: a review. Part 2: Thermal conductivity enhancement techniques, Renew. Sustain. Energy Rev. 60 (2016) 1584–1601, https://doi.org/10.1016/j.rser.2016.03.019.

[7] GY. Eastman, The heat pipe, Sci. Am. 218 (1968) 38–46.

[8] A. Faghri, Review and advances in heat pipe science and technology, J. Heat Transf. 134 (2012) 1–18, https://doi.org/10.1115/1.4007407.

[9] A. Faghri, Washington, D.C (Ed.), first ed., Taylor & Francis, 1995.

[10] WF Lamb, MW Callaghan, F Creutzig, R Khosla, JC Minx, The literature landscape on 1.5°C climate change and cities, Curr. Opin. Environ. Sustain. 30 (2018) 26–34, https://doi.org/10.1016/j.cosust.2018.02.008.

[11] A Crespo, C Barreneche, M Ibarra, W Platzer, Latent thermal energy storage for solar process heat applications at medium-high temperatures – a review, Sol. Energy 192 (2019) 3–34, https://doi.org/10.1016/j.solener.2018.06.101.

[12] A. Abhat, Performance Studies of a Finned Heat Pipe Latent Thermal Energy

Storage System, Pergamon Press, Sun, NY, 1978, pp. 541–546, https://doi.org/10.1016/b978-1-4832-8407-1.50106-9.
[13] A. Abhat, Thermal performance of a finned heat-pipe latent heat store, Int. J. Ambient Energy 5 (1984) 193–206, https://doi.org/10.1080/01430750.1984.9675429.
[14] Z Liu, Z Wang, C Ma, An experimental study on heat transfer characteristics of heat pipe heat exchanger with latent heat storage. Part I: Charging only and discharging only modes, Energy Convers. Manag. 47 (2006) 944–966, https://doi.org/10.1016/j.enconman.2005.06.004.
[15] Z Liu, Z Wang, C Ma, An experimental study on the heat transfer characteristics of a heat pipe heat exchanger with latent heat storage. Part II: Simultaneous charging/discharging modes, Energy Convers. Manag. 47 (2006) 967–991, https://doi.org/10.1016/j.enconman.2005.06.007.
[16] CW Robak, TL Bergman, A Faghri, Enhancement of latent heat energy storage using embedded heat pipes, Int. J. Heat Mass Transf. 54 (2011) 3476–3484, https://doi.org/10.1016/j.ijheatmasstransfer.2011.03.038.
[17] N Sharifi, TL Bergman, MJ Allen, A Faghri, Melting and solidification enhancement using a combined heat pipe, foil approach, Int. J. Heat Mass Transf. 78 (2014) 930–941, https://doi.org/10.1016/j.ijheatmasstransfer.2014.07.054.
[18] MJ Allen, A Faghri, TL Bergman, Robust heat transfer enhancement during melting and solidification of a PCM using a combined heat pipe-metal foam or foil configuration, ASME 2014 8th Int. Conf. Energy Sustain, Boston, U.S.A., 2014, pp. 1–12.
[19] MJ Allen, N Sharifi, A Faghri, TL Bergman, Effect of inclination angle during melting and solidification of a phase change material using a combined heat pipe-metal foam or foil configuration, Int. J. Heat Mass Transf. 80 (2015) 767–780, https://doi.org/10.1115/1.4029970.
[20] S Tiari, M Mahdavi, S Qiu, Experimental study of a latent heat thermal energy storage system assisted by a heat pipe network, Energy Convers. Manag. 153 (2017) 362–373, https://doi.org/10.1016/j.enconman.2017.10.019.
[21] M Mahdavi, S Qiu, S Tiari, Numerical investigation of hydrodynamics and thermal performance of a specially configured heat pipe for higherature thermal energy storage systems, Appl. Therm. Eng. 81 (2015) 325–337, https://doi.org/10.1016/j.applthermaleng.2015.02.031.
[22] M Mahdavi, S Qiu, S Tiari, Improvement of a novel heat pipe network designed for latent heat thermal energy storage systems, Appl. Therm. Eng. 108 (2016) 878–892, https://doi.org/10.1016/j.applthermaleng.2016.07.190.
[23] S Motahar, R. Khodabandeh, Experimental study on the melting and solidification of a phase change material enhanced by heat pipe, Int. Commun. Heat Mass Transf. 73 (2016) 1–6, https://doi.org/10.1016/j.icheatmasstransfer.2016.02.012.
[24] A Saraswat, R Bhattacharjee, A Verma, MK Das, S Khandekar, Investigation of diffusional transport of heat and its enhancement in phase-change thermal energy storage systems, Appl. Therm. Eng. 111 (2017) 1611–1621, https://doi.org/10.1016/j.applthermaleng.2016.06.178.
[25] A Khalifa, L Tan, A Date, A Akbarzadeh, A numerical and experimental study of solidification around axially finned heat pipes for high temperature latent heat thermal energy storage units, Appl. Therm. Eng. 70 (2014) 609–619, https://doi.org/10.1016/j.applthermaleng.2014.05.080.
[26] H Shabgard, TL Bergman, N Sharifi, A Faghri, High temperature latent heat thermal energy storage using heat pipes, Int. J. Heat Mass Transf. 53 (2010) 2979–2988, https://doi.org/10.1016/j.ijheatmasstransfer.2010.03.035.
[27] A Khalifa, L Tan, A Date, A Akbarzadeh, Performance of suspended finned heat pipes in high-temperature latent heat thermal energy storage, Appl. Therm. Eng. 81 (2015) 242–252, https://doi.org/10.1016/j.applthermaleng.2015.02.030.
[28] A Khalifa, L Tan, D Mahony, A Date, A Akbarzadeh, Numerical analysis of latent heat thermal energy storage using miniature heat pipes: a potential thermal enhancement for CSP plant development, Appl. Therm. Eng. 108 (2016) 93–103, https://doi.org/10.1016/j.applthermaleng.2016.07.111.
[29] L Weiss, A Moore, A Hays, F Eboda, E Borquist, Operational enhancements for small scale thermal energy storage devices, Microsyst. Technol. 24 (2018) 2617–2625, https://doi.org/10.1007/s00542-018-3743-3.
[30] A Amini, J Miller, H Jouhara, An investigation into the use of the heat pipe technology in thermal energy storage heat exchangers, Energy 136 (2017) 163–172, https://doi.org/10.1016/j.energy.2016.02.089.
[31] XH Wu, WP Li, Y Wang, ZJ Chang, CX Wang, C Ding, Experimental investigation of the performance of cool storage shelf for vertical open refrigerated display cabinet, Int. J. Heat Mass Transf. 110 (2017) 789–795, https://doi.org/10.1016/j.ijheatmasstransfer.2017.03.071.
[32] Zhao YH, Zhang K, Diao YH. Heat Pipe with Micro-Pore Tubes Array and Making Method Thereof and Heat Exchanging System. US Patent No: US 2011/0203777, 2011.
[33] YH Diao, S Wang, YH Zhao, TT Zhu, CZ Li, FF Li, Experimental study of the heat transfer characteristics of a new-type flat micro-heat pipe thermal storage unit, Appl. Therm. Eng. 89 (2015) 871–882, https://doi.org/10.1016/j.applthermaleng.2015.06.070.
[34] FF Li, YH Diao, YH Zhao, TT Zhu, J Liu, Experimental study on the thermal performance of a new type of thermal energy storage based on flat micro-heat pipe array, Energy Convers. Manag. 112 (2016) 395–403, https://doi.org/10.1016/j.enconman.2016.01.039.
[35] T Wang, Y Diao, T Zhu, Y Zhao, J Liu, X Wei, Thermal performance of solar air collection-storage system with phase change material based on flat micro-heat pipe arrays, Energy Convers. Manag. 142 (2017) 230–243, https://doi.org/10.1016/j.enconman.2017.03.039.
[36] Y Diao, Y Kang, L Liang, Y Zhao, T Zhu, Experimental investigation on the heat transfer performance of a latent thermal energy storage device based on flat miniature heat pipe arrays, Energy 138 (2017) 929–941, https://doi.org/10.1016/j.energy.2017.07.090.
[37] ZY Wang, YH Diao, L Liang, YH Zhao, TT Zhu, FW Bai, Experimental study on an integrated collector storage solar air heater based on flat micro-heat pipe arrays, Energy Build. 152 (2017) 615–628, https://doi.org/10.1016/j.enbuild.2017.07.069.
[38] ZY Wang, YH Diao, YH Zhao, L Liang, TY Wang, Experimental study on the new type of electrical storage heater based on flat micro-heat pipe arrays, Sci. China Technol. Sci. 61 (2018) 219–231, https://doi.org/10.1007/s11431-017-9121-6.
[39] Z Wang, Y Diao, Y Zhao, T Wang, L Liang, Y Chi, Experimental investigation of an integrated collector–storage solar air heater based on the lap joint-type flat micro-heat pipe arrays, Energy 160 (2018) 924–939, https://doi.org/10.1016/j.energy.2018.07.052.
[40] Z Wang, Y Diao, Y Zhao, L Yin, C Chen, L Liang, et al., Performance investigation of an integrated collector–storage solar water heater based on lap-joint-type micro-heat pipe arrays, Appl. Therm. Eng. 153 (2019) 808–827, https://doi.org/10.1016/j.applthermaleng.2019.03.066.
[41] Z Wang, Y Diao, Y Zhao, C Chen, L Liang, T Wang, Thermal performance investigation of an integrated collector–storage solar air heater on the basis of lap joint-type flat micro-heat pipe arrays: simultaneous charging and discharging mode, Energy 181 (2019) 882–896, https://doi.org/10.1016/j.energy.2019.05.197.
[42] YH Diao, L Liang, YH Zhao, ZY Wang, FW Bai, Numerical investigation of the thermal performance enhancement of latent heat thermal energy storage using longitudinal rectangular fins and flat micro-heat pipe arrays, Appl. Energy 233–234 (2019) 894–905, https://doi.org/10.1016/j.apenergy.2018.10.024.
[43] YH Diao, LL Yin, ZY Wang, YH Zhao, L Liang, FW Bai, Numerical analysis of heat transfer characteristics for air in a latent heat thermal energy storage using flat miniature heat pipe arrays, Appl. Therm. Eng. 162 (2019), https://doi.org/10.1016/j.applthermaleng.2019.114247.
[44] TT Zhu, YH Diao, YH Zhao, FF Li, Thermal performance of a new CPC solar air collector with flat micro-heat pipe arrays, Appl. Therm. Eng. 98 (2016) 1201–1213, https://doi.org/10.1016/j.applthermaleng.2016.01.033.
[45] CL Ladekar, SK Chaudhary, SS Khandare, Experimental Investigate for optimization of heat pipe performance in latent heat thermal energy storage, Mater. Today Proc. 4 (2017) 8149–8157, https://doi.org/10.1016/j.matpr.2017.07.156.
[46] C Ladekar, SK Choudhary, SS Khandare, Experimental investigation for the optimization of heat pipe performance in latent heat thermal storage, J. Mech. Sci. Technol. 31 (2017) 2627–2634, https://doi.org/10.1007/s12206-017-0505-6.
[47] VM Shinde, RR Chavan, V Bhagwat V, Experimental analysis of a solar dehydration with phase changing material, Int. J. Eng. Res. Technol. 6 (2017) 327–332, https://doi.org/10.17577/IJERTV6IS030382.
[48] M Faegh, MB. Shafii, Experimental investigation of a solar still equipped with an external heat storage system using phase change materials and heat pipes, Desalination 409 (2017) 128–135, https://doi.org/10.1016/j.desal.2017.01.023.
[49] MS Naghavi, KS Ong, IA Badruddin, M Mehrali, HSC Metselaar, Thermal performance of a compact design heat pipe solar collector with latent heat storage in charging/discharging modes, Energy 127 (2017) 101–115, https://doi.org/10.1016/j.energy.2017.03.097.
[50] A Papadimitratos, S Sobhansarbandi, V Pozdin, A Zakhidov, F Hassanipour, Evacuated tube solar collectors integrated with phase change materials, Sol. Energy 129 (2016) 10–19, https://doi.org/10.1016/j.solener.2015.12.040.
[51] A Papadimitratos, S Sobhansarbandi, V Pozdin, A Zakhidov, F Hassanipour, Evacuated tube solar collectors integrated with phase change materials and silicone oil, Am. Soc. Mech. Eng. Power Div. POWER 2 (2017) 1–9, https://doi.org/10.1115/POWER-ICOPE2017-3520 Charlotte, North Carolina, USA.
[52] P Feliński, R. Sekret, Experimental study of evacuated tube collector/storage system containing paraffin as a PCM, Energy 114 (2016) 1063–1072, https://doi.org/10.1016/j.energy.2016.08.057.
[53] P Feliński, R. Sekret, Effect of a low cost parabolic reflector on the charging efficiency of an evacuated tube collector/storage system with a PCM, Sol. Energy 144 (2017) 758–766, https://doi.org/10.1016/j.solener.2017.01.073.
[54] B Li, X. Zhai, Experimental investigation and theoretical analysis on a mid-temperature solar collector/storage system with composite PCM, Appl. Therm. Eng. 124 (2017) 34–43, https://doi.org/10.1016/j.applthermaleng.2017.06.002.
[55] Y Bai, X He, Y Liu, J Duan, Y Wang, X Han, Experimental investigation of a solar thermal storage heater assembled with finned heat pipe and collective vacuum tubes, Energy Convers. Manag. 166 (2018) 463–473, https://doi.org/10.1016/j.enconman.2018.04.034.
[56] J Wu, T Xian, X Liu, All-weather characteristic studies of a direct expansion solar integrated air source heat pump system based on PCMs, Sol. Energy 191 (2019) 34–45, https://doi.org/10.1016/j.solener.2019.08.057.
[57] W Wu, S Dai, Z Liu, Y Dou, J Hua, M Li, et al., Experimental study on the performance of a novel solar water heating system with and without PCM, Sol. Energy 171 (2018) 604–612, https://doi.org/10.1016/j.solener.2018.07.005.
[58] Z Wang, J Zhang, Z Wang, W Yang, X Zhao, Experimental investigation of the performance of the novel HP-BIPV/T system for use in residential buildings, Energy Build. 130 (2016) 295–308, https://doi.org/10.1016/j.enbuild.2016.08.060.
[59] M Modjinou, J Ji, W Yuan, F Zhou, S Holliday, A Waqas, et al., Performance comparison of encapsulated PCM PV/T, microchannel heat pipe PV/T and conventional PV/T systems, Energy 166 (2019) 1249–1266, https://doi.org/10.1016/j.energy.2018.10.007.
[60] YC Weng, HP Cho, CC Chang, SL Chen, Heat pipe with PCM for electronic cooling, Appl. Energy 88 (2011) 1825–1833, https://doi.org/10.1016/j.apenergy.2010.12.004.

[61] J Krishna, PS Kishore, AB Solomon, Heat pipe with nano enhanced-PCM for electronic cooling application, Exp. Therm. Fluid Sci. 81 (2017) 84–92, https://doi.org/10.1016/j.expthermflusci.2016.10.014.
[62] J Krishna, PS Kishore, A Brusly Solomon, Experimental study of thermal energy storage characteristics using heat pipe with nano-enhanced phase change materials, IOP Conf. Ser. Mater. Sci. Eng. 225 2017, pp. 1–8, , https://doi.org/10.1088/1757-899X/225/1/012058 Hyderabad, India.
[63] SS Chougule, SK. Sahu, Thermal performance of nanofluid charged heat pipe with phase change material for electronics cooling, J. Electron Packag. Trans. ASME 137 (2015) 1–7, https://doi.org/10.1115/1.4028994.
[64] SS Chougule, V. Nirgude V, SP Shewale, AT Pise, SK Sahu, H. Shah, Application of paraffin based nanocomposite in heat pipe module for electronic equipment cooling, Mater. Today Proc. 5 (2018) 23333–23338, https://doi.org/10.1016/j.matpr.2018.11.070.
[65] B Zhuang, W Deng, Y Tang, X Ding, K Chen, G Zhong, et al., Experimental investigation on a novel composite heat pipe with phase change materials coated on the adiabatic section, Int. Commun. Heat Mass Transf. 100 (2019) 42–50, https://doi.org/10.1016/j.icheatmasstransfer.2018.12.006.
[66] Y Wu, Y Tang, Z Li, X Ding, W Yuan, X Zhao, et al., Experimental investigation of a PCM-HP heat sink on its thermal performance and anti-thermal-shock capacity for high-power LEDs, Appl. Therm. Eng. 108 (2016) 192–203, https://doi.org/10.1016/j.applthermaleng.2016.07.127.
[67] X-H Yang, S-C Tan, Z-Z He, J Liu, Finned heat pipe assisted low melting point metal PCM heat sink against extremely high power thermal shock, Energy Convers. Manag. 160 (2018) 467–476, https://doi.org/10.1016/j.enconman.2018.01.056.
[68] ZW Li, LC Lv, J Li, Combination of heat storage and thermal spreading for high power portable electronics cooling, Int. J. Heat Mass Transf. 98 (2016) 550–557, https://doi.org/10.1016/j.ijheatmasstransfer.2016.03.068.
[69] B Shang, Y Ma, R Hu, C Yuan, J Hu, X Luo, Passive thermal management system for downhole electronics in harsh thermal environments, Appl. Therm. Eng. 118 (2017) 593–599, https://doi.org/10.1016/j.applthermaleng.2017.01.118.
[70] H Behi, M Ghanbarpour, M Behi, Investigation of PCM-assisted heat pipe for electronic cooling, Appl. Therm. Eng. 127 (2017) 1132–1142, https://doi.org/10.1016/j.applthermaleng.2017.08.109.
[71] CP Tso, FL Tan, J Jony, Transient and cyclic effects on a pcm-cooled mobile device, Therm. Sci. 19 (2015) 1723–1731, https://doi.org/10.2298/TSCI121206112T.
[72] J Krishna, PS Kishore, A Brusly Solomon, Experimental study of thermal energy storage characteristics using heat pipe with nano-enhanced phase change materials, IOP Conf Ser Mater Sci Eng, 225 2017, https://doi.org/10.1088/1757-899X/225/1/012058.
[73] Z Rao, S Wang, M Wu, Z Lin, F Li, Experimental investigation on thermal management of electric vehicle battery with heat pipe, Energy Convers. Manag. 65 (2013) 92–97, https://doi.org/10.1016/j.enconman.2012.08.014.
[74] Z Rao, Y Huo, X Liu, Experimental study of an OHP-cooled thermal management system for electric vehicle power battery, Exp. Therm. Fluid Sci. 57 (2014) 20–26, https://doi.org/10.1016/j.expthermflusci.2014.03.017.
[75] Q Wang, Z Rao, Y Huo, S Wang, Thermal performance of phase change material/oscillating heat pipe-based battery thermal management system, Int. J. Therm. Sci. 102 (2016) 9–16, https://doi.org/10.1016/j.ijthermalsci.2015.11.005.
[76] J Zhao, Z Rao, C Liu, Y Li, Experimental investigation on thermal performance of phase change material coupled with closed-loop oscillating heat pipe (PCM/CLOHP) used in thermal management, Appl. Therm. Eng. 93 (2016) 90–100, https://doi.org/10.1016/j.applthermaleng.2015.09.018.
[77] Z Rao, Y Huo, X Liu, Experimental study of an OHP-cooled thermal management system for electric vehicle power battery, Exp. Therm. Fluid Sci. 57 (2014) 20–26, https://doi.org/10.1016/j.expthermflusci.2014.03.017.
[78] J Zhao, Z Rao, C Liu, Y Li, Experiment study of oscillating heat pipe and phase change materials coupled for thermal energy storage and thermal management, Int. J. Heat Mass Transf. 99 (2016) 252–260, https://doi.org/10.1016/j.ijheatmasstransfer.2016.03.108.
[79] J Zhao, J Qu, Z Rao, Thermal characteristic and analysis of closed loop oscillation heat pipe/phase change material (CLOHP/PCM) coupling module with different working media, Int. J. Heat Mass Transf. 126 (2018) 257–266, https://doi.org/10.1016/j.ijheatmasstransfer.2018.05.125.
[80] J Zhao, J Qu, Z Rao, Experiment investigation on thermal performance of a large-scale oscillating heat pipe with self-rewetting fluid used for thermal energy storage, Int. J. Heat Mass Transf. 108 (2017) 760–769, https://doi.org/10.1016/j.ijheatmasstransfer.2016.12.093.
[81] J Qu, Z Ke, A Zuo, Z Rao, Experimental investigation on thermal performance of phase change material coupled with three-dimensional oscillating heat pipe (PCM/3D-OHP) for thermal management application, Int. J. Heat Mass Transf. 129 (2019) 773–782, https://doi.org/10.1016/j.ijheatmasstransfer.2018.10.019.
[82] J Zhao, P Lv, Z Rao, Experimental study on the thermal management performance of phase change material coupled with heat pipe for cylindrical power battery pack, Exp. Therm. Fluid Sci. 82 (2017) 182–188, https://doi.org/10.1016/j.expthermflusci.2016.11.017.
[83] Q Huang, X Li, G Zhang, J Zhang, F He, Y Li, Experimental investigation of the thermal performance of heat pipe assisted phase change material for battery thermal management system, Appl. Therm. Eng. 141 (2018) 1092–1100, https://doi.org/10.1016/j.applthermaleng.2018.06.048.
[84] J Gou, W Liu, Y Luo, The thermal performance of a novel internal cooling method for the electric vehicle battery: an experimental study, Appl. Therm. Eng. 161 (2019), https://doi.org/10.1016/j.applthermaleng.2019.114102.
[85] T Yamada, T Koshiyama, M Yoshikawa, T Yamada, N Ono, Analysis of a lithium-ion battery cooling system for electric vehicles using a phase-change material and heat pipes, J. Therm. Sci. Technol. 12 (2017) 1–15, https://doi.org/10.1299/jtst.2017jtst0011.
[86] W Wu, X Yang, G Zhang, K Chen, S Wang, Experimental investigation on the thermal performance of heat pipe-assisted phase change material based battery thermal management system, Energy Convers. Manag. 138 (2017) 486–492, https://doi.org/10.1016/j.enconman.2017.02.022.
[87] C Zhang, S Chen, H Gao, K Xu, Z Xia, S Li, Study of thermal management system using composite phase change materials and thermoelectric cooling sheet for power battery pack, Energies 12 (2019) 1937–1951, https://doi.org/10.3390/en12101937.
[88] JR Turnpenny, DW Etheridge, DA Reay, Novel ventilation cooling system for reducing air conditioning in buildings. Part I: testing and theoretical modelling, Appl. Therm. Eng. 20 (2000) 1019–1037, https://doi.org/10.1016/S1359-4311(01)00003-5.
[89] JR Turnpenny, DW Etheridge, DA Reay, Novel ventilation system for reducing air conditioning in buildings. Part II : testing of prototype, Appl. Therm. Eng. 21 (2001) 1203–1217.
[90] D Etheridge, K Murphy, D Reay, A PCM/heat pipe cooling system for reducing air conditioning in buildings: review of options and report on field tests, Build. Serv. Eng. Res. Technol. 27 (2006) 27–39, https://doi.org/10.1191/0143624406bt142oa.
[91] BW Hu, Q Wang, ZH Liu, Fundamental research on the gravity assisted heat pipe thermal storage unit (GAHP-TSU) with porous phase change materials (PCMs) for medium temperature applications, Energy Convers. Manag. 89 (2015) 376–386, https://doi.org/10.1016/j.enconman.2014.10.017.
[92] Z Liu, B Zheng, Q Wang, S-S Li, Study on the thermal storage performance of a gravity-assisted heat-pipe thermal storage unit with granular high-temperature phase-change materials, Energy 81 (2015) 754–765, https://doi.org/10.1016/j.energy.2015.01.025.
[93] S Qiu, R Galbraith, M White, Phase change material thermal energy storage system design and optimization, Proc. ASME 2013 7th Int. Conf. Energy Sustain, Minneapolis, MN, 2013, pp. 1–8.
[94] S Qiu, L Solomon, G Rinker, Development of an integrated thermal energy storage and free-piston stirling generator for a concentrating solar power system, Energies 10 (2017), https://doi.org/10.3390/en10091361.
[95] C Oshman, C Hardin, J Rea, ML Olsen, N Siegel, G Glatzmaier, et al., Design of a thermosyphon-based thermal valve for controlled high-temperature heat extraction, Appl. Therm. Eng. 126 (2017) 1141–1147, https://doi.org/10.1016/j.applthermaleng.2017.01.038.
[96] C Oshman, J Rea, C Hardin, ML Olsen, J Alleman, G Glatzmaier, et al., Reliability and heat transfer performance of a miniature high-temperature thermosyphon-based thermal valve, Int. J. Heat Mass Transf. 125 (2018) 1079–1086, https://doi.org/10.1016/j.ijheatmasstransfer.2018.04.159.
[97] JE Rea, C Oshman, CL Hardin, A Singh, J Alleman, G Glatzmaier, et al., Experimental demonstration of a latent heat storage system for dispatchable electricity, AIP Conf Proc, 2033 2018, pp. 1218–1229, , https://doi.org/10.1063/1.5067116.
[98] S Qiu, R Galbraith, M White, Phase change material thermal energy storage system design and optimization songgang, Proc. ASME 2013 7th Int. Conf. Energy Sustain. Minneapolis, MN, 2013, pp. 1–8.
[99] GR Kumaresh, F Duan, FL Tan, CP Tso, Thermal designs for mobile phones cooled with use of phase change material and heat pipe, Int. J. Prod. Dev. 18 (2013) 411–432, https://doi.org/10.1504/IJPD.2013.058450.
[100] S Tiari, S Qiu, M Mahdavi, Numerical study of finned heat pipe-assisted thermal energy storage system with high temperature phase change material, Energy Convers. Manag. 89 (2015) 833–842, https://doi.org/10.1016/j.enconman.2014.10.053.
[101] S Tiari, S. Qiu, Three-dimensional simulation of high temperature latent heat thermal energy storage system assisted by finned heat pipes, Energy Convers. Manag. 105 (2015) 260–271, https://doi.org/10.1016/j.enconman.2015.08.004.
[102] S Tiari, M Mahdavi, V Thakore, S Joseph, Thermal analysis of a high-temperature heat pipe-assisted thermal energy storage system with nano-enhanced phase change material, ASME Int. Mech. Eng. Congr. Expo Proc. 6B-2018 (2018) 1–10, https://doi.org/10.1115/IMECE2018-86481.
[103] M Mahdavi, S Tiari, V Pawar, Heat transfer analysis of a low-temperature heat pipe-assisted latent heat thermal energy storage system with nano-enhanced PCM, ASME Int. Mech. Eng. Congr. Expo Proc. 6B-2018 (2018) 1–9, https://doi.org/10.1115/IMECE2018-86609.
[104] A Ebrahimi, MJ Hosseini, AA Ranjbar, M Rahimi, R Bahrampoury, Melting process investigation of phase change materials in a shell and tube heat exchanger enhanced with heat pipe, Renew. Energy 138 (2019) 378–394, https://doi.org/10.1016/j.renene.2019.01.110.
[105] S Tiari, S Qiu, M Mahdavi, Discharging process of a finned heat pipe-assisted thermal energy storage system with high temperature phase change material, Energy Convers. Manag. 118 (2016) 426–437, https://doi.org/10.1016/j.enconman.2016.04.025.
[106] SC Costa, K Mahkamov, M Kenisarin, K Lynn, E Halimic, D Mullen, Solar salt latent heat thermal storage for a small solar organic rankine cycle plant, ASME 2018 12th Int Conf Energy Sustain ES 2018, Collocated with ASME 2018 Power Conf ASME 2018 Nucl Forum, 2018, pp. 1–10, , https://doi.org/10.1115/1.4044557.
[107] X Gui, W Qu, B Lin, X Yuan, Two-dimensional transient thermal analysis of a Phase-Change-Material canister of a heat-pipe receiver under gravity, J. Therm. Sci. 19 (2010) 160–166, https://doi.org/10.1007/s11630-010-0160-z.
[108] G Xiaohong, L Bin, G Yongxian, Y Xiugan, Two-dimensional transient thermal analysis of PCM canister of a heat pipe receiver under microgravity, Appl. Therm.

Eng. 31 (2011) 735–741, https://doi.org/10.1016/j.applthermaleng.2010.10.016.
[109] X Song, Q Song, X Gui, S Liang, D Tang, Influence of void ratio on phase change in thermal storage canister of heat pipe receiver, Heat Transf. Eng. 36 (2015) 1154–1162, https://doi.org/10.1080/01457632.2015.987630.
[110] X Gui, X Song, B Nie, Thermal analysis of void cavity for heat pipe receiver under microgravity, J. Therm. Sci. 26 (2017) 138–143, https://doi.org/10.1007/s11630-017-0922-y.
[111] C Pan, N Vermaak, C Romero, S Neti, S Hoenig, CH Chen, Efficient optimization of a longitudinal finned heat pipe structure for a latent thermal energy storage system, Energy Convers. Manag. 153 (2017) 93–105, https://doi.org/10.1016/j.enconman.2017.09.064.
[112] C Pan, N Vermaak, C Romero, S Neti, S Hoenig, CH Chen, et al., Cost estimation and sensitivity analysis of a latent thermal energy storage system for supplementary cooling of air cooled condensers, Appl. Energy 224 (2018) 52–68, https://doi.org/10.1016/j.apenergy.2018.04.080.
[113] S Lohrasbi, SZ Miry, M Gorji-Bandpy, DD Ganji, Performance enhancement of finned heat pipe assisted latent heat thermal energy storage system in the presence of nano-enhanced H2O as phase change material, Int. J. Hydrog. Energy 42 (2017) 6526–6546, https://doi.org/10.1016/j.ijhydene.2017.01.045.
[114] S Lohrasbi, M Gorji-Bandpy, DD Ganji, Thermal penetration depth enhancement in latent heat thermal energy storage system in the presence of heat pipe based on both charging and discharging processes, Energy Convers. Manag. 148 (2017) 646–667, https://doi.org/10.1016/j.enconman.2017.06.034.
[115] Q Ren, F Meng, P Guo, A comparative study of PCM melting process in a heat pipe-assisted LHTES unit enhanced with nanoparticles and metal foams by immersed boundary-lattice Boltzmann method at pore-scale, Int. J. Heat Mass Transf. 121 (2018) 1214–1228, https://doi.org/10.1016/j.ijheatmasstransfer.2018.01.046.
[116] Q. Ren, Enhancement of nanoparticle-phase change material melting performance using a sinusoidal heat pipe, Energy Convers. Manag. 180 (2019) 784–795, https://doi.org/10.1016/j.enconman.2018.11.033.
[117] M Chang, LC Chow, WS Chang, M Morgan, Transient behavior of heat pipe with thermal energy storage under reversed-pulsed heat loads, AIAA 26th Thermophys. Conf. 1991, Honolulu, Hawaii, 1991, p. 11, , https://doi.org/10.2514/6.1990-1754.
[118] EG Jung, JH. Boo, Thermal analytical model of latent thermal storage with heat pipe heat exchanger for concentrated solar power, Sol. Energy 102 (2014) 318–332, https://doi.org/10.1016/j.solener.2013.11.008.
[119] K Nithyanandam, R. Pitchumani, Computational studies on metal foam and heat pipe enhanced latent thermal energy storage, J. Heat Transf. 136 (2014), https://doi.org/10.1115/1.4026040.
[120] S Almsater, W Saman, F Bruno, Performance enhancement of high temperature latent heat thermal storage systems using heat pipes with and without fins for concentrating solar thermal power plants, Renew. Energy 89 (2016) 36–50, https://doi.org/10.1016/j.renene.2015.11.068.
[121] K Nithyanandam, R. Pitchumani, Design and analysis of metal foam enhanced latent thermal energy storage with embedded heat pipes for concentrating solar power plants, ASME 2013 7th Int. Conf. Energy Sustain. Minneapolis, MN, 2013, pp. 1–10.
[122] H Yang, J Song, B He, G Ding, Numerical study on charging characteristics of heat pipe-assisted cylindrical capsule for enhancing latent thermal energy storage, Sol. Energy 190 (2019) 147–155, https://doi.org/10.1016/j.solener.2019.08.007.
[123] M Bilardo, G Fraisse, M Pailha, E Fabrizio, Modelling and performance analysis of a new concept of integral collector storage (ICS) with phase change material, Sol. Energy 183 (2019) 425–440, https://doi.org/10.1016/j.solener.2019.03.032.
[124] K Nithyanandam, R. Pitchumani, Computational modeling of latent thermal energy storage system with embedded heat pipes, ASME Int. Mech. Eng. Congr. Expo. Proc. Vancouver, British Columbia, Canada, 5 2010 November 12-18, pp. 369–376, , https://doi.org/10.1115/IMECE2010-38682.
[125] K Nithyanandam, R. Pitchumani, Analysis and optimization of a latent thermal energy storage system with embedded heat pipes, Int. J. Heat Mass Transf. 54 (2011) 4596–4610, https://doi.org/10.1016/j.ijheatmasstransfer.2011.06.018.
[126] K Nithyanandam, R. Pitchumani, Computational modeling of dynamic response of a latent thermal energy storage system with embedded heat pipes, ASME 2011 5th Int. Conf. Energy Sustain. Washington, D.C, 2011, pp. 1–10.
[127] H Shabgard, CW Robak, TL Bergman, A Faghri, Heat transfer and exergy analysis of cascaded latent heat storage with gravity-assisted heat pipes for concentrating solar power applications, Sol. Energy 86 (2012) 816–830, https://doi.org/10.1016/j.solener.2011.12.008.
[128] K Nithyanandam, R. Pitchumani, Thermal energy storage with heat transfer augmentation using thermosyphons, Int. J. Heat Mass Transf. 67 (2013) 281–294, https://doi.org/10.1016/j.ijheatmasstransfer.2013.08.007.
[129] K Nithyanandam, R. Pitchumani, Computational studies on a latent thermal energy storage system with integral heat pipes for concentrating solar power, Appl. Energy 103 (2013) 400–415, https://doi.org/10.1016/j.apenergy.2012.09.056.
[130] K Nithyanandam, R. Pitchumani, Design of a latent thermal energy storage system with embedded heat pipes, Appl. Energy 126 (2014) 266–280, https://doi.org/10.1016/j.apenergy.2014.03.025.
[131] K Nithyanandam, R. Pitchumani, Cost and performance analysis of concentrating solar power systems with integrated latent thermal energy storage, Energy 64 (2014) 793–810, https://doi.org/10.1016/j.energy.2013.10.095.
[132] ZJ Zuo, A. Faghri, A network thermodynamic analysis of the heat pipe, Int. J. Heat Mass Transf. 41 (1998) 1473–1484, https://doi.org/10.1016/S0017-9310(97)00220-2.
[133] G Peterson, An Introduction to Heat Pipes: Modeling, Testing, and Applications, Wiley, 1994.
[134] M Chang, LC Chow, WS Chang, M Morgan, Transient behavior of axially grooved heat pipe with thermal energy storage, AIAA/ASME 5th Jt. Thermophys. Heat Transf. Conf. Seattle, WA, USA, 1990 June 18-12,, p. 9.
[135] H jie Song, W Zhang, Y qi Li, Z wei Yang, A bo. Ming, Exergy analysis and parameter optimization of heat pipe receiver with integrated latent heat thermal energy storage for space station in charging process, Appl. Therm. Eng. 119 (2017) 304–311, https://doi.org/10.1016/j.applthermaleng.2017.03.080.
[136] X Liu, G Fang, Z Chen, Dynamic charging characteristics modeling of heat storage device with heat pipe, Appl. Therm. Eng. 31 (2011) 2902–2908, https://doi.org/10.1016/j.applthermaleng.2011.05.018.
[137] N Sharifi, S Wang, TL Bergman, A Faghri, Heat pipe-assisted melting of a phase change material, Int. J. Heat Mass Transf. 55 (2012) 3458–3469, https://doi.org/10.1016/j.ijheatmasstransfer.2016.04.022.
[138] H Shabgard, A Faghri, TL Bergman, CE Andraka, Numerical simulation of heat pipe-assisted latent heat thermal energy storage unit for dish-Stirling systems, J. Sol. Energy Eng. 136 (2014) 1–12, https://doi.org/10.1115/1.4025973.
[139] M Mahdavi, S. Qiu, Mathematical modeling and analysis of steady state performance of a heat pipe network, Appl. Therm. Eng. 91 (2015) 556–573, https://doi.org/10.1016/j.applthermaleng.2015.08.017.
[140] N Sharifi, A Faghri, TL Bergman, CE Andraka, Simulation of heat pipe-assisted latent heat thermal energy storage with simultaneous charging and discharging, Int. J. Heat Mass Transf. 80 (2015) 170–179, https://doi.org/10.1016/j.ijheatmasstransfer.2014.09.013.
[141] R Srikanth, RS Nair, C Balaji, Thermosyphon assisted melting of PCM inside a rectangular enclosure: a synergistic numerical approach, J. Phys. Conf. Ser. 745 (2016), https://doi.org/10.1088/1742-6596/745/3/032130.
[142] Y Cao, A. Faghri, Transient two-dimensional compressible analysis for high-temperature heat pipes with pulsed heat input, Numer. Heat Transf. Part A 18 (1991) 483–502, https://doi.org/10.1080/10407789008944804.
[143] CE Andraka, Dish Stirling advanced latent storage feasibility, Energy Procedia 49 (2014) 684–693, https://doi.org/10.1016/j.egypro.2014.03.074.
[144] N Sharifi, S Wang, TL Bergman, A Faghri, Heat pipe-assisted melting of a phase change material, Int. J. Heat Mass Transf. 55 (2012) 3458–3469, https://doi.org/10.1016/j.ijheatmasstransfer.2016.04.022.
[145] EK. Levy, Theoretical investigation of heat pipes operating at low vapor pressures, J. Eng. Ind. 90 (1968) 547–552, https://doi.org/10.1115/1.3604687.